High Precision Plastic Micro/Nanofabrication and Its Applications for Chemical/Biochemical Microchips

Hidetoshi Shinohara

Major in Nano-Science and Nano-Engineering
Graduate School of Advanced Science and Engineering
(Micro/Nano System Technologies)

Waseda University

February, 2010

Doctoral dissertation committee:

Professor

Dr. Shuichi Shoji (supervisor)

Faculty of Science and Engineering

Waseda University

Professor

Dr. Hiroshi Kawarada

Faculty of Science and Engineering

Waseda University

Associate Professor

Dr. Jeung Sang Go

School of Mechanical Engineering

Pusan National University

Associate Professor

Dr. Takashi Tanii

Faculty of Science and Engineering

Waseda University

Associate Professor

Dr. Takanobu Watanabe

Faculty of Science and Engineering

Waseda University

Acknowledgments

This thesis includes several research achievements during my enrollment at Graduate School of Advanced Science and Engineering of Waseda University. There are many contributors and collaborators in this work.

First of all, I would like to sincerely thank my supervisor, Professor Shuichi Shoji at faculty of Science and Engineering of Waseda University, for his fruitful supports and advices of daily research activities. This work could not have been accomplished without his help. I am glad to have belonged to his laboratory for about six years.

I would like to sincerely thank the dissertation committee, Professor Hiroshi Kawarada, Associate Professor Takashi Tanii, Associate Professor Takanobu Watanabe at faculty of Science and Engineering of Waseda University, and Associate Professor Jeung Sang Go at School of Mechanical Engineering of Pusan National University, for their careful reading of the manuscript and fruitful discussions.

I would like to sincerely thank Associate Professor Jun Mizuno at Nanotechnology Research Center of Waseda University, for his fruitful technical supports and advices. He has kindly supported me since I started research activities at fourth-year undergraduate student.

I am grateful to Associate Professor Tetsushi Sekiguchi at Nanotechnology Research Center of Waseda University, Dr. Tomohiko Edura, and Dr. Takahiro Arakawa for their kindly advices associated Ph.D. studies and the dissertation.

I have also been supported by many students in Shoji laboratory. I would like to thank Mr. Masanori Ishizuka, Mr. Masaaki Abe, Mr. Hiroaki Houjou, and Mr. Yuya Hamagami, for their fundamental training for my starting research activities. Mr. Kentaro Kawai was contemporary Ph.D. student in Shoji laboratory. We could develop through friendly competition. I am happy to complete doctorate together. I would also like to thank Ms. Reiko Nishikiori for kindly support of official trip procedure.

I would also like to thank Imprint group members in Shoji laboratory, Mr. Takafumi Suzuki, Mr. Hiroshi Ono, Mr. Makoto Fukuhara, Mr. Shingo Kataza, Mr. Akira Saeki, Mr. Kentaro Ishibashi, Mr. Katsuyuki Sakuma, Mr. Tomoya Kato, Mr. Noriyasu Nagai, Mr. Shugo Ishizuka, Mr. Tomotaka Shibazaki, Mr. Masao Noguchi, Mr. Shunsuke Matsui, Ms. Naoko Unami, Mr. Shogo Umeda, Mr. Takashi Kasahara, Mr. Takaaki Hori, and Mr. Lingyi Li, for their continuous encouragement. We could develop through friendly competition during daily experiments and discussions. I wish them the best of luck with everything.

Hidetoshi Shinohara

Contents

Chapter 3: Low-Temperature Direct Bonding..............34

Chapter 4: Surface Modification Using Polyurea 72

Chapter 5: Plastic Chemical/Biochemical Microchips

Chapter 6: Conclusion

List of achievements

List of figures

List of tables

List of abbreviations

ATR-FT-IR	Attenuated total reflection Fourier-transform infrared spectrometer
BSA	Bovine serum albumin
COC	Cyclo-olefin copolymer
COP	Cyclo-olefin polymer
DC	Direct current
Deep-RIE	Deep reactive ion etching
DMA	Dynamic mechanical analysis
EOF	Electroosmotic flow
ESI	Electrospray ionization
ICP	Inductively coupled plasma
LOC	Lab-on-a-chip
MCE	Microchip electrophoresis
MDA	4.4'-diaminodiphenylmethane
MDI	4.4'-diphenylmethanediisocyanate
MEMS	Micro electromechanical systems
MPC	2-methacryloyloxiethylphosphorylcholine
MS	Mass spectrometry
NEXAFS	Near edge X-ray absorption fine structure
PC	Polycarbonate
PDMS	Poly-dimethylsiloxane
PEM	Polymer electrolyte membrane
PMMA	Poly-methylmethacrylate
RSD	Residual standard deviation
SEM	Scanning electron microscope
UV	Ultraviolet
VUV	Vacuum ultraviolet
XPS	X-ray photoelectron spectroscopy
µDMFC	Micro direct methanol fuel cell
µ-TA	Micro thermal analysis
µ-TAS	Micro total analysis systems

Chapter 1

<u>Introduction</u>

Plastic [†] materials are used in photonics, electronics, medical, and chemical/biochemical fields. Plastic microfabrication technologies have developed low-cost and functional devices. However, the fabrication precision is not fine enough to obtain micro/nano structures. This chapter introduces the motivation and general fabrication problems on the precision.

1.1 Motivation

Recently, from the standpoint of purely scientific interest and from that of technological validity, chemical/biochemical microchips have been attracting attention. The concept of microchips is the integration of chemical/biochemical, and medical analysis tools onto a chip [2,3]. Preparation, mixing, reaction, detection, and analysis are carried out in the micro-space such as microchannel and microchamber. This strategy is called "micro total analysis systems" (μTAS) or "lab-on-a-chip" (LOC). It brings advantages below;

(1) Chemical and biochemical reaction times can be shortened.
(2) Reaction efficiency can be improved.
(3) Reactant amounts can be reduced.
(4) Analysis equipment can be downsizing.

These merits also enable to inexpensive, fast, and ubiquitous analyses such as home health care testing and on-site analyses.

[†] Meanings of "plastic" are (a) <noun> a synthetic material made from a wide range of organic polymers, (b) <adjective> made of plastic, and (c) <adjective> of or relating to the permanent deformation of a solid without fracture by the temporary application of force [1]. The meaning is mainly (a) or (b) in this thesis. The meaning of (c) is used for discussion about viscoelastic character.

The micro-space structure is usually fabricated by micro electromechanical systems (MEMS) technologies on such substrate materials as Si, glass, and polymers, and then bonded with a lid to form sealed structures. Surface modification is also one of the most important processes for chemical/biochemical microchips to easily control flow behavior of buffer fluids, reagents and biomaterials in microchannels. The core three processes for fabrication of microchips are shown in Figure 1.1.
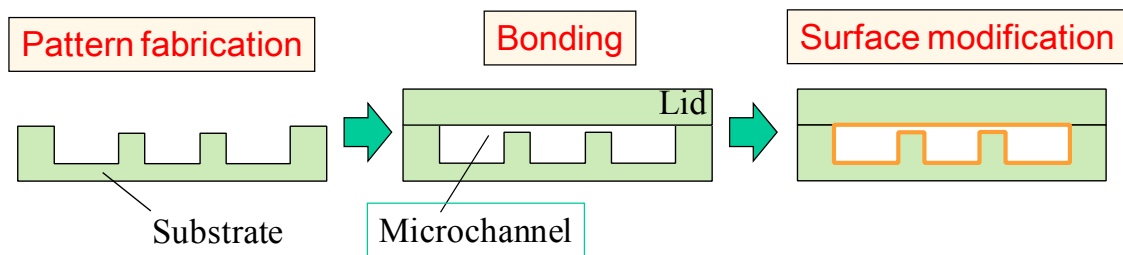
Fig. 1.1: Core three processes for fabrication of chemical/biochemical microchip.

Table 1.1 lists comparison of substrate materials for microchannel fabrication. Conventional Si or glass micro/nanofabrication methods using photolithography and etching have difficulty in reducing the fabrication cost of the microchip to the commercialization level. In the case of multistep-pattern fabrication, multiple photolithography and etching processes are required as shown in Figure 1.2 (a). On the other hand, the use of polymer can provide low-cost mass-manufacturing due to the availability of molding methods. Once a mold has been made, the multistep pattern can be batch transferred by molding with low-cost and high-throughput as shown in Figure 1.2 (b). Thus, polymer is applicable for chemical/biochemical microchips.

High optical transparent polymer has been used for microchannel to easily observe and detect biomaterials by optical methods. Examples of the polymer materials are poly-dimethylsiloxane (PDMS), poly-methylmethacrylate (PMMA), polycarbonate (PC), polystyrene (PS), cyclo-olefin polymer (COP) and cyclo-olefin copolymer (COC). PDMS is the most popular polymers for microchips because of its simple fabrication process [4-7]. Since PDMS is an elastomeric polymer, demolding of PDMS is easier than that of other rigid plastic materials. PDMS can easily bond to other materials by self-adhesiveness, and can bond permanently to Si, glass, and PDMS. However, PDMS has some disadvantages for actual use compared to other materials. For example,

(i) Structural rigidity and strength are insufficient. Supporting plate such as Si, glass, and other plastics is often required for easily handling of the PDMS microchip. In addition, the flow is unstable at high internal pressure in the microchannel by

expansion or shrinkage of its structure.

(ii) Liquid vaporization can be occurred at heated condition because of its high-permeability to gases.

Thus, rigid plastics are also required as materials for low-cost microchip.

Although the size of microstructures in conventional microchip were larger than tens μm, further downsizing to submicron-scale is expected to enhance the abovementioned advantages of μTAS. The precisely-fabricated structures are expected to give precise data according to theoretically designed model. Thus, fine structure ranging from μm to sub-μm is important. Currently, Si, glass and PDMS have been selected as a substrate material. However, the precision for fabrication of plastic microchips is too low to obtain these fine structures. Systematic technologies for the fabrication of plastic microchips have been desired to fabricate the structure smaller than sub-μm precision.

In this thesis, high precision plastic micro/nanofabrication methods are examined by using PMMA and COP. The fabrication methods consist of high precision hot embossing, low-temperature direct bonding, and stable hydrophilic surface treatment. By combining these methods, functional chemical/biochemical microchips are fabricated and examined.

Table 1.1: Comparison of substrate materials for microchannel fabrication.

Material	Pattern fabrication	Advantage	Disadvantage
Si, glass	Photolithography & etching	● Conventional MEMS fabrication process available	● High-cost process
PDMS	Molding	● Easy fabrication	● Insufficient structural rigidity and strength ● High-permeability to gases
Plastic	Molding	● Low-cost process	● Low precision for micro/nanofabrication
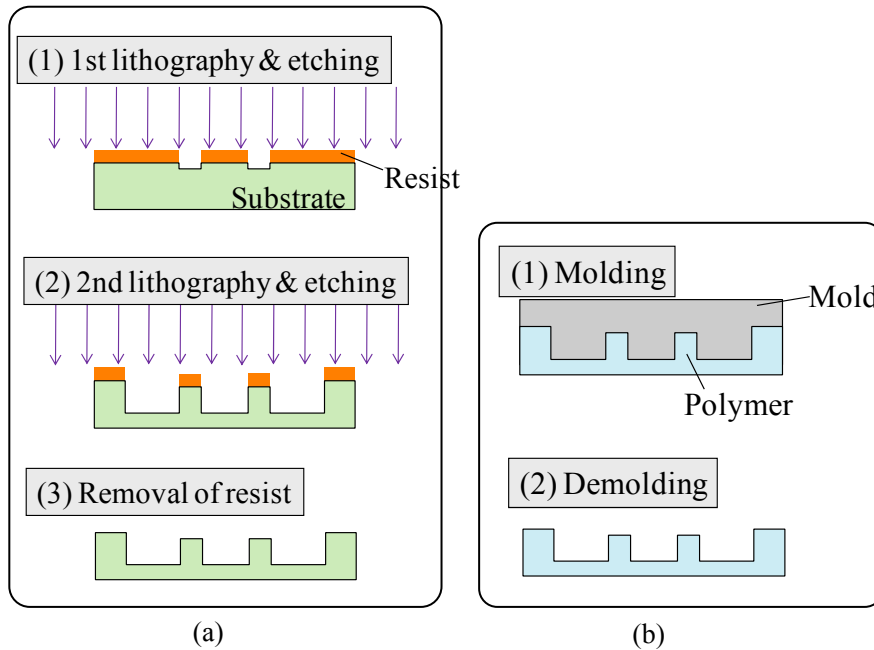
Figure 1.2: Multistep pattern fabrication by (a) photolithography and etching, and (b) molding.

1.2 Required issues on fabrication methods for plastic microchips

1.2.1 Molding methods

Examples of molding methods for fabrication of plastic micro/nanopatterns include injection molding [8-13], hot embossing [8,14-23] and ultraviolet (UV) imprinting [24-27].

Injection molding is a process of injecting melted polymer into a mold. The merit of this method is high-throughput. It is generally used between millimeter and meter scale in industry. In research and development phase, the scale reaches to submicron and micrometer [13].

Hot embossing is the method by pressing a heated plastic in a mold. Compared with injection molding, this method has advantages of lower cost of molds, simpler operation, and higher replication accuracy of micro/nanometer scale patterns.

However, the throughput of this method is lower than that of injection molding because of longer thermal cycle. These injection molding and hot embossing are available for various plastics. Thus, these two methods have general versatility in industry. Table 1.2 and Figure 1.3 show examples of plastics used in these two molding methods [8], and chemical structural formulas of plastics of PMMA and COP [28], respectively.

UV imprinting is a method of pressing mold to UV photocurable resin. Thermal cycle and high-pressure force are not required. The throughput is higher than that of hot embossing. High resolution patterns smaller than 100 nm have been obtained by this method. These hot embossing and UV imprinting have also attracted attention in nanoscale lithography [18,25-27].

Many works on plastic micro/nanopatterns have been done by molding methods. However, conventional molding methods are not sufficiently considered subsequent bonding process. Thus, it was difficult to realize fine micro/nanopatterns in plastic microchip because the micro/nanopatterns are often deformed after bonding process. A molding method adaptable for bonding process is required.

Table 1.2: Examples of plastics used for injection molding and hot embossing [8].

Acronym	Full name	Temperature stability [°C]	Properties	Structure
COC	Cyclo-olefine copolymer	140	High transparency	Amorphous
PMMA	Polymethylmethacrylate	80	High transparency	Amorphous
PC	Polycarbonate	130	High transparency	Amorphous
PS	Polystyrene	80	Transparent	Amorphous
POM	Polyoxymethylene	90	Low friction	Semi crystalline
PFA	Perfluoralkoxy copolymer	260	High chemical resistivity	Semi crystalline
PVC	Polyvinlchloride	60	Cheap	Amorphous
PP	Polypropylene	110	Mechanical properties	Semi crystalline
PET	Polyethylene terephtalate	110	Transparent, low friction	Amorphous/Semi crystalline
PEEK	Polyetheretherketone	250	High temperature resistivity	Semi crystalline
PA	Polyamide	80–120	Good mechanical properties	Semi crystalline
PSU	Polysulfone	150	Chemical and temperature resistivity	Amorphous
PVDF	Polyvinylidenefluoride	150	Chemically inert, piezo-electric	Semi crystalline
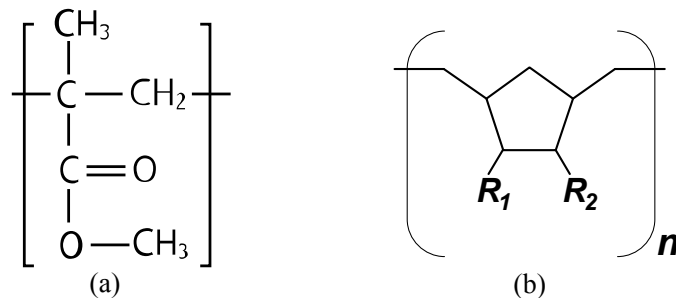
Fig. 1.3: Chemical structural formulas of (a) PMMA and (b) COP [28].

1.2.2 Bonding methods

Variety of plastic bonding methods have been reported including thermal direct bonding [11,18,20,23,29], solvent bonding [16,22], bonding using other intermediate layer such as adhesive and metal layer [10,12,19,30-32].

Plastic bonding process is essential but it causes several fundamental problems:

(1) Deformation of the microstructure causes obstacles to smooth fluidic flow. The deformation is resulted from over-heating, protrusion of adhesives, or dissolved/melted plastics into the channel region.

(2) The adhesives or dissolved/melted plastics also cause scattering and absorption of the light detecting the product materials and / or flowing materials.

To solve these problems, the direct bonding method has been often selected for tens μm scale microstructures under moderate bonding conditions based on glass transition temperature, T_g. However, the heating around T_g causes thermal deformation. To further downsize the microchannel, low-temperature bonding method is required.

1.2.3 Surface modification methods

Surface modification methods for plastics are classified into two categories. One is treatment on the original surface using plasma treatment [33-36] and ultraviolet irradiation [37-43]. Another is coating with other polymer materials [44-57]. In case of hydrophilic surface treatment, capillary pressure can be utilized for liquid pumping in microchannel so that no external flow pump is necessary [58,59].

Performances of the modified surface required for biocompatibility are listed below.

(1) Anti-adhesion of biomaterials
(2) Sufficient adhesion strength to substrate
(3) High stability to maintain modified surface for a long time
(4) Uniformity
(5) Durability in water

The micro/nanostructures should be maintained after the modification.

(6) Thin modified layer without changing sizes of the structures
(7) Low-temperature modification avoiding thermal deformation

However, in case of hydrophilic surface treatment, it is difficult to realize all of the abovementioned performances. In addition, it is also difficult to maintain the property of modified surface during bonding.

1.3 Outline of this thesis

The following chapters describe high precision plastic micromachining methods.

Chapter 2 "**High Precision Hot Embossing**" describes precise structure-controlled hot embossing method of plastic substrates. The author selects hot embossing as molding method from viewpoints of simple operation and general versatility in industry. Flat embossed surface which is required for successive low-temperature bonding is obtained by optimizing mold structure and demolding conditions.

Chapter 3 "**Low-Temperature Direct Bonding**" describes low-temperature direct bonding methods of PMMA and COP. In order to bond at lower than T_g, pretreatments of oxygen plasma, atmospheric-pressure oxygen plasma, UV/O$_3$, vacuum UV (VUV), and VUV/O$_3$ are examined. These methods enable plastic bonding with negligible deformation. The mechanisms of low-temperature direct bonding using oxygen plasma, VUV and VUV/O$_3$ treatments are evaluated using surface analysis methods. PMMA and COP microchips which have fine microchannel of less than 5 μm in depth and 150 μm-wide are fabricated.

Chapter 4 "**Surface Modification Using Polyurea Film**" describes a combined process with surface modification and low-temperature bonding of plastics. The polyurea film is coated on plastic surface and treated by VUV/O$_3$. Highly stable hydrophilic surface is obtained after the treatment. The VUV/O$_3$-treated polyurea film can be used as intermediate layers for low-temperature PMMA bonding. This bonding method is applied for fabrication of electrophoresis microchips.

Chapter 5 "**Plastic Chemical/Biochemical Microchips**" explains plastic chemical/biochemical microchips of μDMFC, MCE-ESI-MS microchip, and plastic blood analysis chip realized by high precision plastic micro/nano fabrication methods.

Chapter 6 concludes this thesis and describes the future research.

References

[1] C. Soanes and A. Stevenson (Ed.), Oxford Dictionary of English, Oxford University Press, (2005).

[2] A. Manz, D. J. Harrison, E. M. J. Verpoorte, J. C. Fettinger, A. Paulus, H. Lüdi, H. M. Widmer, Planar chips technology for miniaturization and integration of separation techniques into monitoring systems: capillary electrophoresis on a chip, *J. Chromatogr.* **593** (1992) 253-258.

[3] T. S. Kim, Y.-S. Lee, T.-D. Chung, N. L. Jeon, S.-H. Lee, K.-Y. Suh, J. Choo, Y.-K. Kim (Ed.), Proc. The 13th Int. Conf. Miniaturized Sys. Chem. Life Sci. (Micro-TAS), (2009).

[4] D. C. Duffy, J. C. McDonald, O. J. A. Schueller, G. M. Whitesides, Rapid prototyping of microfluidic systems in poly(dimethylsiloxane), Anal. Chem. **70** (1998) 4974-4984.

[5] B. E. Slentz, N. A. Penner, E. Lugowska, F. Regnier, Nanoliter capillary electrochromatography columns based on collocated monolithic support structures molded in poly(dimethylsiloxane), Electrophoresis **22** (2001) 3736-3743.

[6] H. Becker and L. E. Locascio, Polymer microfluidic devices, Talanta **56** (2002) 267–287.

[7] T. Arakawa, Y. Shirasaki, T. Aoki, T. Funatsu, S. Shoji, Three-dimensional sheath flow sorting microsystem using thermosensitive hydrogel, Sens. Actuators A **135** (2007) 99-105.

[8] M. Heckele and W. K. Schomburg, Review on micro molding of thermoplastic polymers, J. Micromech. Microeng. **14** (2004) R1-R4.

[9] E. W. Becker, W. Ehrfeld, P. Hagmann, A. Maner, D. Münchmeyer, Fabrication of microstructures with high aspect ratios and great structural heights by synchrotron radiation lithography, galvanoforming, and plastic moulding (LIGA Process), Microelectron. Eng. **4** (1986) 35-56.

[10] R. M. McCormick, R. J. Nelson, M. G. A.-Amigo, D. J. Benvegnu, and H. H. Hooper, Microchannel electrophoretic separations of DNA in injection-molded plastic substrates, Anal. Chem. **69** (1997) 2626-2630.

[11] M. Svedberg, A. Pettersson, S. Nilsson, J. Bergquist, L. Nyholm, F. Nikolajeff, K. Markides, Sheathless electrospray from polymer microchips, Anal. Chem. **75** (2003) 3934-3940.

[12] F. Dang, O. Tabata, M. Kurokawa, A. A. Ewis, L. Zhang, Y. Yamaoka, S. Shinohara,

Y. Shinohara, M. Ishikawa, Y. Baba, High-performance genetic analysis on microfabricated capillary array electrophoresis plastic chips fabricated by injection molding, Anal. Chem. **77** (2005) 2140-2146.

[13] H. Ito, H. Suzuki, K. Kazama, T. Kikutani, Polymer structure and properties in micro- and nanomolding process, Curr. Appl. Phys. **9** (2009) e19-e24.

[14] S. Y. Chou and P. R. Krauss, Imprint of sub-25 nm vias and trenches in polymers, Appl. Phys. Lett. **67** (1995) 3114-3116.

[15] H. Becker and U. Heim, Hot embossing as a method for the fabrication of polymer high aspect ratio structures, Sens. Actuators A **83** (2000) 130-135.

[16] J. Wang, M. Pumera, M. P. Chatrathi, A. Escarpa, R. Konrad, A. Griebel, W. Dörnger, H. Löwe, Towards disposable lab-on-a-chip: poly(methylmethacrylate) microchip electrophoresis device with electrochemical detection, Electrophoresis, **23** (2002) 596-601.

[17] S. J. Park, K. S. Cho, C. G. Choi, Effect of fluorine plasma treatment on PMMA and their application to passive optical waveguides, J. Collo. Interf. Sci. **258** (2003) 424-426.

[18] R. T. Kelly and A. T. Woolley, Thermal bonding of polymeric capillary electrophoresis microdevices in water, Anal. Chem. **75** (2003) 1941-1945.

[19] Y. Zhao and T. Cui, Fabrication of high-aspect-ration polymer-based electrostatic comb drives using the hot embossing technique, J. Micromech. Microeng. **13** (2003) 430-435.

[20] Z. Chen, Y. Gao, J. Lin, R. Su, and Y. Xie, Vacuum-assisted thermal bonding of plastic capillary electrophoresis microchip imprinted with stainless steel template, J. Chromatogr. A **1038** (2004) 239-245.

[21] R.-D. Chien, Hot embossing of microfluidic platform, Int. Comm. Heat Mass Transfer **33** (2006) 645-653.

[22] C. H. Lin, C.H. Chao, C.W. Lan, Low azeotropic solvent for bonding of PMMA microfluidic devices, Sens. Actuators B, **121** (2007) 698-705.

[23] S. Amaya, D. V. Dao, S. Sugiyama, Development of a monolithic PMMA comb-drive micro actuator utilizing hot embossing and ultra-precision machining, Proc. The 22nd IEEE Int. Conf. Micro Elec. Mech. Sys. (IEEE-MEMS), (2009) 713-716.

[24] J. Haisma, M. Verheijen, K. V. D. Heuvel, J. V. D. Berg, Mold-assisted nanolithography: a process for reliable pattern replication, J. Vac. Sci. Tech. B **14** (1996) 4124-4128.

[25] Y. Kawaguchi, F. Nonaka, Y. Sanada, Fluorinated materials for UV nanoimprint

lithography, Microelectron. Eng. **84** (2007) 973-976.

[26] H. Shinohara, M. Fukuhara, T. Hirasawa, J. Mizuno, S. Shoji, Fabrication of magnetic nanodots array using UV nanoimprint lithography and electrodeposition for high density patterned media, J. Photopolym. Sci. Tech. **21** (2008) 591-596.

[27] N. Nagai, H. Ono, K. Sakuma, M. Saito, J. Mizuno, S. Shoji, Copper multilayer interconnection using ultraviolet nanoimprint lithography with a double-deck mold and electroplating. Jpn. J. Appl. Phys. **48** (2009) 115001.

[28] M. Yamazaki, Industrialization and application development of cyclo-olefin polymer, J. Mol. Catal. A **213** (2004) 81–87.

[29] G. A. C. M. Spierings and J. Haisma, Direct bonding of organic materials, Appl. Phys. Lett. **64** (1994) 3246-3248.

[30] B. Graß, A. Neyer, M. Jöhnck, D. Siepe, F. Eisenbeiß, G. Weber, R. Hergenröder, A new PMMA-microchip device for isotachophoresis with integrated conductivity detector, Sens. Actuators B **72** (2001) 249-258.

[31] Y. Zhao and T. Cui, Fabrication of high-aspect-ration polymer-based electrostatic comb drives using the hot embossing technique, J. Micromech. Microeng. **13** (2003) 430-435.

[32] K. F. Lei, S. Ahsan, N. Budraa, W. J. Li, J. D. Mai, Microwave bonding of polymer-based substrates for potential encapsulated micro/nanofluidic device fabrication, Sens. Actuators A **114** (2004) 340-346.

[33] U. Schulz, P. Munzert, N. Kaiser, Surface modification of PMMA by DC glow discharge and microwave plasma treatment for the improvement of coating adhesion, Surf. Coat. Technol. **142-144** (2001) 507-511.

[34] A. Kamińska, H. Kaczmarek, J. Kowalonek, The influence of side groups and polarity of polymers on the kind and effectiveness of their surface modification by air plasma action, Eur. Polym. J. **38** (2002) 1915-1919.

[35] J. Chai, F. Lu, B. Li, D. Y. Kwok, Wettability interpretation of oxygen plasma modified poly(methyl methacrylate), Langmuir **20** (2004) 10919-10927.

[36] J. Lai, B. Sunderland, J. Xue, S. Yan, W. Zhao, M. Folkard, B. D. Michael, Y. Wang, Study on hydrophilicity of polymer surfaces improved by plasma treatment, Appl. Surf. Sci. **252** (2006) 3375–3379.

[37] J. Peeling and D. T. Clark, An ESCA study of the photo-oxidation of the surface of polystyrene film, Polym. Degrad. Stab. **3** (1980-81) 97-105.

[38] J. Peeling and D. T. Clark, ESCA study of the surface photo-oxidation of some non-aromatic polymers, Polym. Degrad. Stab. **3** (1981) 177-185.

[39] T. N. Murakami, Y. Fukushima, Y. Hirano, Y. Tokuoka, M. Takahashi, N.

Kawashima, Surface modification of polystylene and poly(methyl methacrylate) by active oxygen treatment, Collo. Surf. B **29** (2003) 171-179.

[40] A. Hozumi, H. Inagaki, T. Kameyama, The hydrophilization of polystylene substrates by 172-nm vacuum ultraviolet light, J. Collo. Interf. Sci. **278** (2004) 383-392.

[41] H. Kaczmarek, H. Chaberska, The influence of UV-irradiation and support type on surface properties of poly(methyl methacrylate) thin films, Appl. Surf. Sci. **252** (2006) 8185-8192.

[42] G. A. Diaz-Quijada, R. Peytavi, A. Nantel, E. Roy, M. G. Bergeron, M. M. Dumoulin, T. Veres, Surface modification of thermoplastics-towards the plastic biochip for high throughput screening devices, Lab Chip **7** (2007) 856-862.

[43] Y.-J. Kim, Y. Taniguchi, K. Murase, Y. Taguchi, H. Sugimura, Vacuum ultraviolet-induced surface modification of cyclo-olefin polymer substrates for photochemical activation bonding, Appl. Surf. Sci. **255** (2009) 3648-3654.

[44] E. Ruckenstein and S. V. Gourisankar, Preparation and characterization of thin film surface coatings for biological environments, Biomater. **7** (1986) 403-422.

[45] R. Larsson, G. Selén, H. Björdklund, P. Fagerholm, Intraocular PMMA lenses modified with surface-immobilized heparin: evaluation of biocompatibility in vitro and in vivo, Biomater. **10** (1989) 511-516.

[46] N. B. Mateo and B. D. Ratner, Relating the Surface properties of intraocular lens materials to endothelial cell adhesion damage, Invest. Ophthalmol. Vis. Sci. **10** (1989) 853-860.

[47] B. D. Ratner, Surface Modification of Polymers: chemical, biological and surface analytical challenges, Biosens. Bioelec. **10** (1995) 797-804.

[48] M. Morpurgo, F. M. Veronese, D. Kachensky, J. M. Harris, Preparation and characterization of poly(ethylene glycol) vinyl sulfone, Bioconjugate Chem. **7** (1996) 363-368.

[49] Y. Iwasaki, A. Mikami, K. Kurita, N. Yui, K. Ishihara, N. Nakabayashi, Reduction of surface-induced platelet activation on phospholipid polymer, J. Biomed. Mater. Res. **36** (1997) 508-515.

[50] K. Ishihara, H. Nomura, T. Mihara, K. Kurita, Y. Iwasaki, N. Nakabayashi, Why do phospholipid polymers reduce protein adsorption?, J. Biomed. Mater. Res. **39** (1998) 323-330.

[51] N. Tirelli, M. P. Lutolf, A. Napoli, J. A. Hubbell, Polyethylene glycol/ block copolymers, Rev. Molec. Biotech. **90** (2002) 3-15.

[52] C. Oehr, Plasma surface modification of polymers for biomedical use, Nucl. Instr.

And Meth. In Phys. Res. B **208** (2003) 40-47.

[53] J. Liu, T. Pan, A. T. Woolley, M. L. Lee, Surface-modified poly(methyl methacrylate) capillary electrophoresis microchips for protein and peptide analysis, Anal. Chem. **76** (2004) 6948-6955.

[54] T. Goda, T. Konno, M. Takai, T. Moro, K. Ishihara, Biomimetic phosphorylcholine polymer grafting from polydimethylsiloxane surface using photo-induced polymerization, Biomater. **27** (2006) 5151-5160.

[55] H. Bi, W. Zhong, S. Meng, J. Kong, P. Yang, B. Liu, Construction of a biomimetic surface on microfluidic chips for biofouling resistance, Anal. Chem. **78** (2006) 3399-3405.

[56] F. Kitagawa, K. Kubota, K. Sueyoshi, K. Otsuka, One-step immobilization of cationic polymer onto a poly(methyl methacrylate) microchip for high-performance electrophoretic analysis of proteins, Sci. Tech. Adv. Mater. **7** (2006) 558-565.

[57] F. Kitagawa, K. Kubota, K. Otsuka, One-step preparation of amino-PEG modified PMMA microchips for electrophoretic separation of biogenic compounds, Proc. The 12th Int. Conf. Miniaturized Sys. Chem. Life Sci. (Micro-TAS), (2008) 1138-1140.

[58] E. Delamarche, A. Bernard, H. Schmid, A. Bietsch, B. Michel, H. Biebuyck, Microfluidic networks for chemical patterning of substrates: design and application to bioassays, J. Am. Chem. Soc. **120** (1998) 500-508.

[59] L. Sainiemi, T. Nissilä, V. Jokinen, T. Sikanen, T. Kotiaho, R. Kostiainen, R. A. Ketola, S. Franssila, Fabrication and fluidic characterization of silicon micropillar array electrospray ionization chip, Sens. Actuators B **132** (2008) 380-387.

Chapter 2

<u>High Precision Hot Embossing</u>[*]

2.1 Introduction

Ideal hot embossing is schematically illustrated in Figure 2.1 (a). Hot embossing is a fabrication method of microchannel structures on plastic plate. Si is often used as the mold material in terms of smooth surface and easy fabrication by deep reactive ion etching (Deep-RIE) [5]. The embossed surface should be as flat as possible for void-free bonding. Actually, several μm level failures such as burr, crack and slope at the top edge of the channel pattern are often remained as illustrated in Figure 2.1 (b). These failures can be eliminated after conventional bonding with low precision, because adhesives or dissolved/melted plastics can compensate the failures. However, these failures result in the failure of low-temperature bonding[†]. Adaptable hot embossing method for low-temperature bonding with high precision is required.

In this work, the failures at the top edge of the channel pattern are minimized and realizes flat surface after hot embossing. The author focuses on mold structure and hot embossing conditions. A Si mold fabrication method for high precision hot embossing is described in Section 2.2. Section 2.3 describes high precision hot embossing method.

---

[*]This chapter is based on the published papers listed in the reference section [1-4].
[†]Low-temperature bonding method will be described in Chapters 3 and 4.
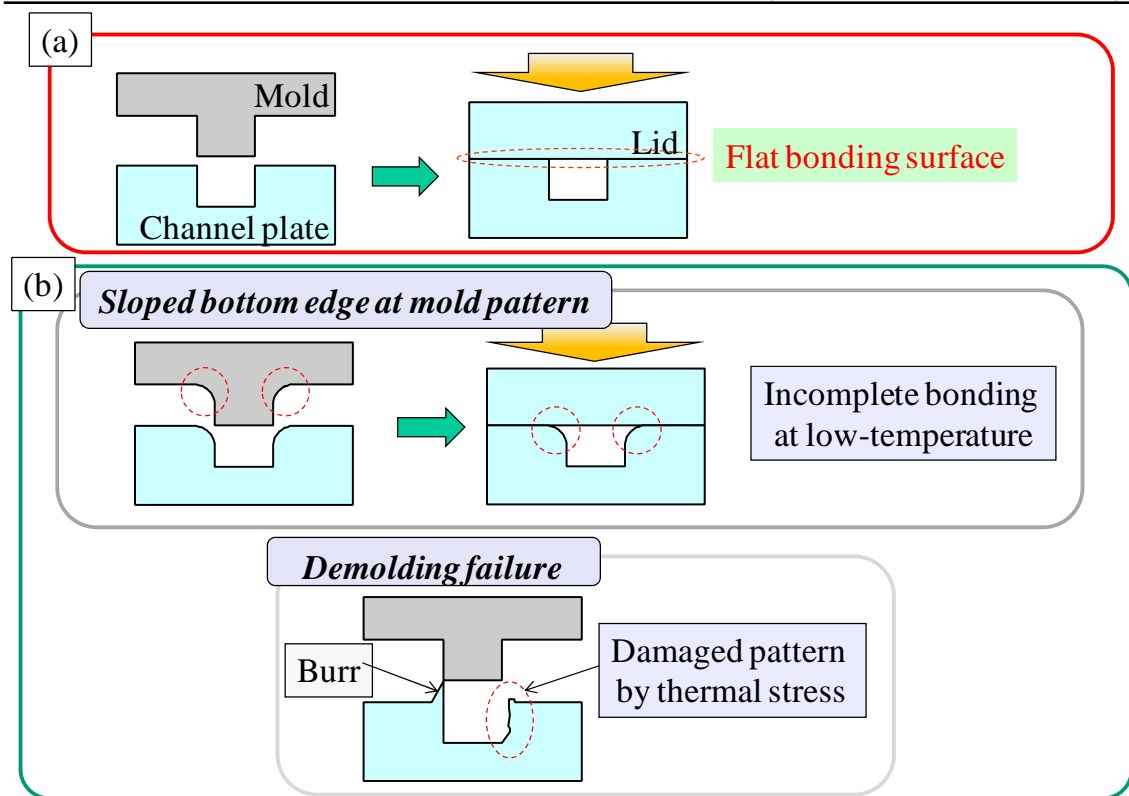
Fig. 2.1: Conceptual diagram of (a) ideal and (b) actual hot embossing.

2.2 Si mold fabrication

2.2.1 Si mold fabrication using Deep-RIE

Figure 2.2 shows typical Si mold fabrication process [5]. First, photoresist or SiO_2 is coated on Si wafer (Figure 2.2 (a)). Pattern is formed by conventional photolithography method (Figure 2.2 (b)). Then, Si is etched by Deep-RIE (Figure 2.2 (c)). Finally, the resist layer is removed (Figure 2.2 (d)).

Figure 2.3 shows conventional Deep-RIE process [6] using Bosch process. This process repeats isotropic etching by SF_6-RIE and CF_x-passivation from C_4F_8 gas. This process provides fast anisotropic etching. However, there are left ripple-shape structures on the etched sidewall called scallop resulted from etching/passivation cycles. Thus, the shape at the bottom edge of the etched area is roundly sloped. Etching conditions were examined to realize smaller scallops of Deep-RIE [7] by decreasing the slope at the bottom edge.

(a)

Resist

Si wafer

(b)

(c)

(d)
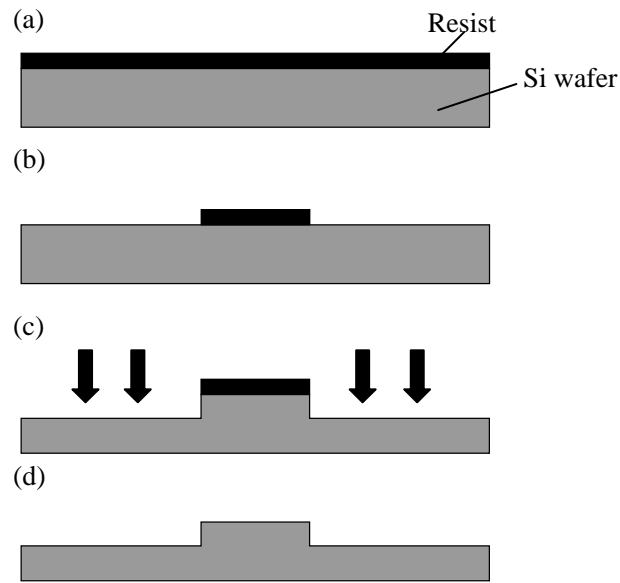
Fig. 2.2: Si mold fabrication process; (a) resist coating, (b) patterning, (c) Si etching, and (d) removal of resist layer [5].

Resist

Si

Isotropic Etching

Passivation layer

**Deposition
(Sidewall Passivation)**

**Removal of bottom
passivation layer by
ion bombardment**

Isotropic Etching

Scallop structures

Resulting profile
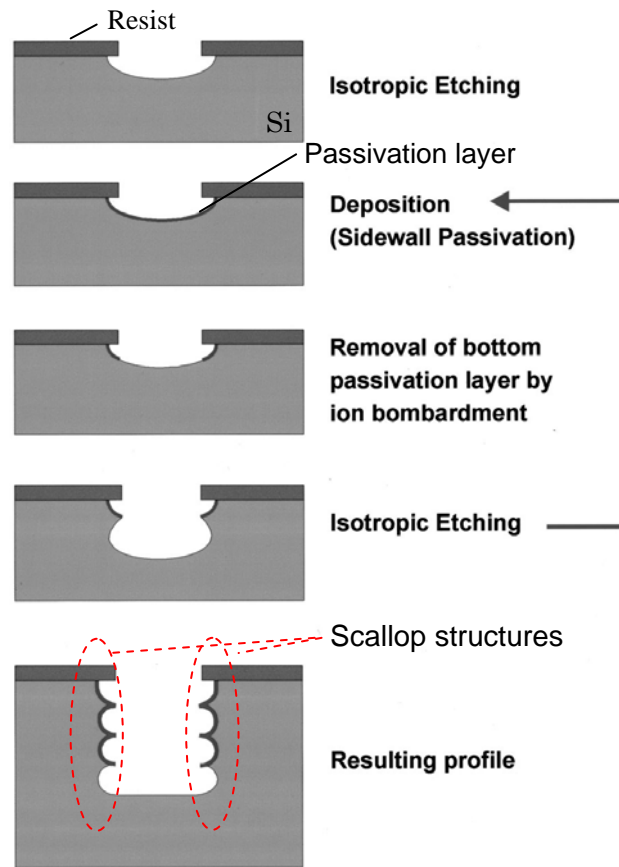
Fig. 2.3: Process flow of conventional Deep-RIE process [6].

2.3.1 Experimental procedure

Si Deep-RIE process was performed by an inductively coupled plasma (ICP) system (MUC-21 from Sumitomo Precision Co., Ltd.). Process conditions of conventional Deep-RIE and small-scallop types [7] are listed in Table 2.1. Conventional type is fitted for the fabrication of high-aspect ratio structures such as trench or through holes. The etching rate for mold fabrication is about 1.9 μm/min. In case of small-scallop type, the effect of passivation process is larger than conventional type so that the scallop structure can be minimized at appropriate etching rate of about 0.9 μm/min.

For evaluation of bottom edge shape of the mold, micrometer-scale pattern with width of 30 ~ 50 μm, and height of 10 ~ 50 μm were fabricated with Deep-RIE conditions in Table 2.1. The degree of roundness was evaluated by measuring vertical-size difference between ideal vertical shape and the actual shape f defined in Figure 2.4. The vertical-size difference was measured from cross-sectional scanning electron microscope (SEM) image.

Table 2.1: Process conditions of conventional Deep-RIE and small-scallop types [7].

				Conventional type	Small-scallop type
Cycle Time	Etch	On Time (sec)		12.0	7.0
	Pass	On Time (sec)		8.0	5.0
Gases	Etch	C_4F_8	(sccm)	0	35
		SF_6	(sccm)	130	90
	Pass	C_4F_8	(sccm)	85	190
		SF_6	(sccm)	0	0
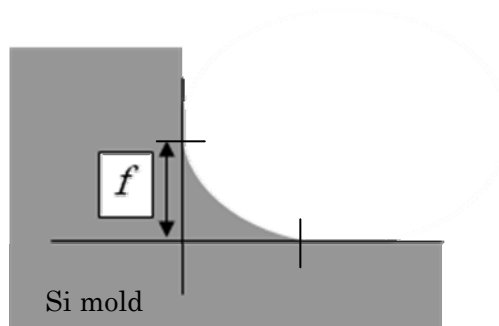
Fig. 2.4: Definition of vertical-size difference f between ideal vertical shape and the actual shape in Si mold.

2.3.2 Results and discussion

Figure 2.5 shows dependence of vertical-sides difference f on height of Si pattern. In case of conventional Deep-RIE type, the f was larger than 1 µm at pattern higher than 17 µm, and the f was linearly increased with increasing pattern height. Cross-sectional SEM image of bottom edge shape (pattern height: 27 µm) is shown in Figure 2.6 (a). In small scallop type, the value of f was clearly smaller than that in conventional type at same pattern height. Cross-sectional SEM image of the edge shape (pattern height: 19 µm) is shown in Figure 2.6 (b). The f was smaller than 0.5 µm at the pattern height of 19 µm. On the other hand, the sidewall was tapered to be a trapezoidal shape with taper angle of about 5 °. It is because that the resist near the edge was faceted and gradually worn off during the Deep-RIE process [8]. The taper is advantageous for demolding; on the other hand, the taper can be prevented by making the resist thicker.
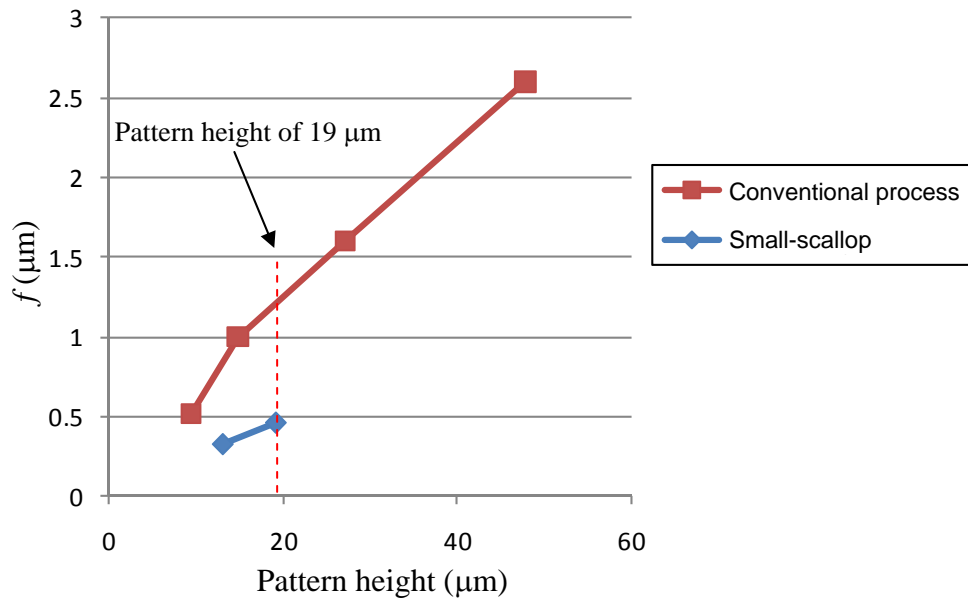
Fig. 2.5: Dependence of vertical-sides difference f on height of Si pattern.
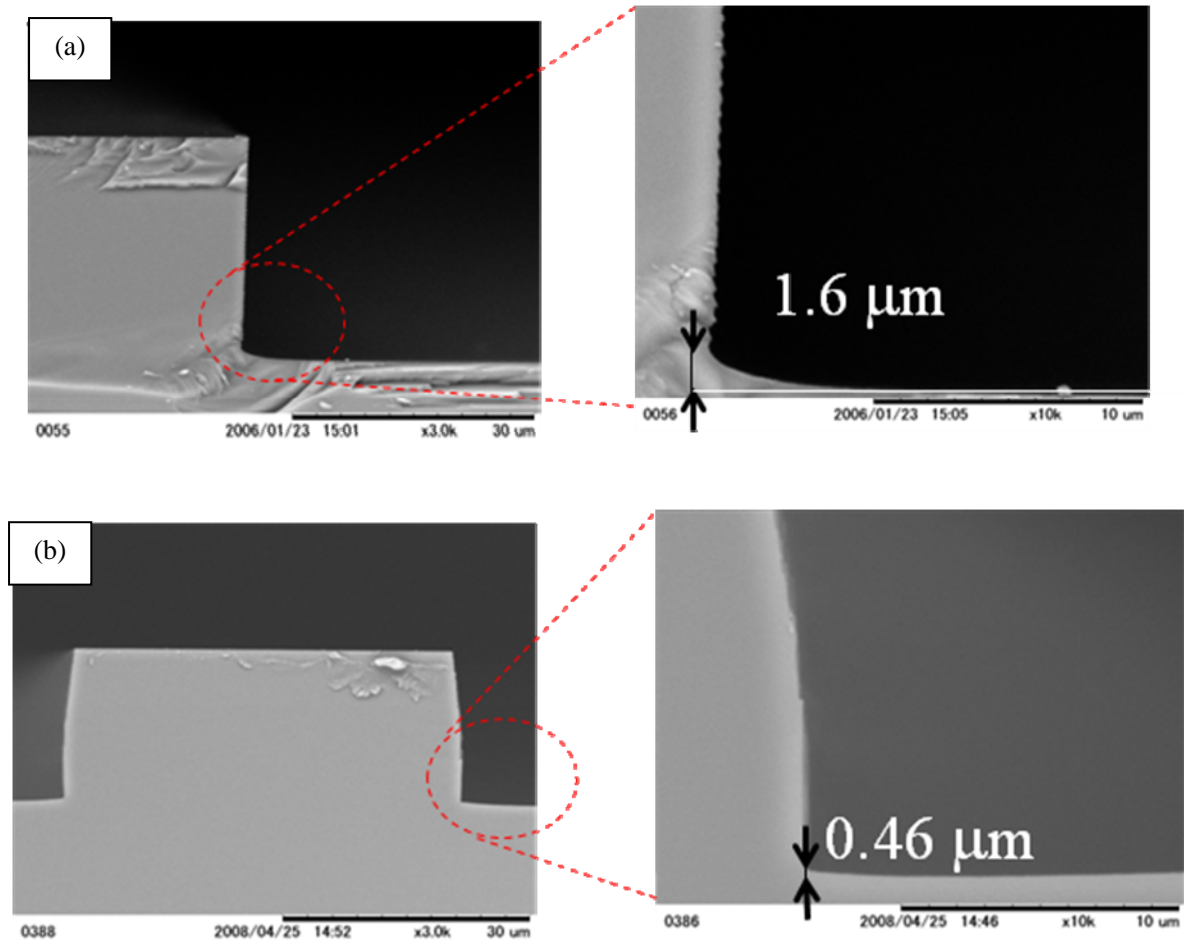
Fig. 2.6: Cross-sectional SEM images of bottom edge and its value of vertical-size difference between ideal vertical shape and the actual shape *f*. The Si mold was fabricated with Deep-RIE conditions of (a) conventional type (pattern height: 27 µm) and (b) small-scallop type (pattern height: 19 µm).

2.3 High precision hot embossing

2.3.1 Concept of high precision hot embossing

Typical hot embossing process is shown in Figure 2.7. The mold and plastic substrate are heated up to molding temperature higher than glass transition temperature T_g of the plastic (Figure 2.7 (a)). Embossing pressure P_h is applied at a constant temperature T_h (Figure 2.7 (b)). The mold and plastic are cooled holding the embossing pressure (Figure 2.7 (c)). After that, the mold and plastic are released at a temperature T_d (Figure 2.7 (d)).

To decide hot embossing parameters, temperature characteristics of viscoelastic properties, storage modulus G′, loss modulus G″ and *Tan δ* of the plastic are often considered. *Tan δ* is defined as

$$Tan\ \delta = G''/G'. \tag{2.1}$$

G′ and G″ are components of complex elastic modulus G*:

$$G* = G' + iG'' \tag{2.2}$$

G′ and G″ correspond elastic element and viscous element of the plastic, respectively. These properties are decided by using dynamic mechanical analysis (DMA). Figure 2.8 shows examples of visco-elastic properties of poly-methylmethacrylate (PMMA) [9]. The states categorize three parts:

(1) Glassy state (< T_g): The polymer chains are locked. The G′ is large and stable.

(2) Glass transition (around T_g): The polymer chain segments start to move. The G′ is decreased with increasing temperature. The G″ and *Tan δ* have peaks in this part.

(3) Rubbery state (> T_g): The polymer chain segments are free to move while-wide range molecular movement is small. The G′ and G″ are decreased with increasing temperature.

At much higher temperature 200 °C, the polymer changes melting state. In hot embossing process, the glass transition or rubbery state are used while the melting state is used in injection molding.

From the DMA results, the T_g is defined by G′onset, G″ peak, or *Tan δ* peak [10]. G′ can be indicator to decide T_h and P_h [11].

The demolding temperature T_d is an important parameter for precise hot embossing. Ng et al. decided the T_d to be T_h- 10 ^{o}C for T_h of 120 ^{o}C and 130 ^{o}C in PMMA hot embossing from the reason that the embossed depth could reach maximum at the T_d [12]. On the other hand, since the T_d higher than T_g causes large destruction of the embossed pattern in demolding process, a T_d lower than T_g is often selected. Yi et al. automatically demolded Ni mold and cyclo-olefin polymer (COP) substrate by tangential force originated from the difference in the thermal expansion coefficient of the mold and the COP [13]. The temperature at the mold was kept higher than that at the COP to generate the tangential force. Peng et al. showed that T_d was an important factor to reduce the surface roughness of the embossed substrate [14]. Song et al.
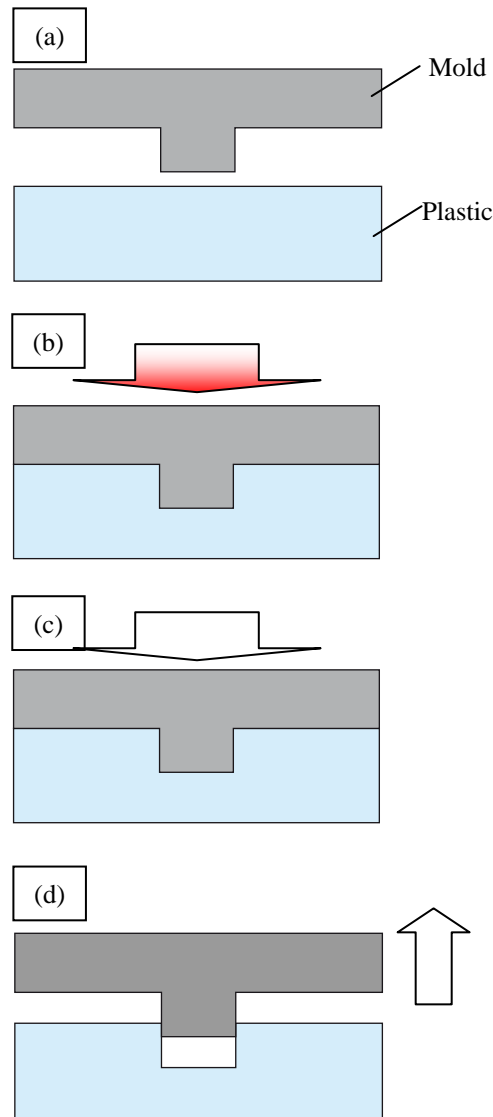
Fig. 2.7: Schematic diagram of hot embossing process; (a) heating mold and plastic, (b) pressing mold and holding, (c) cooling and holding, and (d) demolding.

optimized the T_d using the finite element analysis [15]. At $T_d = 70\ ^{\circ}$C, the local stress of a PMMA pattern in demolding process showed minimum value. However, research on the burr and damage of structures during demolding process has not been conducted.

The plastic is being deformed by thermal stress during cooling/holding process (Figure 2.7 (c)) even at glassy state. Two types of the deformation can be categorized: elastic/plastic deformation[‡], and viscous deformation[§]. During cooling/holding process, the thermal stress is released as permanent destruction of the pattern in elastic/plastic deformation type. The thermal stress is expected to be absorbed in the material in viscous deformation type, while the pattern is easily deformed by external force for demolding. Since elastic/plastic and viscous deformations correspond to G′ and G′′ in visco-elastic properties, $Tan\ \delta$ indicates which deformations are dominant at a temperature. The transition point from viscous to plastic/elastic deformation corresponds to rising edge of the $Tan\ \delta$ curve at glassy state around 80 $^{\circ}$C as shown in Figure 2.9 [17]. In this work, the optimized T_d is suggested for the transition point because the influences of both the thermal stress and the external demolding force are reduced around that point. The author optimizes the T_d by measuring the burr height and width of the embossed patterns.
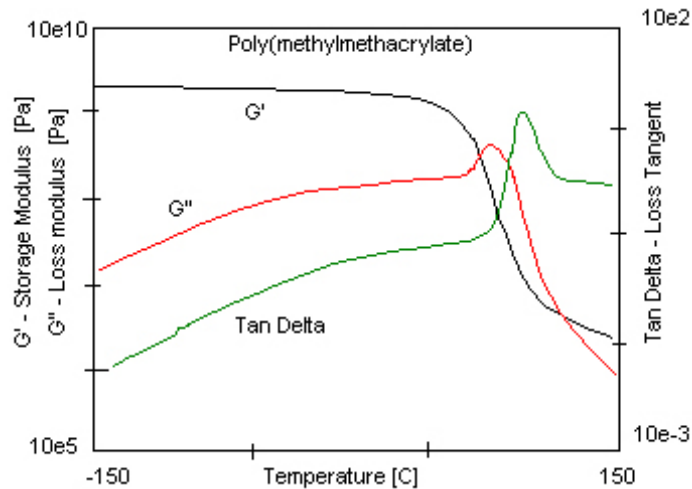
Fig. 2.8: Examples of visco-elastic properties of PMMA [9].

[‡]Elastic deformation is a change in shape of a material at low stress that is recoverable after removal of the stress. When the stress is sufficient to permanently deform the material, the deformation is called plastic deformation [16].
[§]Viscous deformation is an unrecoverable change in shape of a material after applied a stress.
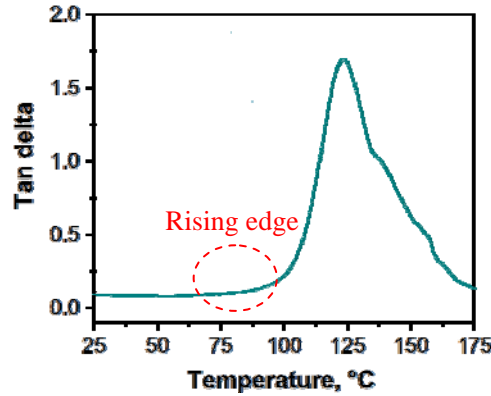
Fig. 2.9: Example of temperature dependence of *Tan δ* of PMMA (extracted from Ref. [17]).

2.3.2 Experimental procedure

Optimization of demolding temperature

The microchannel pattern to examine the demolding temperature is designed in Figure 2.10. The microchannel is 50 μm wide and 19 μm deep. It has two 50 μm-wide, 100 μm-long, and ~4 μm-gap dams [2]. Two microchannel patterns (types I and II) are evaluated.

Sample preparation is described below. Firstly, Si mold was fabricated by Deep-RIE. The Deep-RIE condition was selected for small-scallop type described in Section 2.2. A mold lubricant (EGC-1720 from Sumitomo 3M, Ltd.) was coated over the surface of the mold for easy demolding. The microchannel region was formed on a PMMA plate (Comoglass from Kuraray Co., Ltd.) by using the hot embossing equipment (EVG520HE from EV Group Co.). The PMMA plate is $20 \times 40 \times 1$ mm^3. Typical embossing conditions were P_h = 2.4 MPa and T_h = 125 $^{\circ}$C. Various T_d were tested at 75 $^{\circ}$C, 78 $^{\circ}$C, 80 $^{\circ}$C, 82 $^{\circ}$C, 84 $^{\circ}$C, 86 $^{\circ}$C and 88 $^{\circ}$C.

Eight points of edge profiles in an embossed plate were observed by a laser microscope (VK-8510 from KEYENCE Co.). These measured points are two edges in each dam structure (dams 1 and 2) and two edges in channel structures (channels 1 and 2) as shown in Figure 2.11 (a). The edge heights were defined as shown in Figure 2.11 (b) and (c). The dent or burr height was measured as the difference from its flat surface level. Both types I and II were measured at edge heights and widths of dams 1 and 2. In addition, type I was measured at edge heights and width of channel 1, while type II was measured at those of channel 2. These sizes were compared to the mold. It is

difficult to observe the bottom edge shape in the mold precisely due to the limitation of the laser microscope measurement. Thus, poly-dimethylsiloxane (PDMS) replica directly transferred from the mold was substituted for the mold.
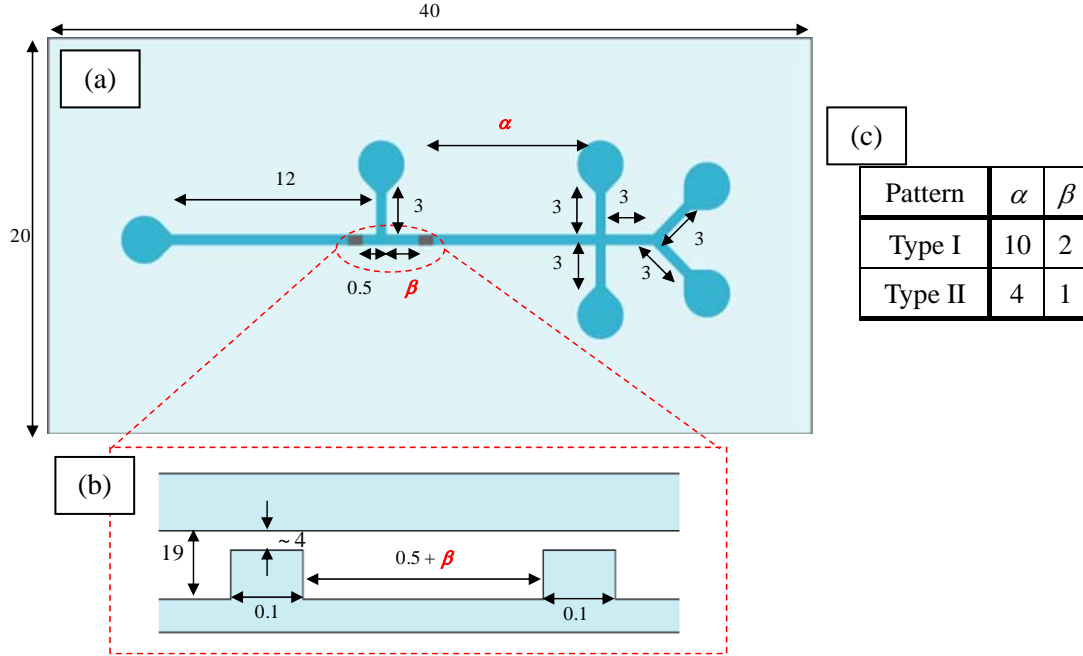
Fig. 2.10: Design of the microchannel pattern for evaluation of demolding temperature (unit: μm). (a) Whole design, (b) cross section of two dams (image after bonding with lid) and (c) differences between two patterns (types I and II).
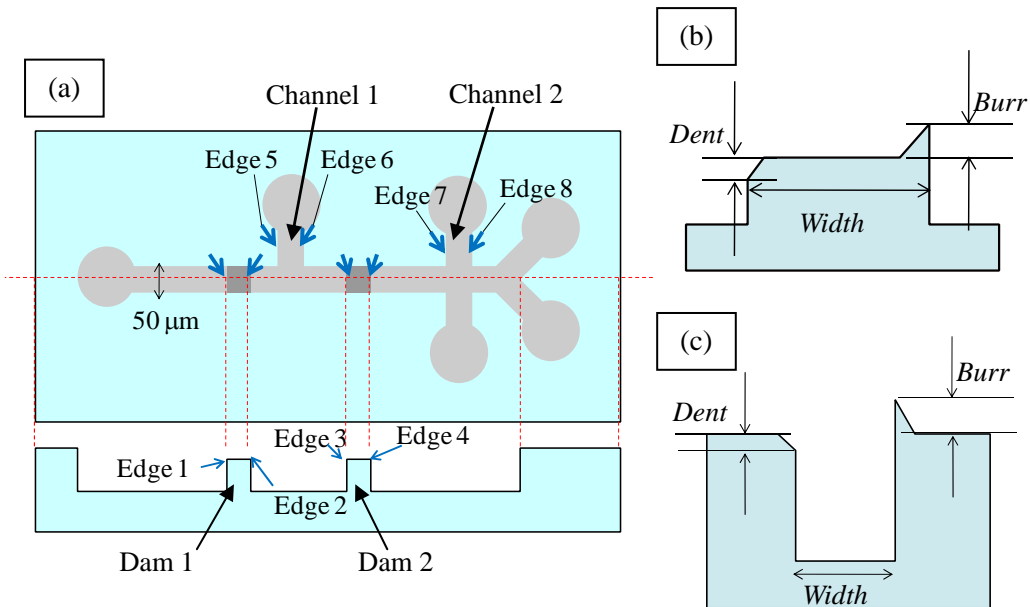
Fig. 2.11: (a) Measured points of edge profiles as indicated blue arrows, and definition of edge height in (b) dams and (c) channel structures.

Application for other patterns

  The optimized demolding conditions were applied for other two 3D microstructure fabrications. One is 5 μm-deep microchannel pattern [3] and the other is double-deck microchannel-array pattern with 300 μm-wide and 85 μm-deep channels, and 6 μm-wide and 5 μm-deep microchannels [1]. The embossed patterns were observed by SEM.

2.3.3 Results and discussion

Optimization of demolding temperature

  Figures 2.12 and 2.13 show size differences with embossed samples and PDMS replica at the various demolding temperatures. Profiles of dam structures of PDMS replica and embossed samples at T_d = 80 ^{o}C and 78 ^{o}C are shown in Figure 2.14. The differences were minimized to be less than 1 μm under the demolding temperature T_d of 80 ^{o}C. Since the surface viscosity at the T_d higher than 82 ^{o}C was large, the pattern edge could be stretched along the demolded direction. On the other hand, at the T_d lower than 78 ^{o}C, the pattern was damaged by thermal stress originated from plastic/elastic deformation. At the T_d of 75 ^{o}C, the mold was often released spontaneously from the embossed plate. This result indicates that the thermal internal stress was relaxed by plastic/elastic deformation during the cooling from 78 ^{o}C to 75 ^{o}C. However, the differences of type II at T_d = 75 ^{o}C were smaller than those of type I. These results indicate that the magnitude of the damage by the plastic/elastic deformation depends on pattern sizes and areas.
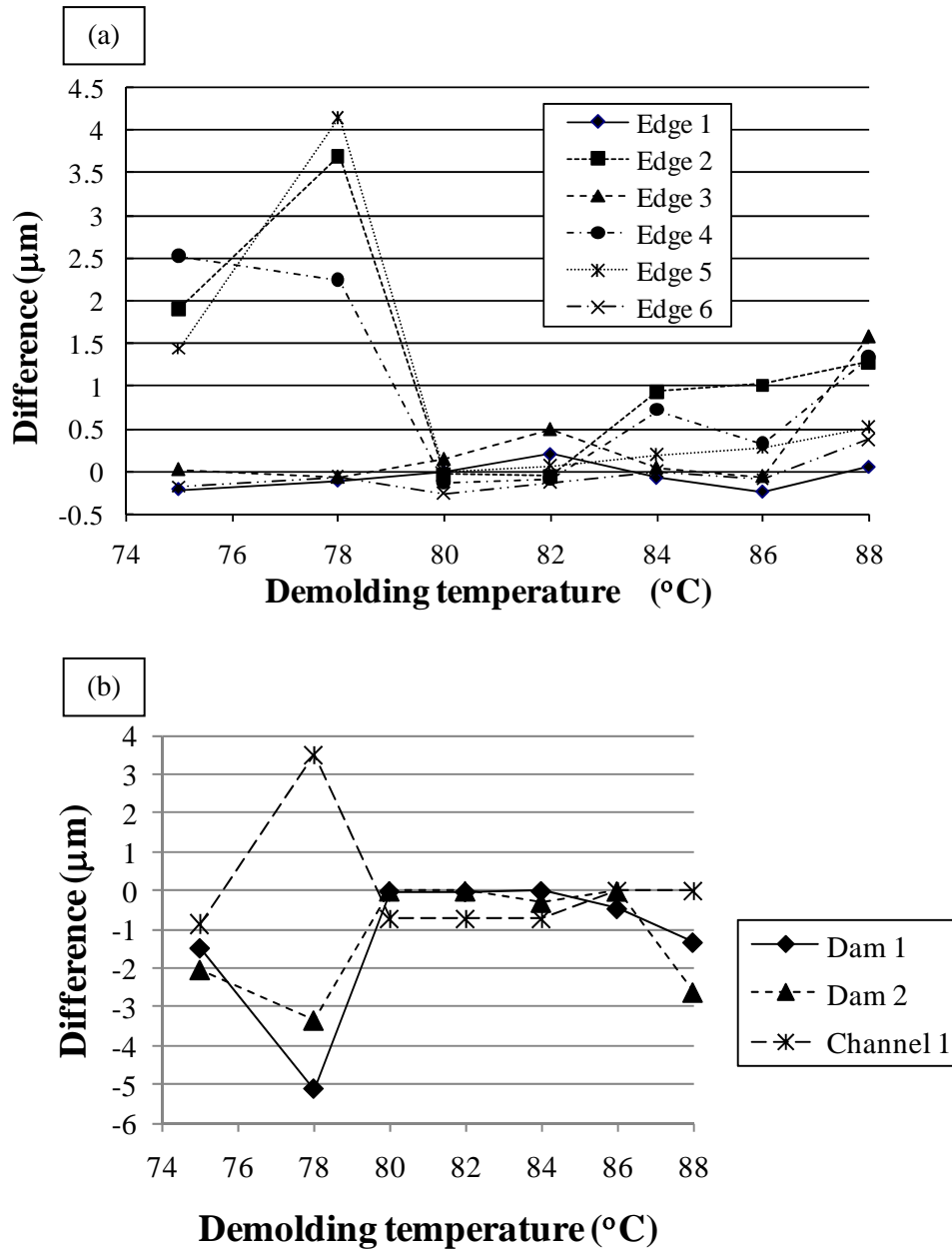
Fig. 2.12: Size differences of type I and PDMS replica at various demolding temperature: (a) difference of edge height and (b) difference of pattern width.
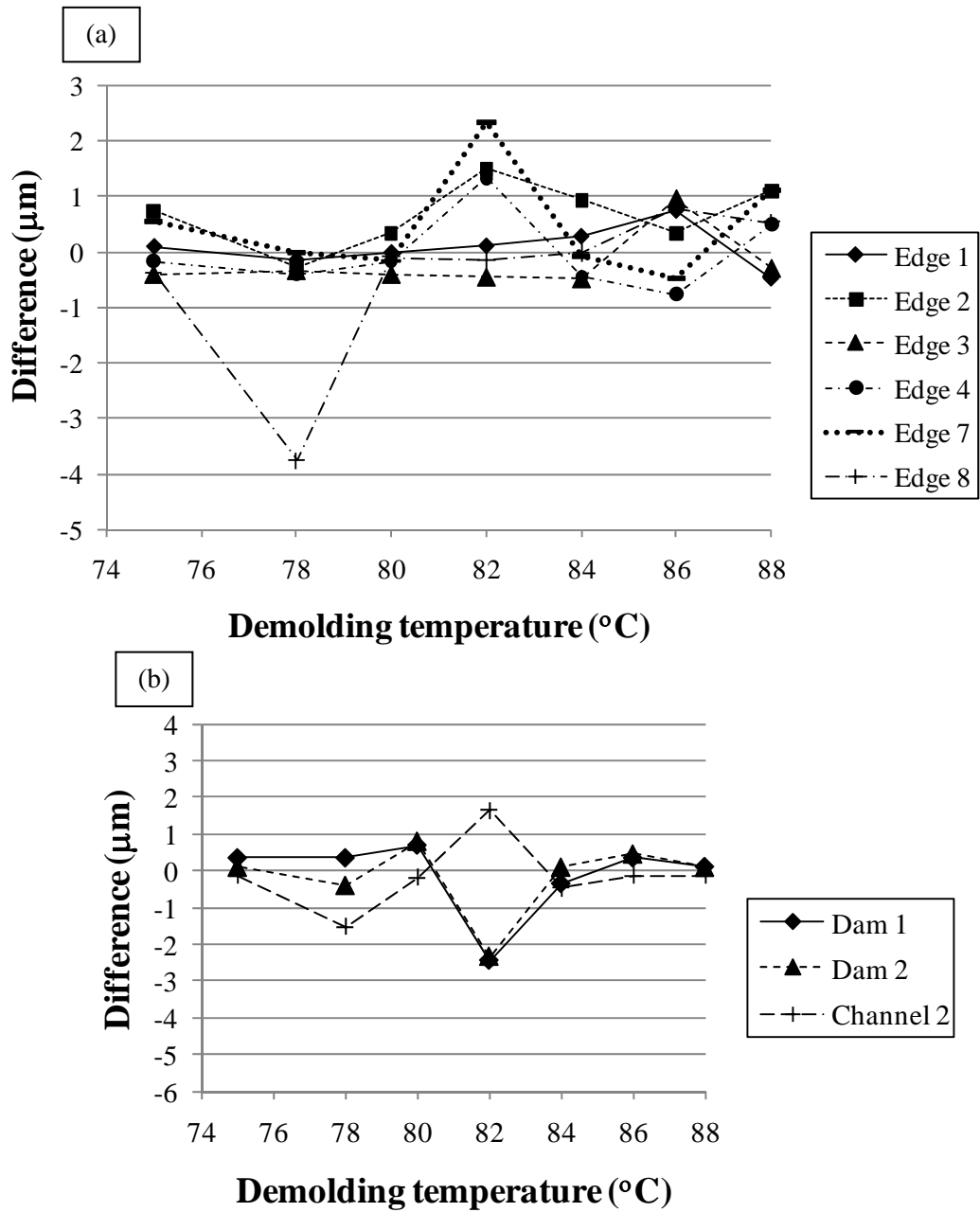
Fig. 2.13: Size differences of type II and PDMS replica at various demolding temperature: (a) difference of edge height and (b) difference of pattern width.
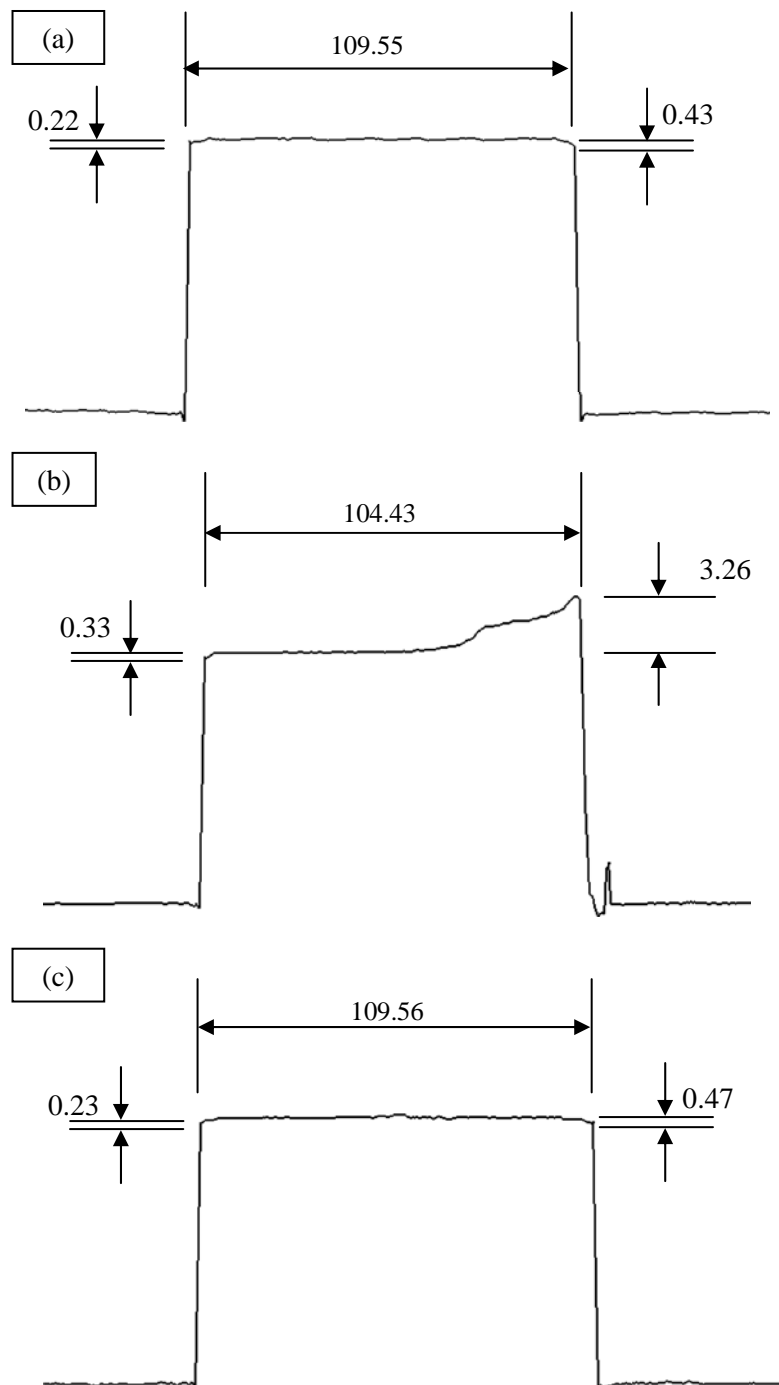
Fig. 2.14: Profiles of dam structures in type I (dam 1 in Fig 2.10 (a)) and their sizes (unit: μm); (a) PDMS replica, and embossed patterns demolded at (b) 78 °C and (c) 80 °C.

Application for other patterns

The obtained demolding conditions were applied for other two 3D microstructure fabrications. Figure 2.15 shows SEM images of embossed shallow microchannel pattern (depth: 5 μm) on PMMA. Pattern failure was not observed at demolding temperature T_d of 80 °C while it was observed at the T_d of 75 °C. Figure 2.16 shows SEM images of microchannel pattern arrayed on PMMA. The microchannel array was successfully formed at the T_d of 80 °C while that was deformed at the T_d of 75 °C. These results indicate that the optimized demolding conditions are applicable for fabrication of other fine micropatterns.
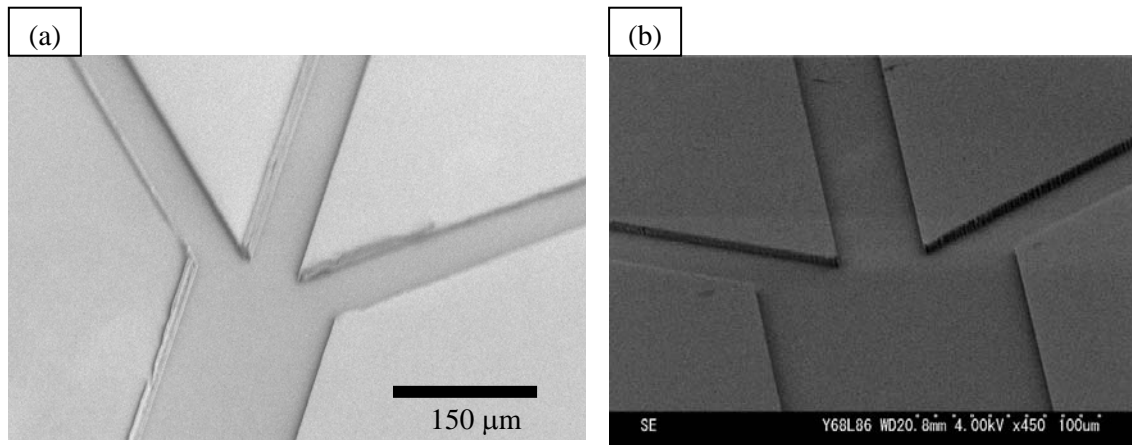
Fig. 2.15: SEM images of embossed microchannel pattern (depth: 5 μm) on PMMA plate demolded at (a) 75 °C and (b) 80 °C [3].
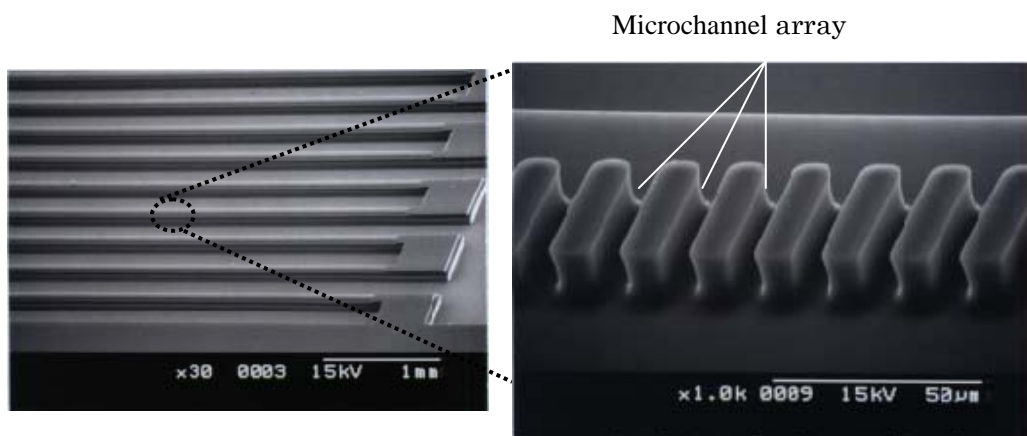
Fig. 2.16: SEM images of embossed microchannel array pattern on PMMA plate demolded at 80 °C [1].

2.4 Conclusion

Flat embossed surface which is required for successive low-temperature bonding was realized by optimization of mold structure and demolding conditions.

The shape of the bottom edge of Si mold fabricated by conventional Deep-RIE was roundly sloped. The depth difference between the bottom edge and flat surface were approximately 1.6 µm in the case of 30 µm etching depth. Etching condition to realize smaller scallops of Deep-RIE was chosen to decrease the slope at the bottom edge making less than 0.5 µm.

In hot embossing process, a Si mold with 19 µm-height and 50 µm-wide channel pattern was used. PMMA plate was used as the substrate. The failures were characterized by measuring the burr height of the patterns. The failures were minimized to be less than 1 µm under the demolding temperature of 80 $^{\circ}$C.

This is a new finding to optimize the edge profile on embossed pattern evaluating the relationship between demolding temperature and the pattern failure. By combining low-temperature bonding method, this hot embossing method can be applied for actual plastic-MEMS devices with fine micro/nanostructures.

References

[1]   J. Mizuno, H. Shinohara, M. Ishizuka, T. Suzuki, G. Tazaki, Y. Kirita, T. Nishi, S. Shoji, PMMA micro-channel array for blood analysis fabricated by hot embossing, Proc. The 9th Int. Conf. Miniaturized Sys. Chem. Life Sci. (Micro-TAS), (2005) 1340-1342.

[2]   H. Shinohara, J. Mizuno, F. Kitagawa, K. Otsuka, S. Shoji, Fabrication of highly dimension controlled PMMA microchip by hot embossing and low temperature direct bonding, Proc. The 10th Int. Conf. Miniaturized Sys. Chem. Life Sci. (Micro-TAS), (2006) 158-160.

[3]   H. Shinohara, J. Mizuno, S. Shoji, Low temperature direct bonding of poly(methyl methacrylate) for polymer microchips, IEEJ Trans. Electr. Electron. Eng. **2** (2007) 301-306.

[4]   H. Shinohara, J. Mizuno, S. Shoji, Precise structure controlled plastic hot embossing method for low-temperature direct bonding, Int. Conf. Electron. Packaging (ICEP), (2010) (accepted).

[5]   H. Shinohara, J. Mizuno, S. Shoji, Fabrication of a microchannel device by hot embossing and direct bonding of poly(methyl methacrylate), Jpn. J. Appl. Phys. **46** (2007) 3661-3664.

[6]   B. Volland, F. Shi, P. Hudek, H. Heerlein, I. W. Rangelow, Dry etching with gas chopping without rippled sidewalls, J. Vac. Sci. Tech. B **17** (1999) 2768-2771.

[7]   Shoji Lab. (Waseda Univ.) Tech. Rep. (April 1, 2005) (in Japanese).

[8]   M. Madou, Fundamentals of microfabrication, CRC Press, 1997.

[9]   http://www.rheosci.co.jp/apps/b01.html   (accessed   on   October   2009)   (in Japanese)

[10] Homepage of TA instruments (in Japanese):
     http://www.tainstruments.co.jp/products/dma.html (accessed on October 2009)

[11] Y. Hirai, T. Yoshikawa, N. Takagi, S. Yoshida, Mechanical properties of poly-methyl methacrylate (PMMA) for nano imprint lithography, J. Photopolym. Sci. Tech. **16** (2003) 615-620.

[12] S. H. Ng, R. T. Tjeung, Z. Wang, Hot embossing on polymethyl methacrylate, Proc. Electronics Packaging Technology Conference (EPTC), (2006) 615-621.

[13] L. Yi, W. Xiaodong, Y. Fan, Microfluidic chip made of COP (cyclo-olefin polymer) and comparion to PMMA (polymethylmethacrylate) microfluidic chip, J. Mater. Process. Technol. **208** (2008) 63-68.

[14] B.-Y. Peng, C.-W. Wu, Y.-K. Shen, Y. Lin, Microfluidic chip fabrication using hot embossing and thermal bonding of COP, Polym. Adv. Technol. (2009), doi: 10.1002/pat.1447.

[15] Z. Song, B. H. You, J. Lee, S. Park, Study on demolding temperature in thermal imprint lithography via finite element analysis, Microsyst. Technol. **14** (2008) 1593-1597.

[16] Homepage of NDT Resource Center:
http://www.ndt-ed.org/EducationResources/CommunityCollege/Materials/Structure/deformation.htm (accessed on January 2010)

[17] F. A. Zhang, D.-K. Lee, T. J. Pinnavaia, PMMA–mesocellular foam silica nanocomposites prepared through batch emulsion polymerization and compression molding, Polymer **50** (2009) 4768-4774.

Chapter 3

Low-Temperature Direct Bonding[*]

3.1 Introduction

Many thermal direct bonding methods of plastic plates are carried out at a temperature around or higher than the glass transition temperature T_g [12-15]. When two plastic surfaces come into contact at an atomic scale, interatomic bonds such as hydrogen bonds are formed. In particular, the polymer chains are mobile at a temperature around or higher than the T_g, and effects similar to the welding of polymers occur [12]. Because of the applied pressure and heat during the direct bonding process, deformation of the microchannel was often observed. Thus, smaller pressure and lower bonding temperature should be applied to eliminate the deformation. However, it is difficult to realize strong bonding under the conventional bonding condition. In addition, it is also difficult to fabricate shallow microchannels in which depth is less than several-μm. Submicrometer-scale accuracy of the plastic bonding are required for downsizing and functionalization of the microchannel.

The author proposes novel methods of low-temperature direct bonding using poly-methylmethacrylate (PMMA) and cyclo-olefin polymer (COP) as shown in Figure 3.1. Plastic surface is pretreated before bonding. Examples of typical pretreatment methods are using oxygen plasma, atmospheric-pressure oxygen plasma, UV/O$_3$[†], vacuum UV (VUV) and VUV/O$_3$. To evaluate the pretreated plastics and investigate the bonding mechanisms, surface analyses are carried out (Section 3.5). Prototype PMMA and COP microchips, microchips with shallow microchannel and Au-electrode-embedded microchannel, are fabricated by the methods (Section 3.6).

Firstly, the author describes concept of low-temperature direct bonding and the methods in Sections 3.2 and 3.3. Section 3.4 describes measurement of bond strength of plastics prepared by the low-temperature direct bonding.

---

[*]This chapter is based on the published papers listed in the reference section [1-11].
[†]UV treatment under oxygen atmosphere

Force, Heat

Lid　　Channel plate

(a)　　　　　　　　　　(b)
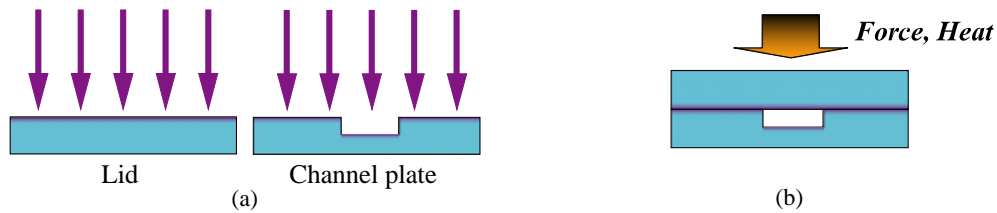
Fig. 3.1: Low-temperature direct bonding process: (a) surface pretreatment and (b) direct bonding.

3.2 Concept of low-temperature direct bonding

3.2.1 Surface pretreatment

The effects of surface pretreatment on direct bonding are illustrated in Figure 3.2.

In general, polar functional groups such as -OH (hydroxyl groups), -C-O (carbon single bond with oxygen atom), -C=O (carbonyl groups), and -O-C=O (carboxylic acids or esters) are increased or generated on plastic surface after oxygen plasma treatment [16-23] or UV irradiation [23-33]. The polar groups increase dipolar interactions between two treated plates such as -OH···OH (hydrogen bond) and -C=O···C=O as shown in Figure 3.3 (a).

High energy plasma species or UV photons cause main or side chain cleavage of the polymer. Since this chain cleavage causes degradation of the plastic, the T_g on the treated surface is decreased [23,29,34]. The degraded layer is called low-T_g layer in this chapter. The low-T_g layer acts as an adhesion for the direct bonding; the layer is diffusion-bonded to each other as shown in Figure 3.3 (c).

R, R': hydrocarbon group

(a)　　　　　　　　　　(b)
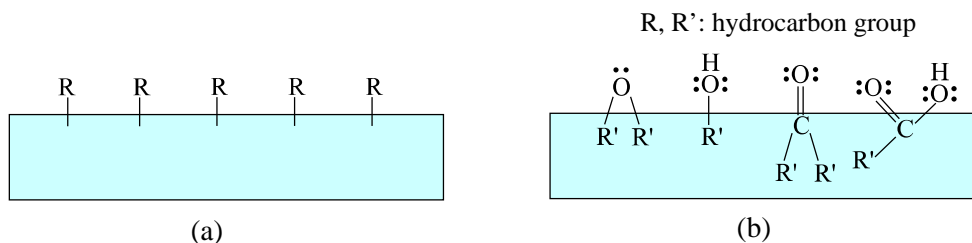
Fig. 3.2: Possible surface chemical structures of plastic: (a) untreated and (b) treated by oxygen plasma or UV light.
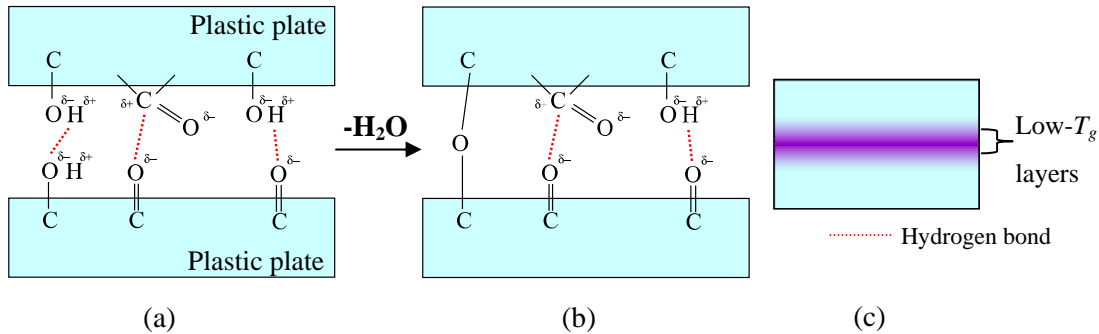
Fig. 3.3: Effects of surface pretreatment on direct bonding: bonding by dipolar interactions (a) at room temperature and (b) after annealing; (c) diffusion bonding by low- T_g layers.

It is important for low-temperature direct bonding to reduce geometric damage to the surface after the pretreatment. Features of surface pretreatments of oxygen plasma, atmospheric-pressure plasma, UV/O_3, VUV and VUV/O_3 for low geometric damage are described below.

Oxygen plasma

Oxygen plasma treatment in this thesis is defined as a treatment by oxygen plasma generated in a vacuum chamber. Isotropic oxygen plasma is used to reduce geometric damage to the surface.

Atmospheric-pressure plasma

Atmospheric-pressure plasma treatment in this thesis is defined as a treatment by oxygen plasma under atmospheric pressure. High density active plasma is expelled from a nozzle. Since the region between the nozzle and the sample is not electrically-biased, the geometric damage after atmospheric-pressure plasma treatment is smaller than that after conventional plasma treatment.

UV/O_3

UV/O_3 treatment is defined as a treatment by UV irradiation in the presence of oxygen. The low-pressure UV lamp radiates 185 nm and 254 nm lights. In the presence of O_2, the 185-nm UV is absorbed by O_2 to generate the atomic species in ground state $O(^3P)$. $O(^3P)$ can react with O_2 to form O_3. If this O_3 absorbs the 254-nm UV, excited oxygen atoms $O(^1D)$ with 190 kJ/mol excitation energy are generated [35]. These O_3,

O(^{1}D), and the VUV light reaching on the sample play an important role on surface treatment. This treatment method is widely used for surface cleaning/activation of various kinds of inorganic materials with low geometric damage [36-38].

VUV and VUV/O$_3$

VUV light is irradiated from a dielectric-barrier discharge excimer lamp filled with Xe gas. Central wavelength of the VUV light is 172 nm.

VUV treatment in this thesis is defined as a treatment only by VUV light irradiation. Since photon energy of VUV light is larger than that of conventional UV light, dissociation of polymer chemical bonds (e.g. C-C, C-H) by direct VUV irradiation is more effective than that by conventional UV irradiation.

VUV/O$_3$ treatment is defined as a treatment by VUV light irradiation in the presence of oxygen. The VUV generates not only O$_3$ and O(^{1}D) in the same manner as the 185-nm and 254-nm UV lights, but is also absorbed directly by O$_2$ in the chamber to generate O(^{1}D) [39]. Since absorption coefficient of O$_2$ at the 172-nm UV light are approximately 20 times greater than that at the 185-nm [40], the generation efficiency of O(^{1}D) by VUV/O$_3$ treatment is better than that by UV/O$_3$. The VUV light intensity reached on the sample surface is controllable by the oxygen pressure p and distance between the VUV-light window and the sample surface d (refer to Chapter 4).

3.2.2 Thermal annealing

Thermal annealing is required during or after direct bonding for achieving high-yield. Expected effect of thermal annealing during or after direct bonding process were described below. Some hydrogen bonds in Figure 3.3 (a) are expected to change to covalent bonds (-C-O-C-) by dehydration during thermal annealing as shown in Figure 3.3 (b). At the bonded interface, local elastic/plastic deformation at elevated temperature is easier than that at room temperature. The deformation is expected to increase real contact area. Even lower than T_g, surface viscosity is increased with increasing temperature. The increase in viscosity increases surface adhesion force.

3.3 Surface pretreatment and bonding methods

3.3.1 Surface pretreatment methods

Surface pretreatment conditions in this chapter are listed in Table 3.1.

Oxygen plasma was generated in a plasma-activated bonding system (EVG810LT from EV Group Co.) [41,42] with parallel electrodes in the vacuum chamber. The radiofrequency of 397 kHz used in this system is lower than that of other conventional plasma treatment systems of 13.56 MHz. This chamber is designed to reduce potential surface etching effect during the plasma irradiation [42].

Atmospheric-pressure plasma was generated by plasma cleaning unit (Aiplasma from Panasonic Electric Works, Ltd.) [19] supplying mixed gas consisted of 98 % Ar and 2 % O_2. The unit used dielectric-barrier discharge [43] as the plasma source.

UV/O_3 treatment was performed in cleaning equipment (NL-UV253 from Nippon Laser & Electronics Lab.) with three low-pressure UV lamps.

Equipment for VUV and VUV/O_3 treatments (UER20-172 from Ushio Inc.) is shown in Figure 3.4 [44]. The specifications of the lamp are a central wavelength of 172 nm, the irradiance of 10 mW/cm^2 and the full width at half maximum of 14 nm [45]. For VUV treatment, nitrogen gas was firstly introduced into the chamber to reduce density of oxygen gas, and then the gases were evacuated. The evacuation continued during the VUV irradiation. For VUV/O_3 treatment, oxygen gas was introduced into the chamber to setup pressure p after evacuation. The chamber was not evacuated during the VUV irradiation.

Table 3.1: Surface pretreatment conditions for low-temperature bonding.

Treatment type	P (W)	p (Pa)	t (sec)	d (mm)
Oxygen plasma	100 - 200	40 - 80 (O_2-rich)	30	-
Atmospheric-pressure plasma	80	1.0×10^5	0.6	-
UV/O_3	-	1.0×10^5 (O_2-rich)	1200	-
VUV	-	$< 6.0 \times 10^3$ (N_2-rich)	30	12
VUV/O_3	-	3.0×10^4 - 5.0×10^4 (O_2-rich)	600 - 1800	12

P: plasma power, p: chamber pressure, t: treatment time, d: distance between VUV-lamp window and sample surface
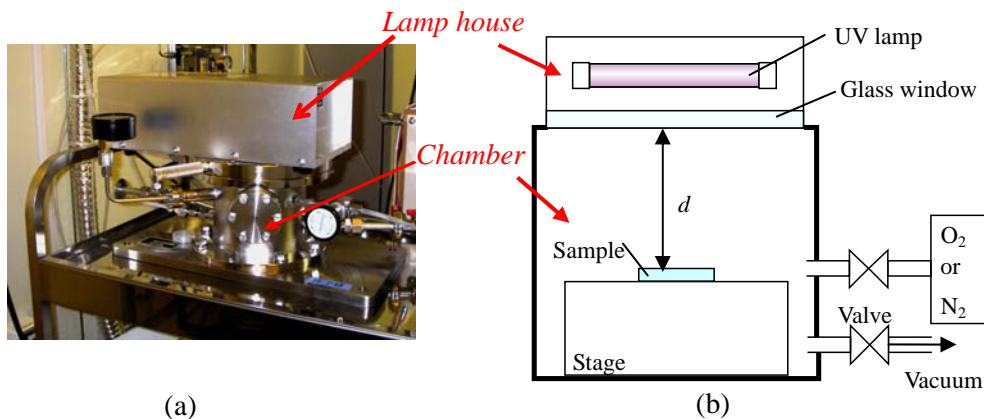
Fig. 3.4: VUV-irradiation equipment: (a) whole view and (b) schematic diagram [44].

3.3.2 Direct bonding methods

After pretreatment, the two plates were exposed to the atmosphere. To minimize airborne molecular contamination, the plates were introduced into the bonding equipment within 10 min since the surface was pretreated. These plates were bonded to each other using a hot embossing system (EVG520HE from EVG Co.) at atmospheric pressure. The equipment ensures the high uniformity of pressure and temperature to within ±1%. Top and bottom side heaters are equipped and temperature can be controlled independently. In this bonding process, both heaters were set a same temperature of lower than T_g. A pressure was applied to the sample and holding for a set time. In this thesis, the set temperature and time are defined as annealing temperature and annealing time, respectively. On the other hand, some of the samples bonded at room temperature were thermally annealed on a hot plate.

3.4 Measurement of bond strength

3.4.1 Experimental procedure

Bare PMMA or COP plates were used. These surfaces of the plates were pretreated and bonded with abovementioned methods described in subsections 3.3.1. and 3.3.2.

Figure 3.5 shows tensile test equipment (MODEL 1307 from Aikoh Engineering Co, Ltd.) for evaluating bond strength. The bonded sample was glued with stainless plates by epoxy adhesive (Araldite from Vantico Ltd.), and pulled perpendicularly by

the equipment.

Figure 3.6 shows schematic diagram of razor blade method for investigation of thermal annealing effect after COP room temperature bonding. A razor is parallelly inserted into the interface between two plates. Surface energy between two plates (γ) can be written as [46]

$$\gamma = 3Ex^3y^2 \,/\, (32L^4), \tag{3.1}$$

where E is modulus of elasticity, x is thickness of the substrate, $2y$ is thickness of the razor blade, and L is crack length.
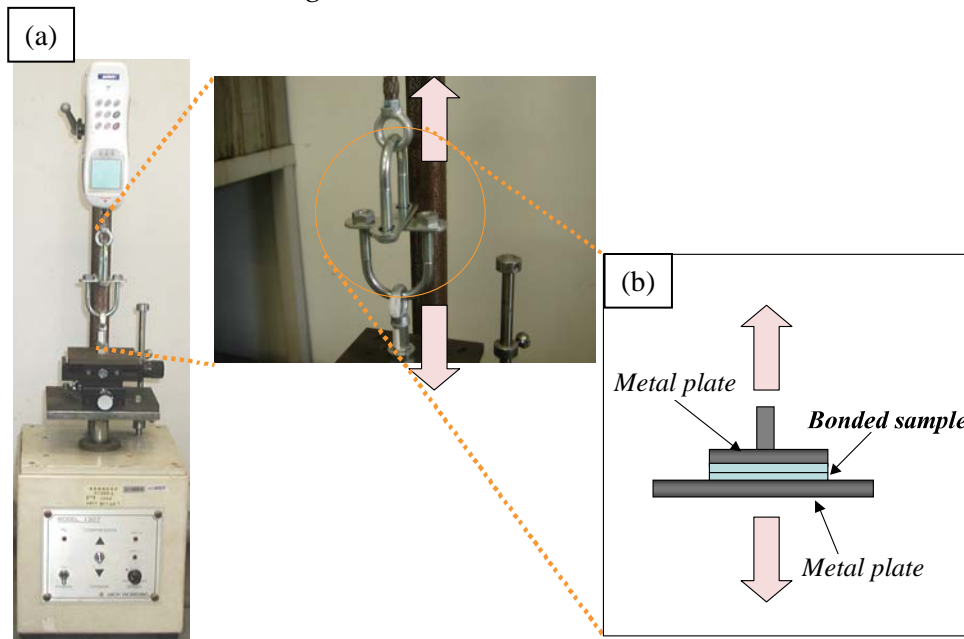
Fig. 3.5: Tensile test for evaluating bond strength; (a) photograph of the tensile test equipment and (b) principle of the tensile test [6].
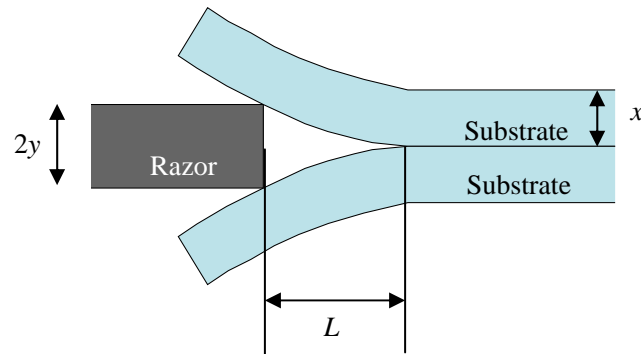
Fig. 3.6: Schematic diagram of razor blade method for the evaluation of bond strength [46].

Commercially available PMMA or COP plates were used for these tests. Table 3.2 shows trade names of these plastic plates, their thickness and thermal properties. In general, plastic properties are slightly different from each other depending on their preparation methods, average molecular weights, and additive agents.

Table 3.2: PMMA and COP plates used for bond strength measurements.

Common name	Trade name	Manufacturer	Thickness (mm)	Deflection temperature under load (^{o}C)	Vicat softening point (^{o}C)	T_g (^{o}C)
PMMA	Acrylite E-IR	Mitsubishi Rayon Co., Ltd.	1	90 [47]	-	-
PMMA	Comoglass	Kuraray Co., Ltd.	1	92 [48]	104 [48]	-
PMMA	Technolloy S001	Sumitomo Chemical Co., Ltd.	0.25	-	-	107 [49]
COP	Zeonex 480	Zeon Co.	1	123 [46]	-	138 [50]

3.4.2 Experimental results

Bond strength between two PMMA plates (Acrylite E-IR) is shown in Figure 3.7. In this figure, red broken lines indicate the values for direct bonding at temperature of 95 $^{\circ}$C, applied pressure of 1.25 MPa and annealing time of 25 min, without any pretreatments [51]. The bond strengths of the samples using pretreatment were same or stronger than that of the sample without pretreatment.

Among three bonding parameters of annealing temperature, applied pressure and annealing time, long annealing time or high annealing temperature is effective to increase the chemical reactions at the bonding interface. On the other hand, high applied pressure enhances intimate contact between surfaces. Especially after pretreatment of atmospheric-pressure plasma, the bonding became clearly stronger with increasing these bonding parameters. In case of UV/O_3 pretreatment, the bonding is weakest among these four pretreatments. The VUV/O_3-treated bonding is stronger (about 0.9 MPa) in most cases.

Figure 3.8 shows bond strengths between different-type PMMA plates (Comoglass and Technolloy) and between same-type PMMA plates (Comoglass and Comoglass). Oxygen plasma pretreatment at plasma power P of 200 W and chamber pressure p of 80 Pa were used in this case. Bonding stronger than 1 MPa was realized in both cases. This result indicates that the low-temperature direct bonding was also applicable between different-type PMMA plates.

Figure 3.9 shows bond strength between two COP plates. Pretreatments of oxygen plasma at plasma power P of 100 W, chamber pressure p of 40 Pa, VUV, and VUV/O_3 for 10 min were used in this case. The bonding was performed at room temperature with applied pressure of 2.5 MPa for 5 min. Strong bonding (> 1 MPa) was realized by pretreatment and room temperature bonding.

Figure 3.10 shows dependence of the surface energy between two COP plates on annealing temperature after room temperature bonding measured by razor blade method. Oxygen plasma was used in this case. The surface energy was significantly increased with increase in the annealing temperature.
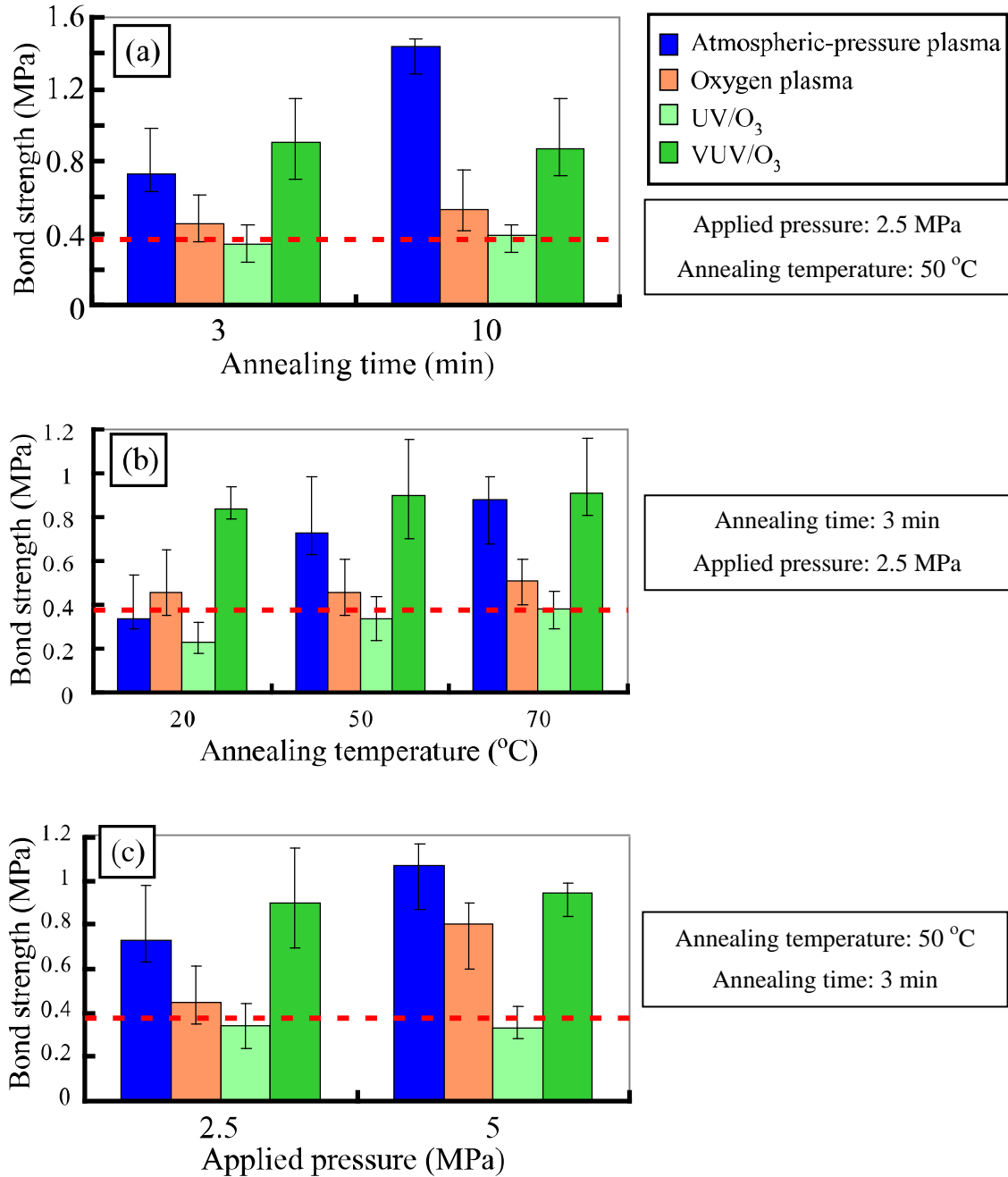
Fig. 3.7: Bond strength between two PMMA plates bonded by pretreatments of atmospheric-pressure plasma, oxygen plasma (P = 200 W, p = 80 Pa), UV/O_3 and VUV/O_3 (p = 5.0 × 10^4 Pa, t = 30 min): (a) dependence of the bond strength on annealing time, (b) dependence of the bond strength on annealing temperature, and (c) dependence of the bond strength on applied pressure [6].
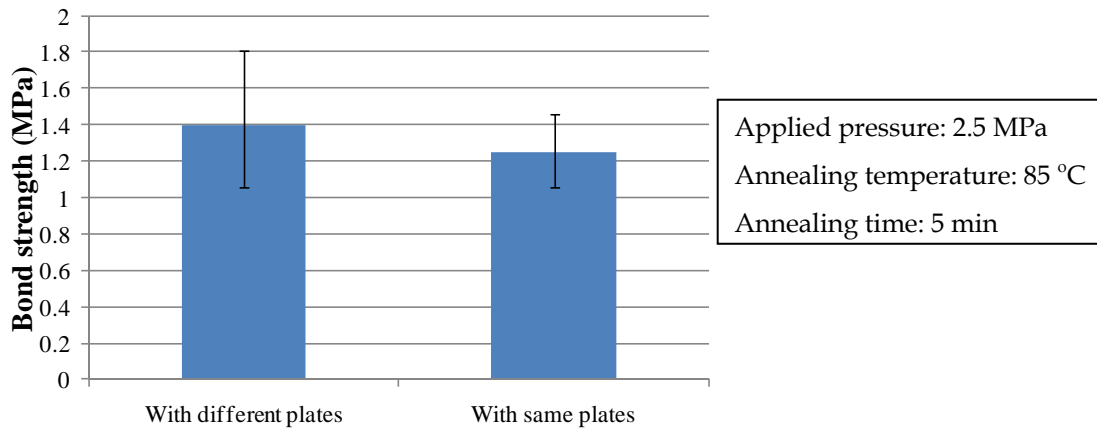
Fig. 3.8: Bond strength of PMMA plates (with different type plates and with same type plates) bonded by pretreatments of oxygen plasma (P = 200 W, p = 80 Pa).
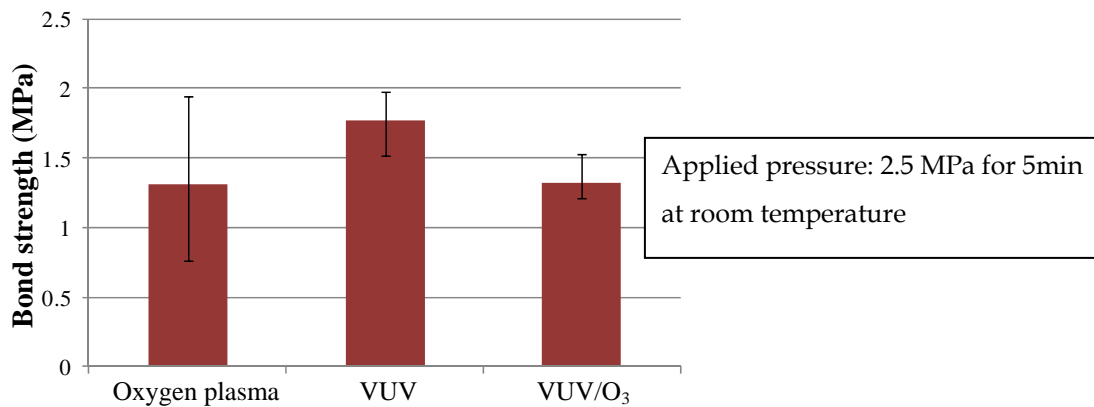
Fig. 3.9: Bond strength between COP plates bonded by pretreatments of oxygen plasma (P = 100 W, p = 40 Pa), VUV (t = 30 sec) and VUV/O$_3$ (p = 5.0 × 10^4 Pa, t = 10 min).
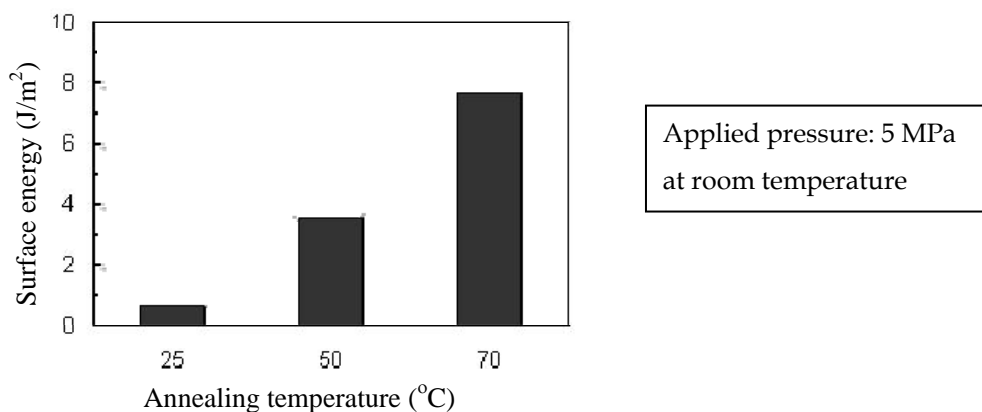
Fig. 3.10: Dependence of surface energy between two COP plates on annealing temperature; the two plates were bonded with the applied pressure of 5 MPa at room temperature [2,3].

3.5 Evaluation of pretreated plastics

3.5.1 Experimental procedure

Bare PMMA or COP plates were used for surface analysis by attenuated total reflection Fourier-transform infrared spectrometer (ATR-FT-IR), contact angle measurements and micro thermal analysis (μ-TA). For X-ray photoelectron spectroscopy (XPS) and near edge X-ray absorption fine structure (NEXAFS) analysis, thin PMMA or COP films were prepared by spin-coating of PMMA/toluene or COP/toluene solutions onto Si wafers. The films were thinner than 150 nm.

ATR-FT-IR measurements (equipment: SpectrumOne from PerkinElmer, Inc.) were performed by using Ge prism. The ATR was single reflection type, and the incident angle was 65 $^{\circ}$.

XPS measurements (equipment: 5400MC from PerkinElmer, Inc.) were performed by using AlKα (1486.6 eV) radiation operating at 150 W (15 kV, 10 mA) to investigate the chemical structure on the surface at shallower point with tens nm than ATR-FT-IR. All

spectra were compensated assuming that the C1s C-C/C-H peak appears at a binding energy of 285.0 eV. The C1s and O1s spectra were decomposed by fitting mixed Gaussian-Lorenzian functions, according to expected chemical assignments [21,28,31,33,52,53].

To confirm results of ATR-FT-IR and XPS, surface free energy γ_s on the sample surface was calculated by measuring contact angles θ of water (H_2O), glycerin ($C_3H_5(OH)_3$), formamide ($HCONH_2$) and diiodomethane (CH_2I_2) on the sample surface. The surface free energy is defined by Owens-Wendt theory [54]:

$$\gamma_s = \gamma_s^p + \gamma_s^d, \tag{3.2}$$

$$\gamma_l = \gamma_l^p + \gamma_l^d, \tag{3.3}$$

$$\gamma_l (1 + \cos \theta) = 2(\gamma_s^p \gamma_l^p)^{0.5} + 2(\gamma_s^d \gamma_l^d)^{0.5}, \tag{3.4}$$

where γ_l is the surface tension of the liquid and the superscripts 'p' and 'd' refer to the polar and dispersive components. When γ_l and γ_l^d are known values, γ_s, γ_s^p and γ_s^d are obtained by measuring θ of more than two different liquids. In our case, the surface energies of samples were calculated using a computer program [55].

NEXAFS analyses on PMMA surface were carried out for supplementation of XPS results. These analyses were performed at the BL12 in the SAGA Light Source (SAGA-LS), Japan. The X-ray incident angle was 90 $^{\circ}$.

For investigation of thermal properties on PMMA surface, μ-TA was measured by combining nano-thermal analysis unit (from Anasys Instruments Corp.) with atomic force microscope (AFM) system (SPM-9600 from Shimadzu Co.) with contact mode. The probe contacted on the sample surface is heating up and the deflection signal of the probe is increased due to thermal expansion. The signal is decreased at the softening or melting point of the surface [56]. The rate of temperature rise of the probe was +5 $^{\circ}$C/sec.

3.5.2 Results and discussion

Increase in polar functional groups

　Figure 3.11 (a) shows ATR-FT-IR spectra of PMMA before and after surface treatments. Figure 3.11 (b) shows these spectra minus the untreated spectrum shown in Figure 3.11 (a). Spectra changes in the VUV and VUV/O_3 treatments suggest that C-O-C/C-C components of main- or side-chain were decreased, while -OH and C=O (ketone or aldehyde components) [26,30] were generated. O-C=O (carboxylic acids or esters) component in the spectrum of VUV/O_3-treated PMMA was also increased. The change of the spectrum of oxygen plasma-treated PMMA was smallest among that of others.

　Figure 3.12 shows ATR-FT-IR spectra of COP. The spectrum of untreated COP suggests that the COP has many cyclopentane rings [57]. Spectra changes in the VUV and VUV/O_3 treatments suggest that -OH, C=O, O-C=O, C=C and C-H (CH, CH_2 and CH_3) components were generated by the reactions of cyclopentane ring-opening and dehydrogeneration. The increase in C=C and C-H components suggests that main- or side-chain cleavage also occurred on the treated surfaces. A broad -OH peak was detected from the spectrum of oxygen plasma-treated COP; however, the change of the spectrum was smaller than those of the other spectra, as well as the spectrum of oxygen plasma-treated PMMA. This is because the plasma-treated surface layer is thinner than the detection depth represented by the ATR-FT-IR spectrum [17].
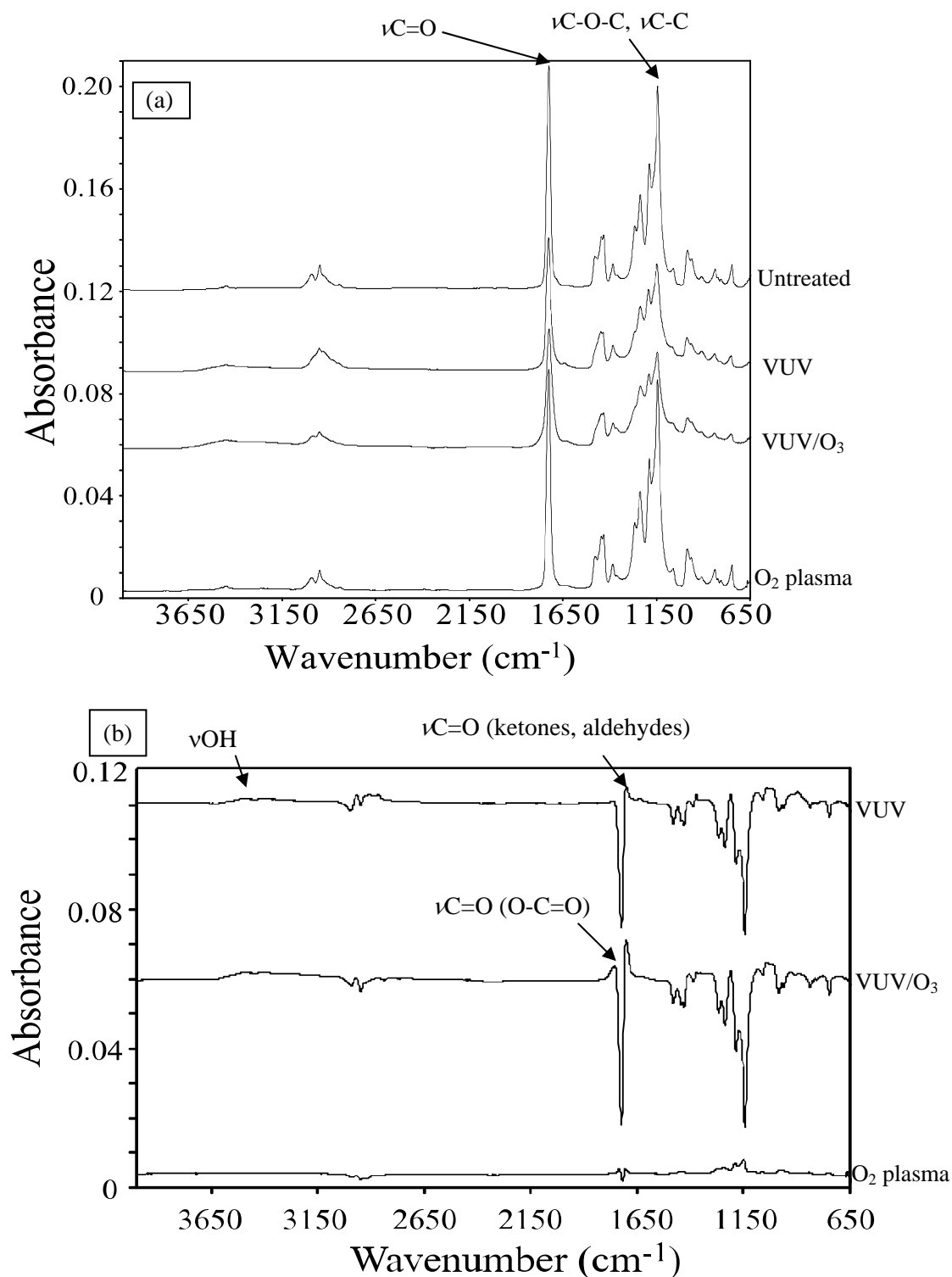
Fig. 3.11: (a) ATR-FT-IR spectra of untreated, VUV (t = 1 min), VUV/O$_3$ (p = 5.0 × 10^4 Pa, t = 10 min) and O$_2$ plasma (P = 200 W, p = 80 Pa) treated PMMA samples; (b) subtracted spectra by the untreated spectrum (ν: stretching vibration) [8].
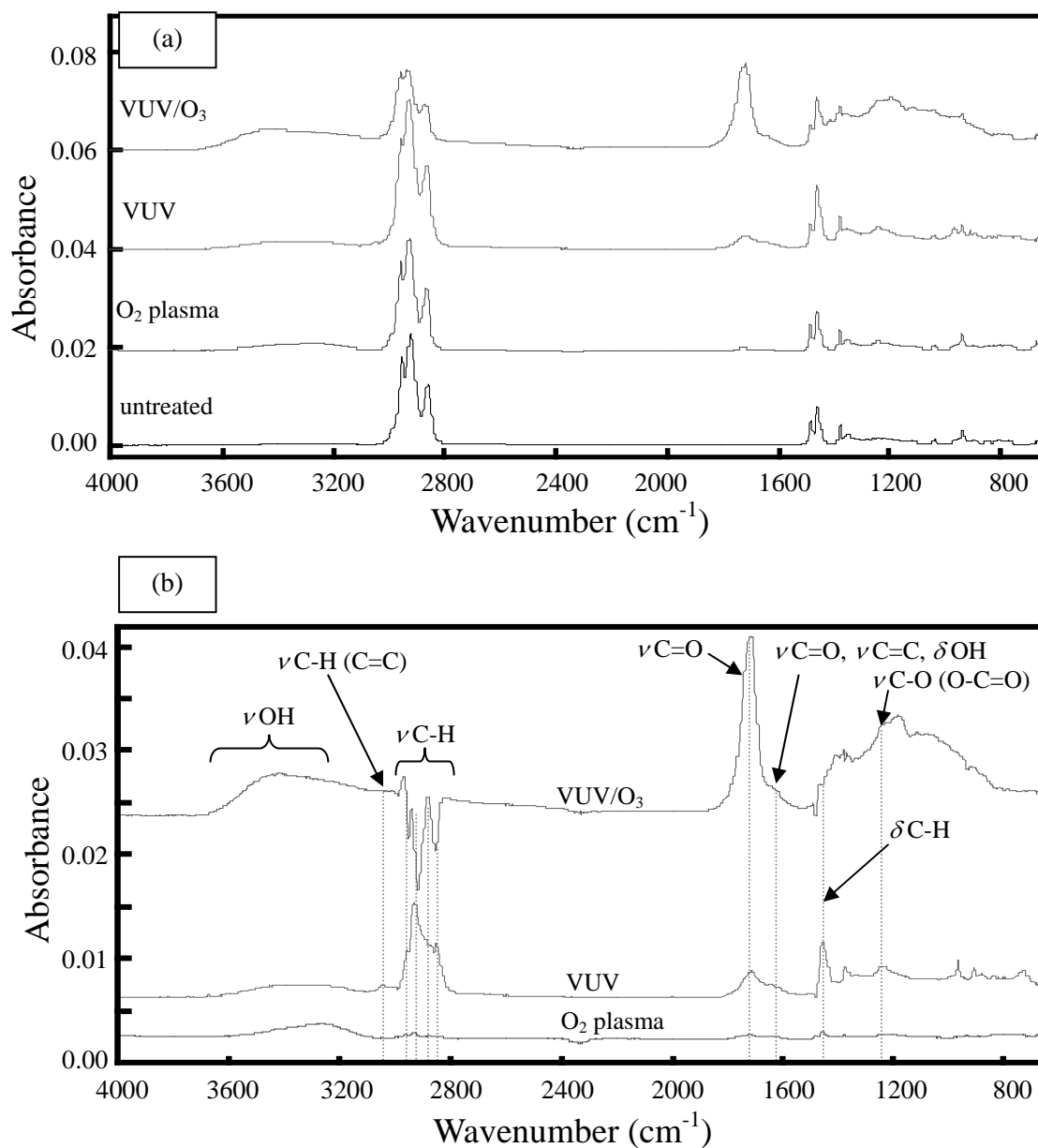
Fig. 3.12: (a) ATR-FT-IR spectra of untreated, VUV (t = 1 min), VUV/O$_3$ (p = 5.0 × 10^4 Pa, t = 5 min) and O$_2$ plasma (P = 100 W, p = 40 Pa) treated COP samples; (b) subtracted spectra by the untreated spectrum (ν: stretching vibration, δ: bending vibration) [9].

Figure 3.13 shows C1s XPS spectra of PMMA. The VUV and VUV/O_3 spectra shows that C=O/O-C-O components were generated. In case of VUV/O_3 and oxygen plasma, The O-C=O peaks in VUV/O_3- and oxygen plasma-treated PMMA were increased. Their O1s spectra are shown in Figure 3.14. From the spectra of VUV- and VUV/O_3-treated PMMA, O-C (ethers or alcohols) peaks were generated. The O=C and O*-C=O peaks (the asterisk corresponds to the analyzed oxygen) in the spectra of VUV/O_3- and oxygen plasma-treated PMMA were increased. These ATR-FT-IR and XPS results indicate that the oxidized polar components such as -OH, C=O (including ketone or aldehyde), and O-C=O (ester or carboxylic groups) were increased after VUV or VUV/O_3 treatments. The oxidized polar components were also increased after oxygen plasma treatment, while newly generated component could not be determined.
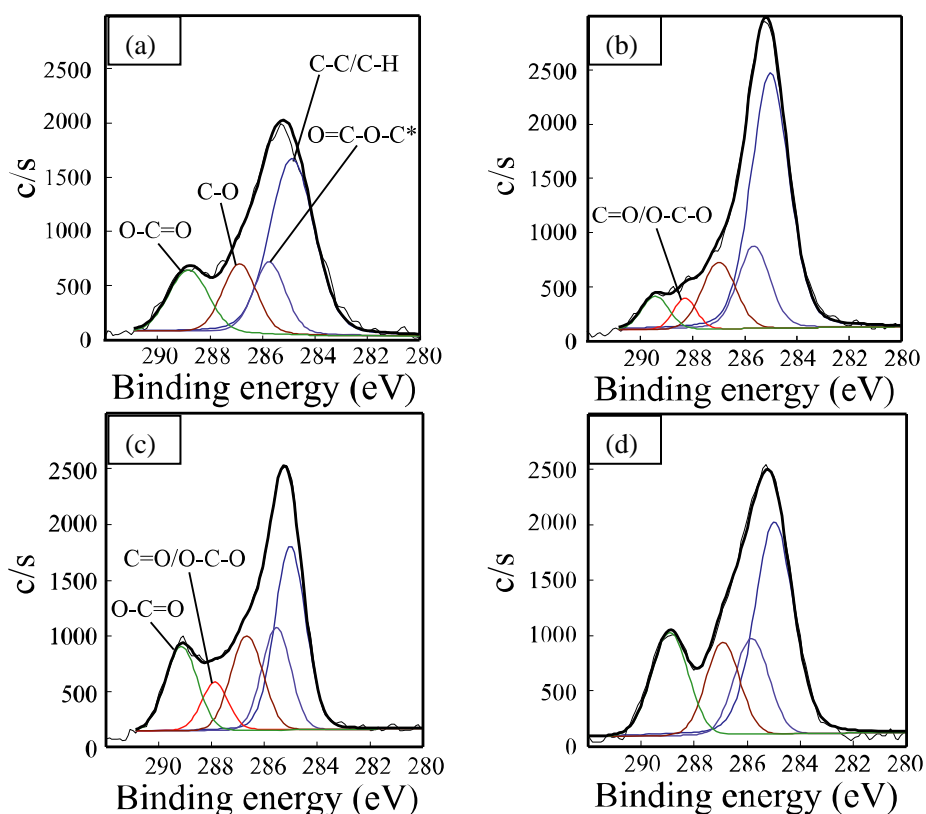
Fig. 3.13: C1s XPS spectra of (a) untreated PMMA, (b) VUV (t = 1 min), (c) VUV/O_3 (p = 5.0 × 10^4 Pa, t = 10 min) and (d) O_2 plasma (P = 200 W, p = 80 Pa) treated PMMA samples [8]. The asterisk indicates the carbon that was analyzed.
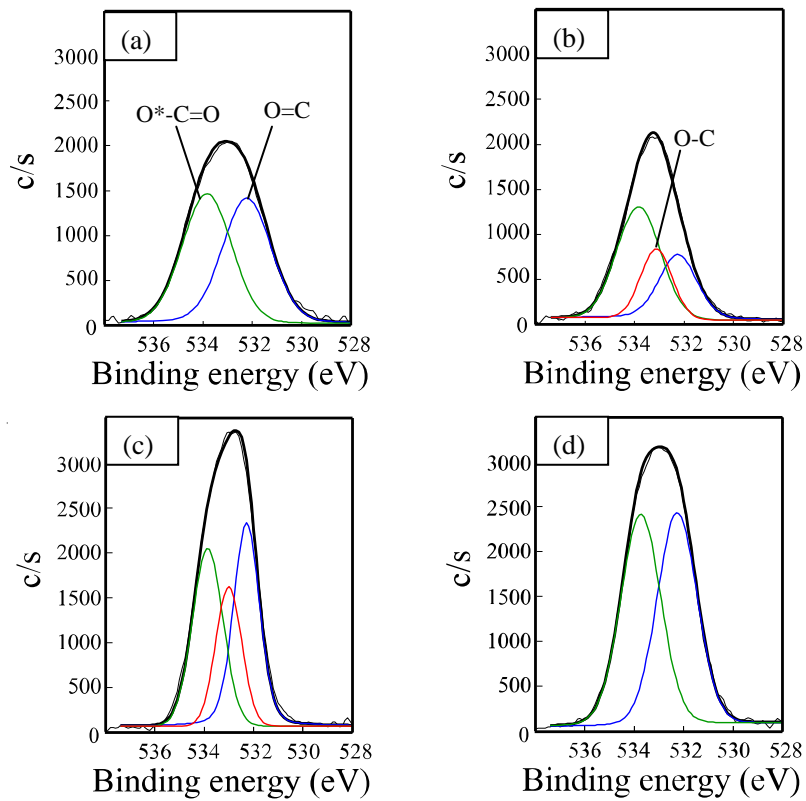
Fig. 3.14: O1s XPS spectra of (a) untreated PMMA, (b) VUV (t = 1 min), (c) VUV/O_3 (p = 5.0 × 10^4 Pa, t = 10 min) and (d) O_2 plasma (P = 200 W, p = 80 Pa) treated PMMA samples [8]. The asterisk indicates the oxygen that was analyzed.

51

The C1s and O1s XPS spectra of COP are shown in Figures 3.15 and 3.16. All C1s and O1s spectra after treatments show that the components originating in oxygen were generated. These results support the ATR-FT-IR results of VUV- and VUV/O_3-treated COP in Figure 3.12.

Figures 3.17 and 3.18 show the calculation results of γ_s, γ_s^p and γ_s^d of PMMA and COP surfaces. Increase in γ_s^p was observed in each case. The increase in γ_s^p corresponds to the polar group formation detected in the ATR-FT-IR and XPS.

The polar groups increases dipolar interactions between two treated plates as shown in Figure 3.3 (a).
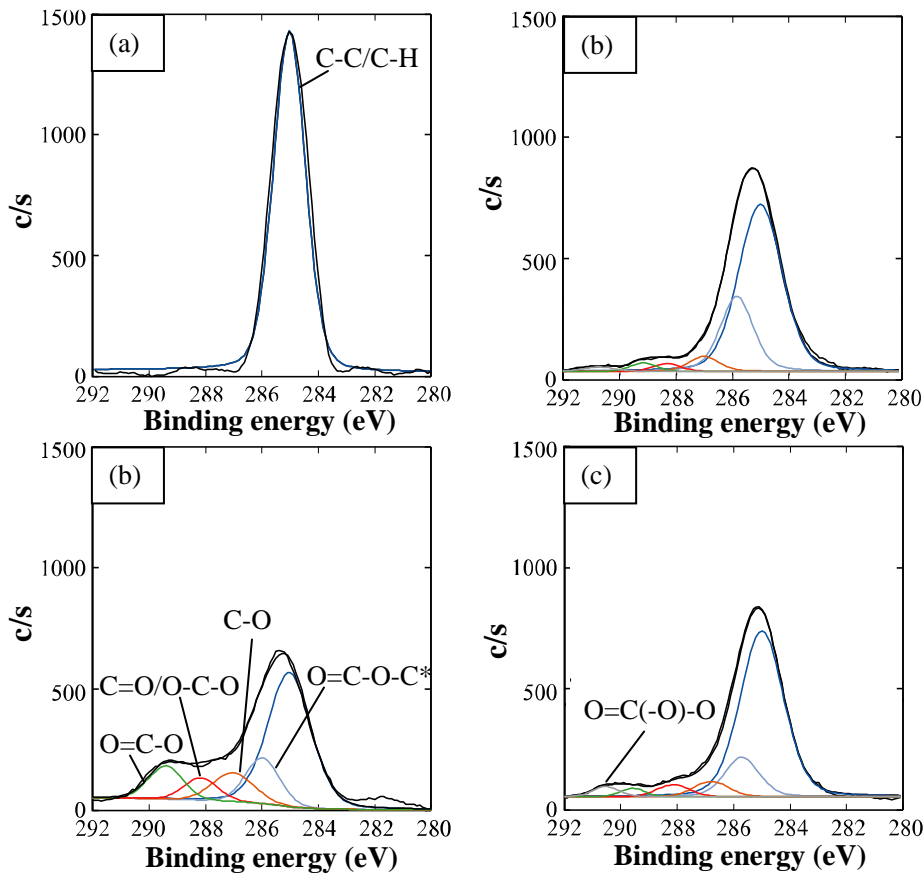
Fig. 3.15: C1s XPS spectra of (a) untreated COP, (b) VUV (t = 1 min), (c) VUV/O_3 (p = 5.0 × 10⁴ Pa, t = 10 min) and (d) O_2 plasma (P = 100 W, p = 40 Pa) treated COP samples [9]. The asterisk indicates the carbon that was analyzed.
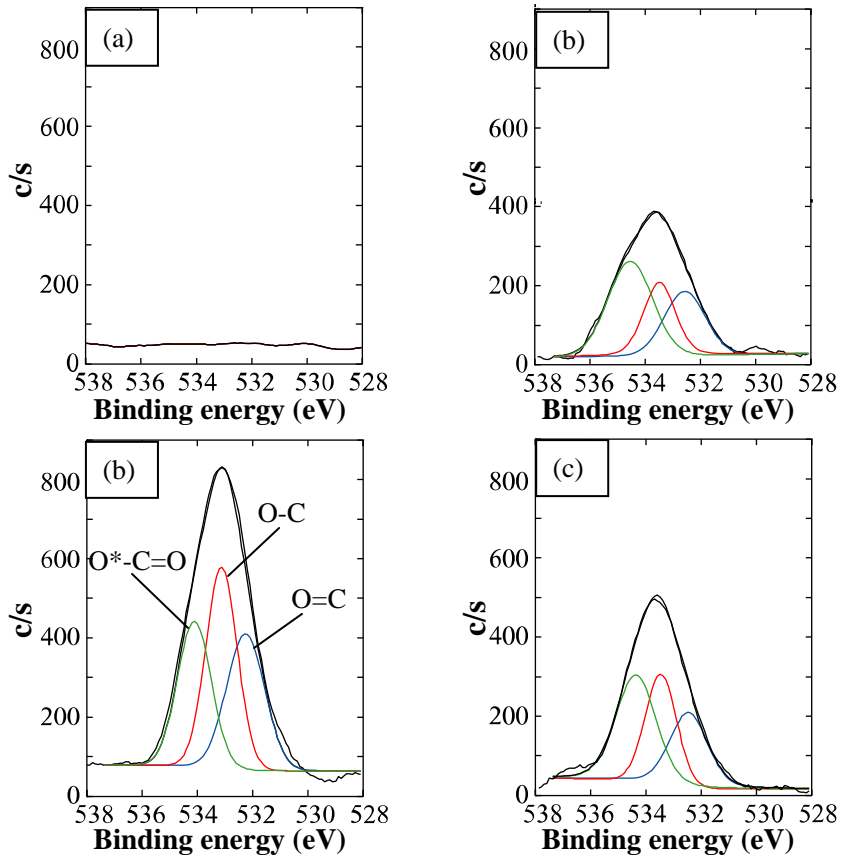
Fig. 3.16: O1s XPS spectra of (a) untreated COP, (b) VUV (t = 1 min), (c) VUV/O$_3$ (p = 5.0 × 10^4 Pa, t = 10 min) and (d) O$_2$ plasma (P = 100 W, p = 40 Pa) treated COP samples. The asterisk indicates the oxygen that was analyzed.
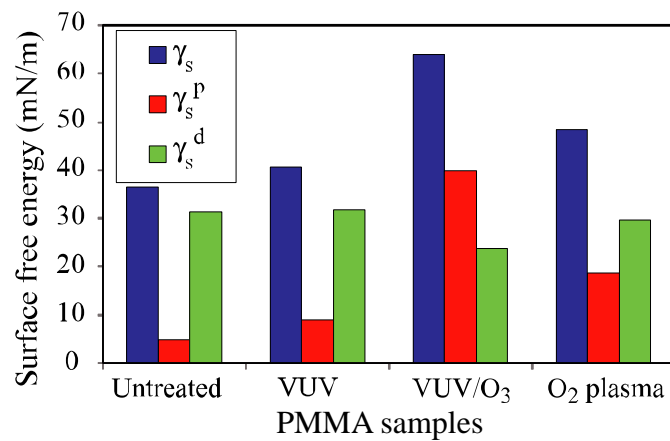
Fig. 3.17: Surface free energies on untreated, VUV (t = 1 min), VUV/O$_3$ (p = 3.0 × 10^4 Pa, t = 10 min) and oxygen plasma (P = 200 W, p = 80 Pa) treated PMMA samples [8].

53
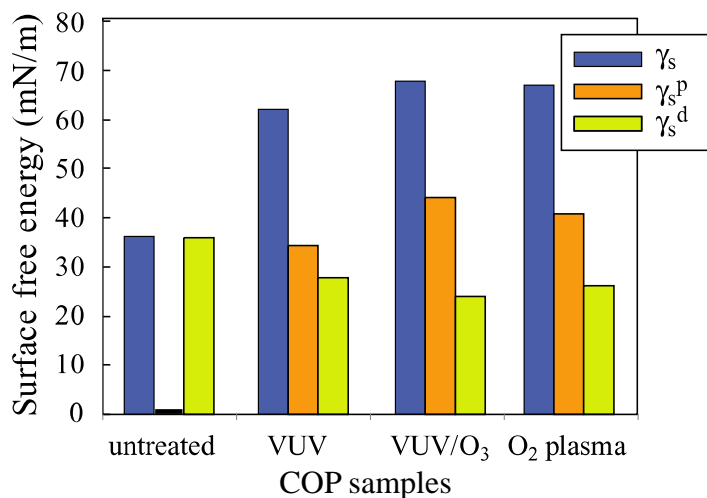
Fig. 3.18: Surface free energies on untreated, VUV (t = 1 min), VUV/O_3 (p = 5.0 × 10⁴ Pa, t = 10 min) and oxygen plasma (P = 100 W, p = 40 Pa) treated COP samples [9].

Figure 3.19 shows NEXAFS spectra of untreated, VUV and VUV/O_3-treated PMMA. Expected peak assignments were referred to other literatures [58-62]. Since peak 1 (π*(C=C) transition) was also observed in spectrum of untreated PMMA, the peak was generated by X-ray irradiation damage [61]. Peak 2 (π*(C=C) transition) was generated after VUV irradiation. Peak 3 (π*(C=C) transition) originated in cross-linking according to Ref. [62]. Figure 3.20 shows the spectrum of oxygen plasma-treated PMMA. Peak 3 was also generated after oxygen plasma treatment.

Based on these surface analysis results including ATR-FT-IR, XPS, surface free energy measurements, and NEXAFS, the author proposed examples of chemical changes of PMMA surface after the treatments as shown in Figure 3.21. In cross-linked structure, the surface occupancy of O-C=O (ester) is relatively increased with decrease of -CH_3 (Figure 3.21 (c)). It is expected that the increase in dipolar interactions between two treated PMMA surfaces are originated in the increase in O-C=O component. In addition, after VUV and VUV/O_3 treatments, polar groups is incorporated or substituted as shown in Figure 3.21 (a) and (b) [16,21]. The generated polar groups cause increase in the dipolar interactions.
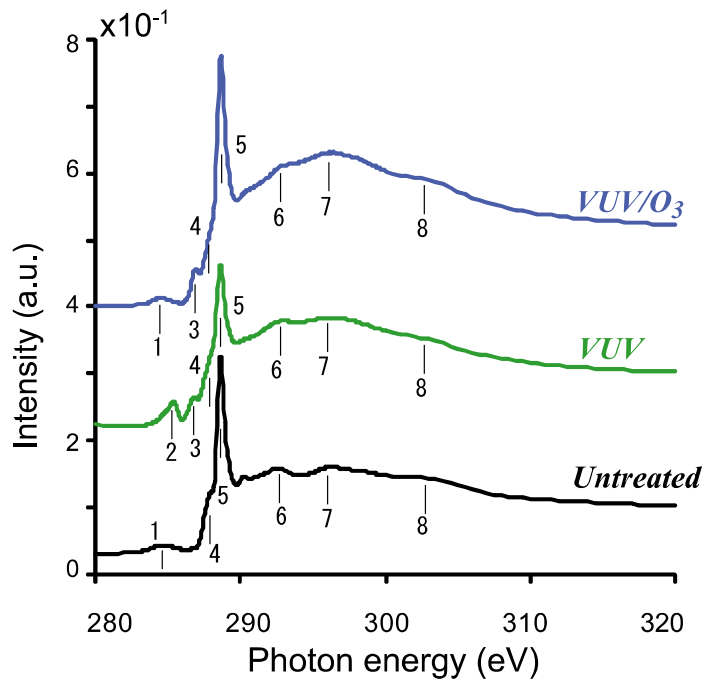
Fig. 3.19: C-K edge NEXAFS spectra of untreated, VUV (t = 30 sec) and VUV/O$_3$ (p = 3.0 × 10^4 Pa, t = 5 min) treated PMMA; 1-3: π*(C=C), 4: π*(C-H), 5: π*(C=O), 6: σ*(C-C, C-O), 7: σ*(C=O), 8: multiple scattering [10].
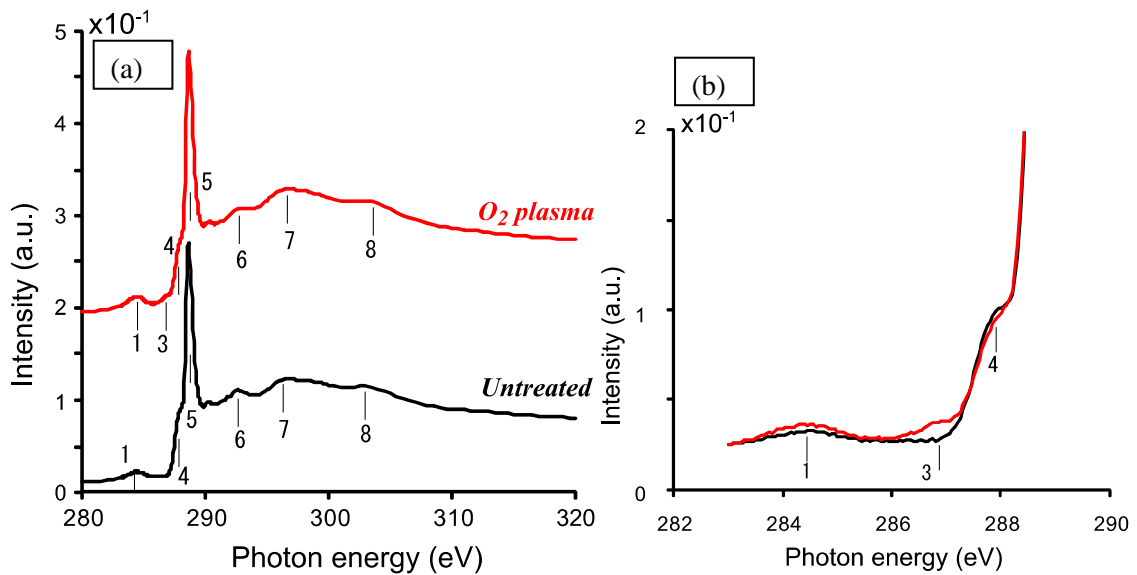
Fig. 3.20: C-K edge NEXAFS spectra of untreated and oxygen plasma (P = 200 W, p = 80 Pa) treated PMMA: (a) range of 280-320 eV and (b) 283-288.5 eV (overwrittened). 1,3: π*(C=C), 4: π*(C-H), 5: π*(C=O), 6: σ*(C-C, C-O), 7: σ*(C=O), 8: multiple scattering [10].
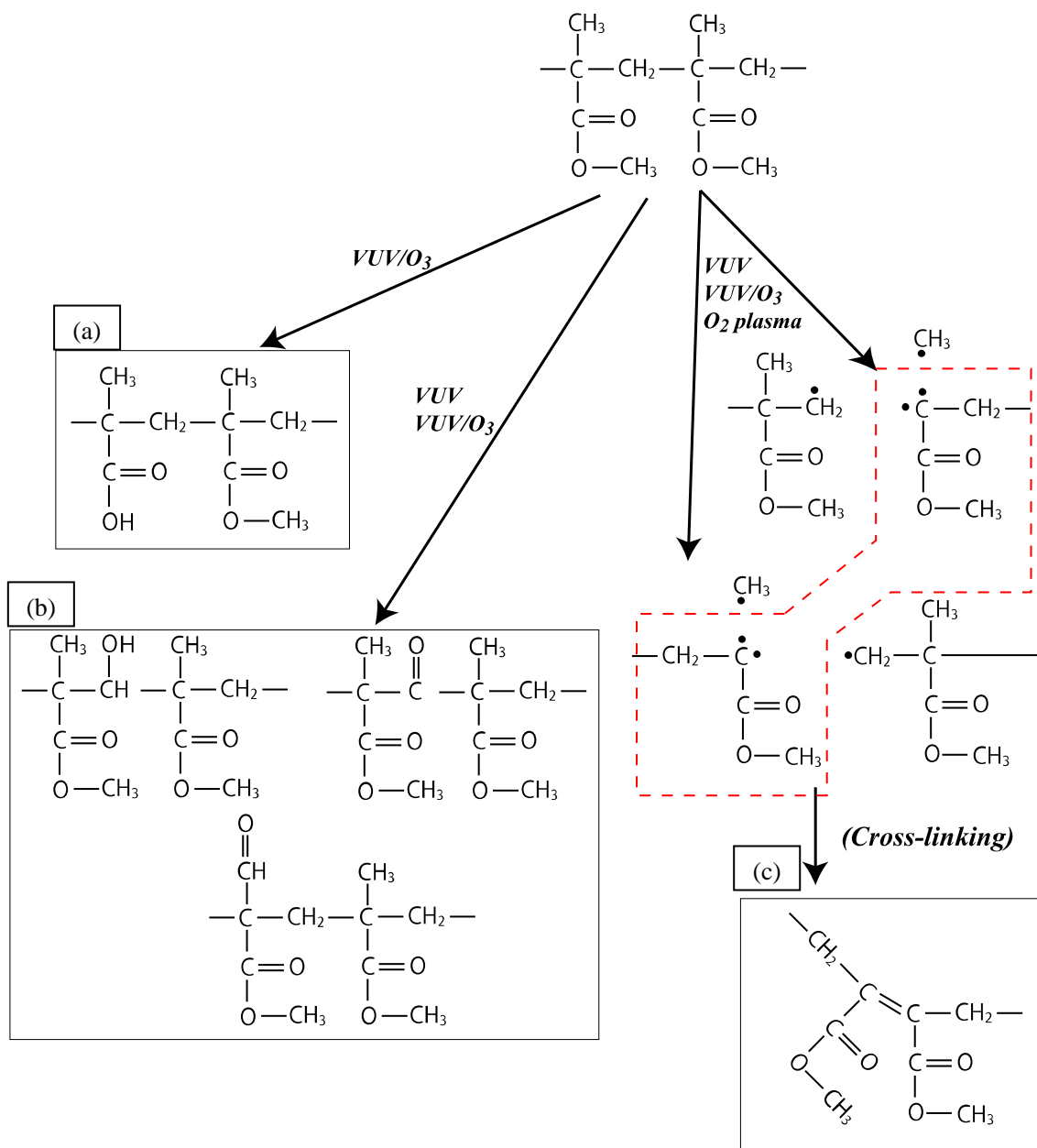
Fig. 3.21: Examples of the chemical changes of PMMA after the treatments: (a) carboxylic acid; (b) alcohol, ketone, and aldehyde [16,21]; (c) cross-linked structure [10].

Generation of low-T_g layer

Main or side chain cleavage of polymer chains causes degradation of the plastics so as to generate low-T_g layer on the surface. Figure 3.22 shows results of µ-TA on PMMA surface. The first softening points as indicated with blue and green arrows in the curves of VUV- and VUV/O_3-treated PMMA were decreased (~60 ^{o}C). On the other hand, the softening point of the oxygen plasma-treated sample was not changed with red arrow. These results indicate that the T_g on the PMMA surface was decreased after VUV and VUV/O_3 treatments.

Thermal annealing effect

Figure 3.23 shows changes in surface free energies on oxygen plasma-treated COP surfaces after thermal annealing at 120 ^{o}C. After the annealing, γ_s^p decreased while γ_s^d increased. These results suggest that the generated polar groups (e.g. -OH, -COOH) were consumed by the dehydration reaction. This reaction could also have occurred at the interface of the two COPs during the bonding process. H_2O also could be consumed during annealing, and some hydrogen bonds change to covalent bonds (-C-O-C-), as shown in Figure 3.3 (a) and (b).
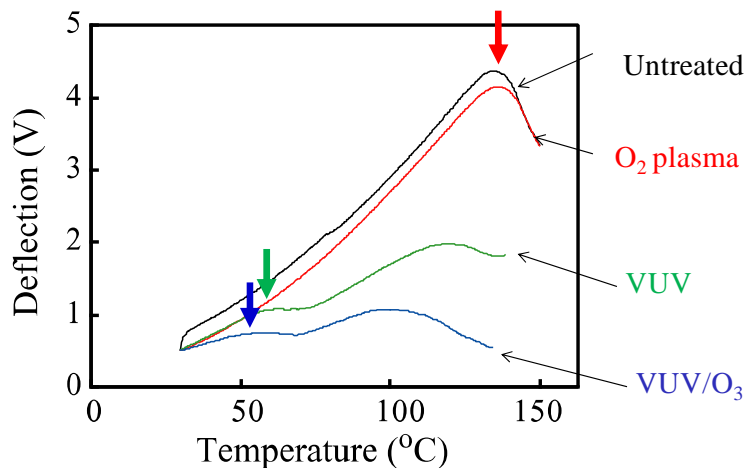
Fig. 3.22: Results of µ-TA on untreated, VUV (t = 30 sec), VUV/O_3 (p = 3.0 × 10^4 Pa, t = 5 min) and oxygen plasma (P = 200 W, p = 80 Pa) treated PMMA samples [8].
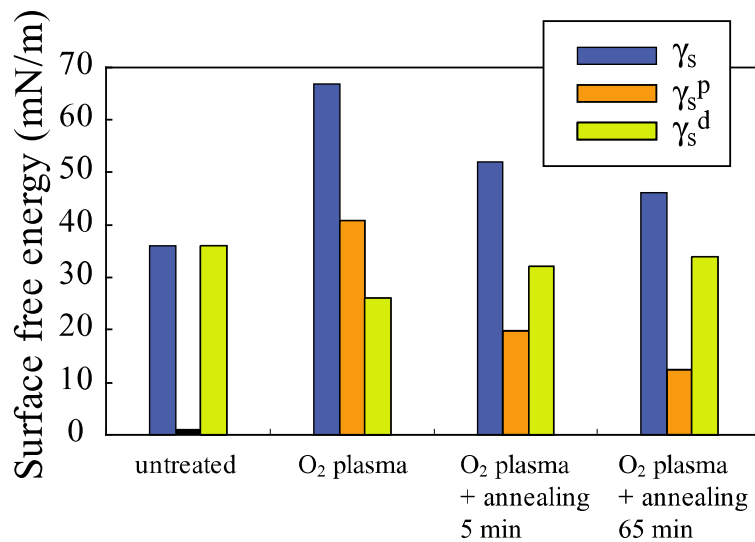
Fig. 3.23: Changes in surface free energies (γ_s, γ_s^p and γ_s^d) on oxygen plasma-treated (P = 100 W, p = 40 Pa) COP surfaces after thermal annealing at 120 $^{\circ}$C [9].

3.6 Applications for microchannel fabrication

3.6.1 Shallow microchannel

Fabrication process

Fabrication process of a microchip with shallow microchannel is shown in Figure 3.24. A silicon mold was fabricated by conventional photolithography and deep reactive ion etching (Deep-RIE) (Fig. 3.24 (a)). The micro-channel region was fabricated by embossing a plastic plate (Fig. 3.24 (b)). Then the surface of the micro-channel plate and the PMMA lid were pretreated (Fig. 3.24 (c)). Finally, the microchip was fabricated by direct bonding of the plates to each other (Fig. 3.24 (d)).
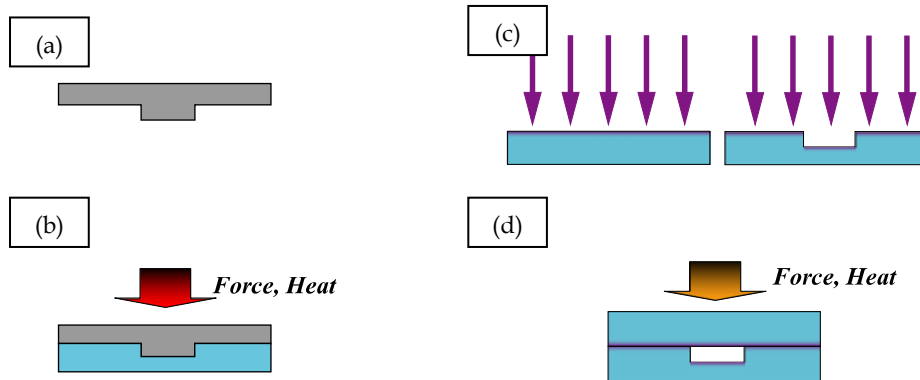
Fig. 3.24: Fabrication process of microchip with shallow microchannel: (a) Si mold fabrication; (b) hot embossing; (c) surface pretreatment; and (d) direct bonding.

Fabrication results

A prototype PMMA microchip which has fine channel with depth of 5 μm and width of 150 μm is shown in Figure 3.25. Figure 3.26 shows COP microchannels with depth of 1 μm and width of 150 μm. The shallow microchannel was successfully fabricated without deformation and significant voids.

Figure 3.27 shows a PMMA microchip which has two dams with a gap of less than 5 μm. The dam structures were maintained after low-temperature bonding. The flow behaviors of the dams were evaluated with de-ionized water including fluorescent beads. The water was introduced from port E. There was no leakage or obstacles for smooth flow. Large microbeads with diameter of 5.7 μm were completely trapped and filled between two dams, while small microbeads with diameter of 1.0 μm passed through the dams, as shown in Figure 3.27 (c).

These results indicate that these bonding method described in this chapter can be applicable to fabricate fine microchannels with several μm gaps.
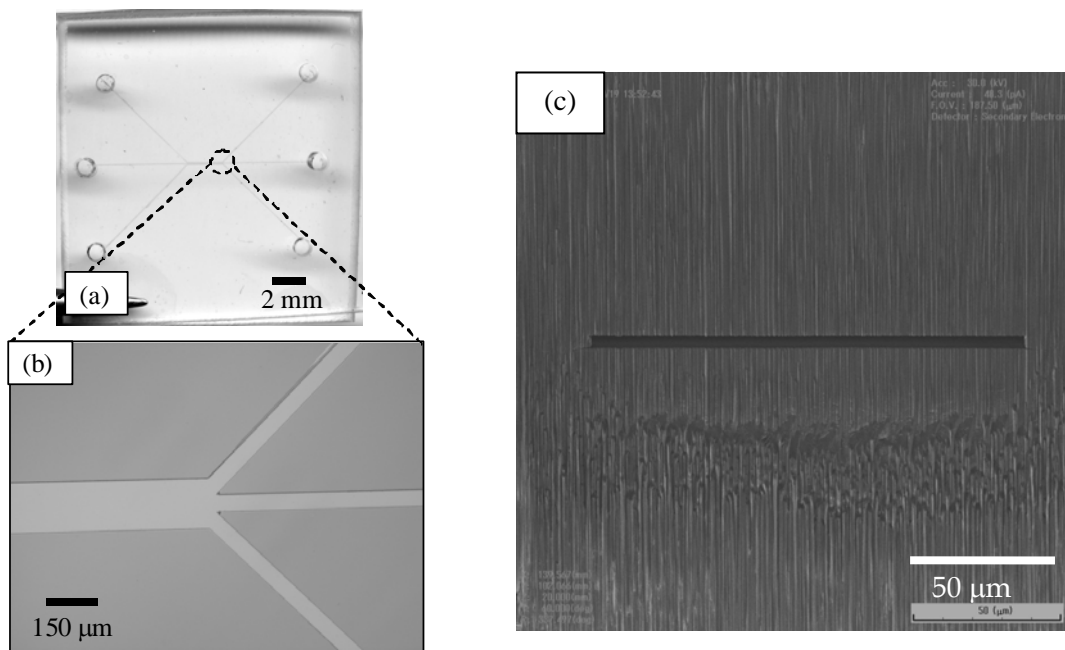
Fig. 3.25: A shallow PMMA microchannel: (a) whole and (b) magnified view of the microchip; (c) cross-section of the microchannel (width: 150 μm, depth: 5 μm) [6].
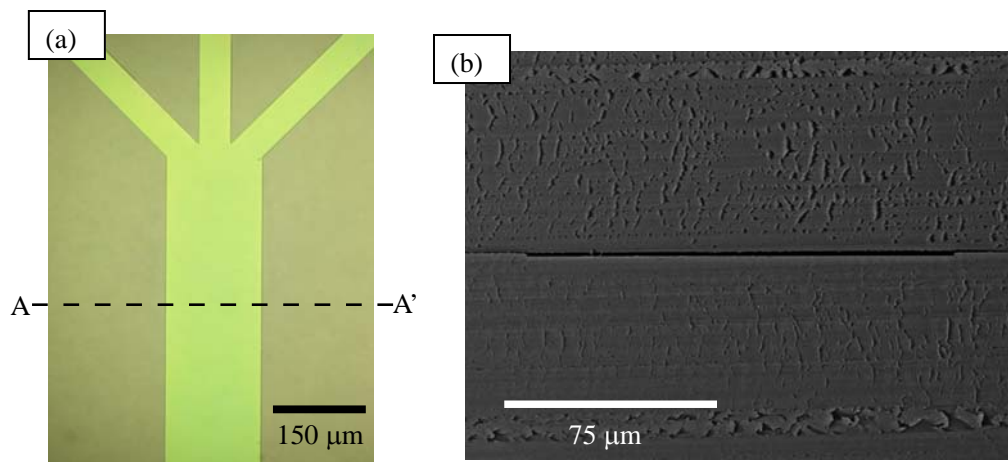
Fig. 3.26: Shallow COP microchannel: (a) photomicrograph and (b) cross-section SEM image (along line A-A' in (a)) [9].
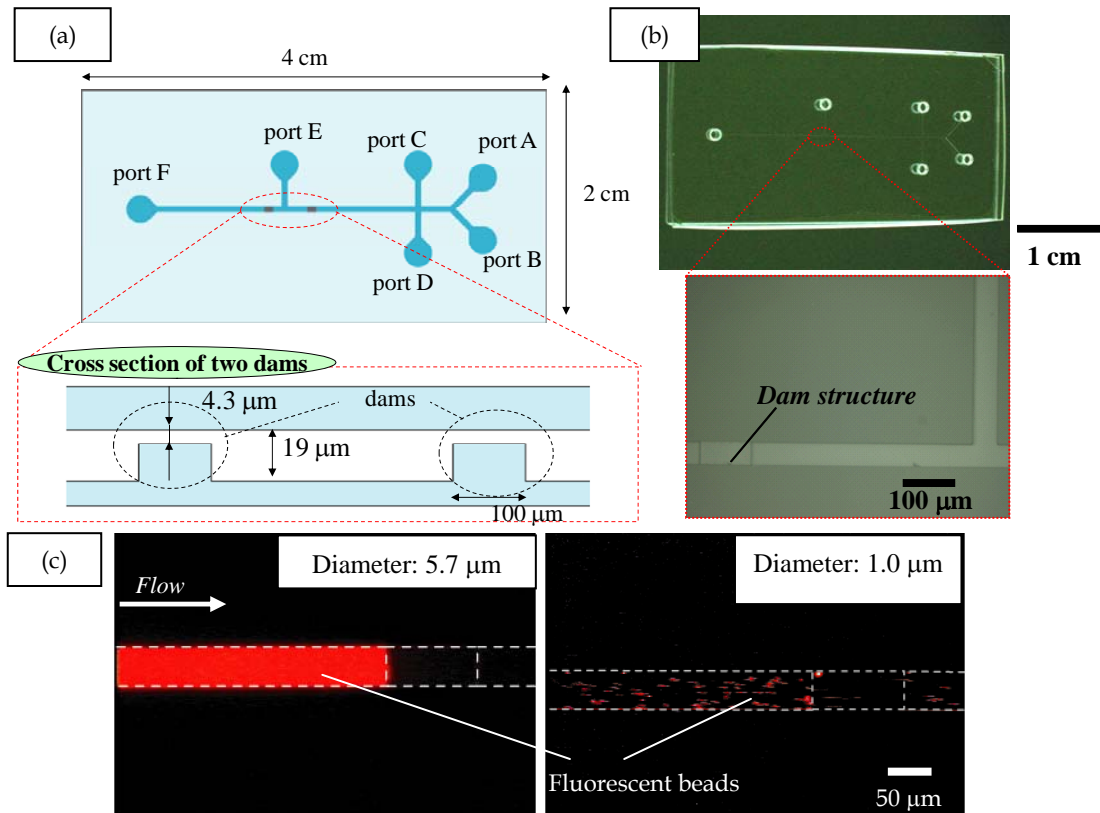
Fig. 3.27: A PMMA microchip which has two dams with shallow gap (< 5 μm): (a) design, (b) whole view and photomicrograph near a dam, and (c) flow behavior near a dam [5].

3.6.2 Au-embedded COP microchannel

Experimental procedure

Figure 3.28 shows fabrication process of an Au-embedded microchip. Au film of 200 nm thickness is deposited on bare COP plate by electron beam evaporation (Figure 3.28 (a)). Au electrode pattern was formed by conventional photolithography (Figure 3.28 (b)) and wet etching techniques (Figure 3.28 (c)). Using the other COP plate, micro-channel plate was fabricated by hot embossing (Figure 3.28 (d)). The two plates were treated by oxygen plasma activation bonding system (EVG810LT) (Figure 3.28 (e)).   The treatment was carried out under the following conditions; plasma power P

of 100 W, oxygen pressure p of 0.4 mbar, and treatment time t of 30 sec. Finally, the two plates were bonded together with applied pressure of 3 MPa, at a temperature of 120 $^{\circ}$C and the annealing time of 10 min (Figure 3.28 (f)).

Adhesion strength between COP and Au film was measured by microindentation tester [62] (MH4000 from NEC San-ei Instruments, Ltd.). For comparison, the adhesion strengths between PMMA and Au, between quartz glass and Au film, and between Si and Cr film were also measured. All metal films (thickness: ~200 nm) were coated by electron beam evaporation.

The bonding strength between COP and Au film coated on COP was evaluated by a tensile test method explained in Section 3.4.

The flow behavior in the fabricated microchip was observed by introducing de-ionized water including negative-charged fluorescent beads (diameter: 5 μm).
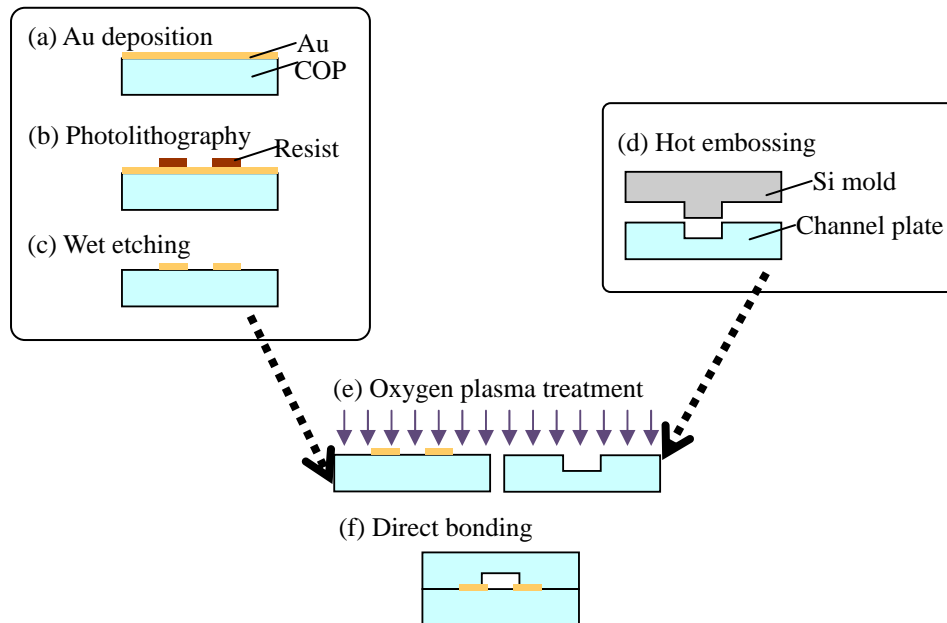
Fig. 3.28: Fabrication process of Au-embedded COP microchip.

Results and discussion

Figure 3.29 shows the adhesion strength of Au-COP, Au-quartz, and Cr-Si. The Au-COP adhesion was stronger than that of Au-quartz and as same as that of Cr-Si. Strong Au-COP adhesion was obtained compared to other conventional polymer materials, such as poly-dimethylsiloxane (PDMS), PMMA, and polycarbonate (PC) [13,63].

The bonding strength of Au-COP was approximately 0.3 MPa. The strength value

measured by the microindentation method cannot be compared simply with that by the tensile test [62]. However, the two COP plates were separated at the direct-bonded interface. This result indicates that the bonding strength of Au-COP was weaker than that of adhesion strength. On the other hand, the strength of COP-COP was larger than 1 MPa as explained in Section 3.4. Further experiments and optimizations of surface pretreatment and bonding conditions are required to realize strong Au-COP bonding.
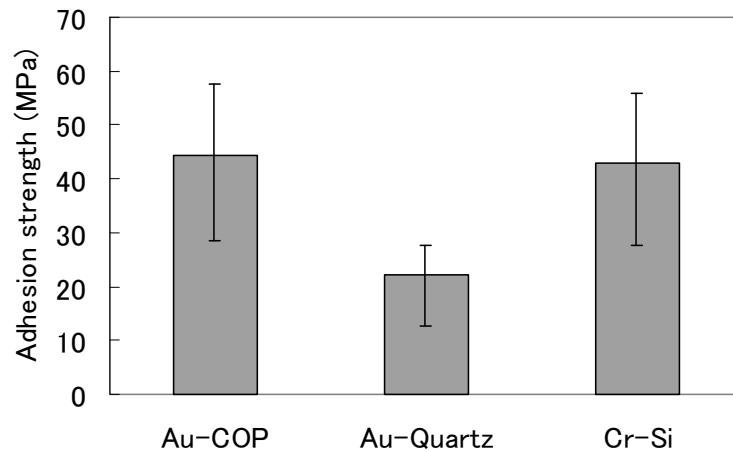
Fig. 3.29: Adhesion strength of Au-COP, Au-Quartz and Cr-Si measured by microindentation method [7].

Figures 3.30 and 3.31 show the designed structure and image of the fabricated microchip. The microchannels are 50 μm wide and 20 μm deep. There are three pairs of Au electrodes, and each pair of the electrodes is faced on either side of the microchannels. The gap between the two electrodes is 25 μm. There was no void at the interface between COP and Au as well as the interface of two COP surfaces.

The flow behaviors in the microchannel were evaluated with de-ionized water including negative-charged fluorescent beads (diameter: 5 μm). There was no leakage or obstacles to smooth fluidic flow at the bonded interfaces and at the exposed Au electrodes as shown in Figure 3.32 (a).

Then, direct current (DC) voltage of + 5 V was applied to the electrodes of #1 or #2 in Figure 3.30. The beads were drawn to the voltage-applied electrodes, and the flow behaviors changed by voltage switching as shown in Figure 3.32 (b) and (c). These results indicate that the electrical continuity of Au electrode was kept after the bonding process. Au-embedded COP structure is widely applicable for practical microchips.
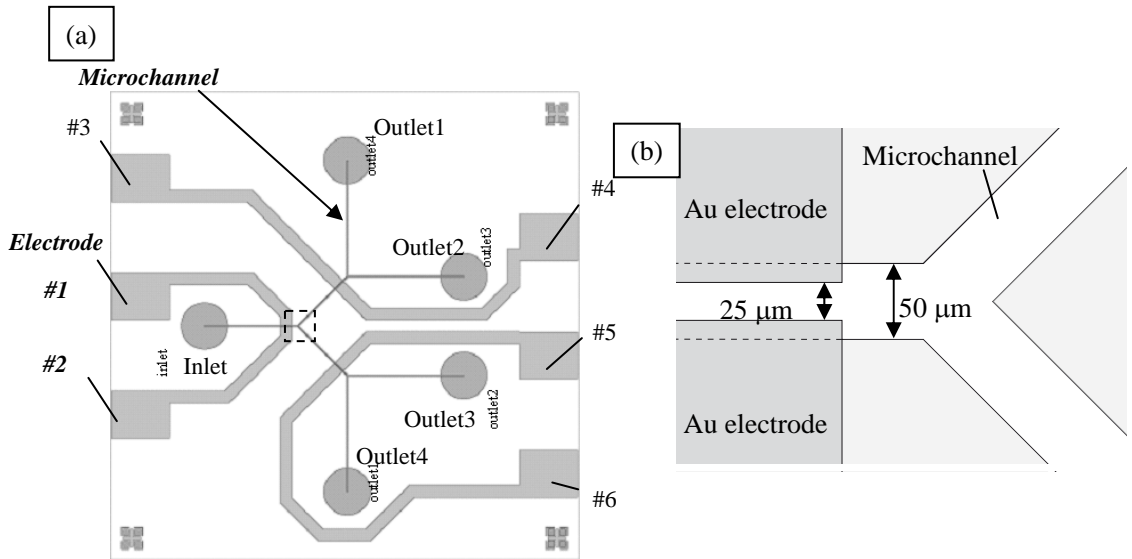
Fig. 3.30: Design of prototype Au-embededed microchip: (a) whole view and (b) magnified view of Y-junction (enclosed with dash line in (a)) [11].
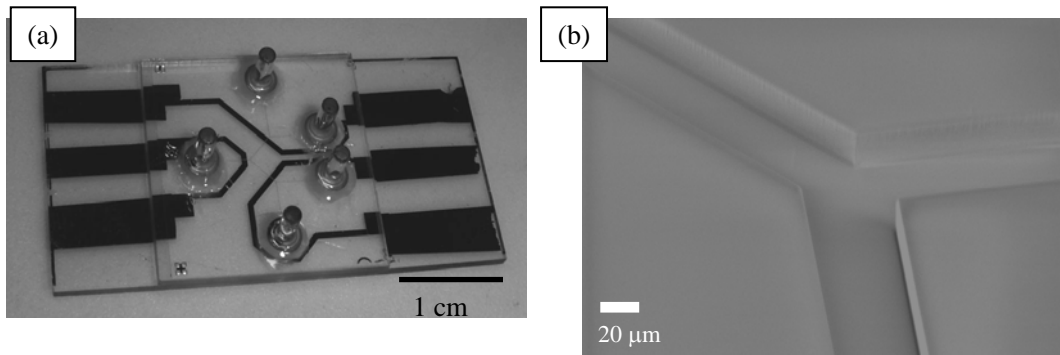
Fig. 3.31: Fabricated Au-embedded microchip: (a) whole view of the microchip, and (b) SEM image of embossed microchannel at Y-junction [11].
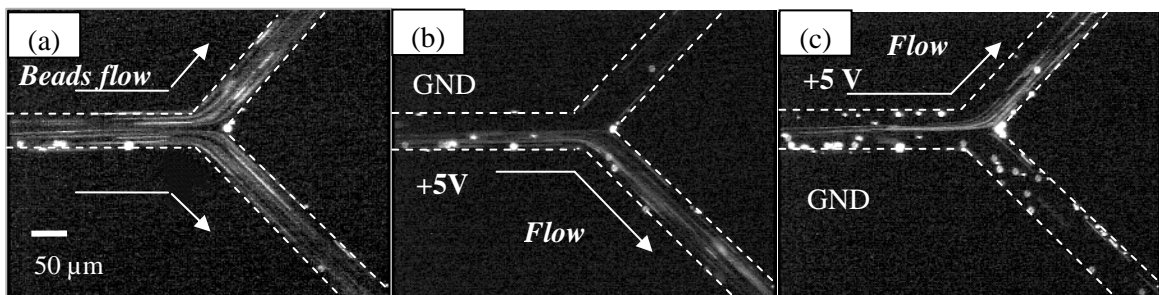
Fig. 3.32: Flow behavior in the microchip: (a) without voltage, (b) voltage applied to lower electrode, and (c) voltage applied to upper electrode [11].

3.6 Conclusion

In order to bond plastics directly at a temperature lower than T_g of the plastic, various pretreatments such as oxygen plasma, atmospheric-pressure plasma, UV/O$_3$, VUV and VUV/O$_3$ were evaluated and optimum conditions were investigated. Appropriate bond strength was realized even at room temperature, and the bond strength is increased with increasing temperature.

The mechanisms of low-temperature bonding using oxygen plasma, VUV and VUV/O$_3$ treatments were investigated using surface analysis methods. The bonding mechanisms are described below: Each bonding is partly originated in increasing dipolar interactions between polar functional groups on two treated plates such as –OH···OH (hydrogen bond) and -C=O···C=O. Decrement of surface free energies on oxygen plasma-treated samples changes some of the hydrogen bonds to covalent bonds (-C-O-C-) during annealing. Low-T_g layer is generated on the surface after VUV and VUV/O$_3$ pretreatments, and the layer is diffusion-bonded to each other. This is the world's first research to propose the low-temperature bonding mechanisms by showing specific surface chemical changes after pretreatment. These bonding mechanisms become guidelines to other low-temperature bonding methods such as using other kinds of plastics and other pretreatment methods.

PMMA and COP microchips with a microchannel of less than 5 μm in depth and 150 μm wide were fabricated. This is the world's first results to realize such shallow and fine channel structures using plastic material. These results indicate that this bonding method can be applicable for fine microstructures which have several μm gaps. In addition, an Au-electrode-embedded COP microchip was fabricated by hot embossing and low-temperature direct bonding. The fabrication method of this microchip has remarkable advantage for integrating electrodes in a plastic microchip.

References

[1] T. Suzuki, H. Shinohara, M. Ishizuka, J. Mizuno, S. Shoji, Proc. The 12th Cheminas (2005) 10 (in Japanese).

[2] J. Mizuno, H. Ishida, S. Farrens, V. Dragoi, H. Shinohara, T. Suzuki, M. Ishizuka, T. Glinsner, F. P. Lindner, S. Shoji, Cyclo-olefin polymer direct bonding using low temperature plasma activation bonding, Proc. The 13th Int. Conf. Solid-State Sens. Actuators Microsys. (Transducers), (2005) 1346-1349.

[3] J. Mizuno, S. Farrens, H. Ishida, V. Dragoi, H. Shinohara, T. Suzuki, M. Ishizuka, T. Glinsner, S. Shoji, Cyclo-olefin polymer direct bonding using low temperature plasma activation bonding, Proc. Int. Conf. MEMS, NANO, and Smart Sys. (ICMENS), (2005) 346-349.

[4] H. Shinohara, M. Ishizuka, J. Mizuno, S. Shoji, Low temperature direct bonding of PMMA for polymer microchips, Proc. Asia-Pacific Conf. Transducers and Micro-Nano Tech. (APCOT), (2006) 95-FT-A0062 (in CD-ROM).

[5] H. Shinohara, J. Mizuno, F. Kitagawa, K. Otsuka, S. Shoji, Fabrication of highly dimension controlled PMMA microchip by hot embossing and low temperature direct bonding, Proc. The 10th Int. Conf. Miniaturized Sys. Chem. Life Sci. (Micro-TAS), (2006) 158-160.

[6] H. Shinohara, J. Mizuno, S. Shoji, Low temperature direct bonding of poly(methyl methacrylate) for polymer microchips, IEEJ Trans. Electr. Electron. Eng. **2** (2007) 301-306.

[7] H. Shinohara, F. Kitagawa, J. Mizuno, K. Otsuka, S. Shoji, Highly stable and reproducible cyclo-olefin polymer nano-electrospray tip for electrophoresis-mass spectrometry, Proc. The 4th Asia-Pacific Conf. Transducers and Micro/Nano Technol. (APCOT), (2008) 2S45 (in CD-ROM).

[8] H. Shinohara, J. Mizuno, S. Shoji, Studies on low-temperature direct bonding methods of PMMA and COP using surface pretreatment, Proc. Int. Conf. Electron. Packaging　(ICEP), (2009) 748-753.

[9] H. Shinohara, T. Suzuki, J. Mizuno, S. Shoji, Studies on low-temperature bonding mechanism of VUV and plasma pretreated cyclo-olefin polymer, Proc. The 15th Int. Conf. Solid-State Sens. Actuators Microsys. (Transducers), (2009) 1039-1042.

[10] H. Shinohara, J. Mizuno, S. Shoji, NEXAFS studies on VUV and oxygen plasma pretreated PMMA surfaces for investigation of low-temperature bonding mechanisms, Proc. The 22nd Int. Microprocesses and Nanotech. Conf. (MNC),

(2009) 726-727.

[11] H. Shinohara, J. Mizuno, S. Shoji, Au-electrode-embedded cyclo-olefin polymer microchip using low-temperature direct bonding, IEEJ Trans. E (submitted).

[12] G. A. C. M. Spierings and J. Haisma, Direct bonding of organic materials, Appl. Phys. Lett. **64** (1994) 3246-3248.

[13] M. Svedberg, A. Pettersson, S. Nilsson, J. Bergquist, L. Nyholm, F. Nikolajeff, K. Markides, Sheathless electrospray from polymer microchips, Anal. Chem. **75** (2003) 3934-3940.

[14] R. T. Kelly and A. T. Woolley, Thermal bonding of polymeric capillary electrophoresis microdevices in water, Anal. Chem. **75** (2003) 1941-1945.

[15] Z. Chen, Y. Gao, J. Lin, R. Su, and Y. Xie, Vacuum-assisted thermal bonding of plastic capillary electrophoresis microchip imprinted with stainless steel template, J. Chromatogr. A **1038** (2004) 239-245.

[16] L. Lianos, D. Parrat, T. Q. Hoc, T. M. Duc, Secondary ion mass spectrometry time of flight and in situ x-ray photoelectron spectroscopy studies of polymer surface modifications by a remote oxygen plasma treatment, J. Vac. Sci. Technol. A **12** (1994) 2491-2498.

[17] U. Schulz, P. Munzert, N. Kaiser, Surface modification of PMMA by DC glow discharge and microwave plasma treatment for the improvement of coating adhesion, Surf. Coat. Technol. **142-144** (2001) 507-511.

[18] A. Kamińska, H. Kaczmarek, J. Kowalonek, The influence of side groups and polarity of polymers on the kind and effectiveness of their surface modification by air plasma action, Eur. Polym. J. **38** (2002) 1915-1919.

[19] Y. Sawada, Applications of atmospheric-pressure glow plasma, J. Plasma Fusion Res. **79** (2003) 1022-1028 (in Japanese).

[20] M. Noeske, J. Degenhardt, S. Strudthoff, U. Lommatzsch, Plasma jet treatment of five polymers at atmosphrcie pressure: surface modifications and the relevance for adhesion, Int. J. Adhes. Adhes. **24** (2004) 171-177.

[21] J. Chai, F. Lu, B. Li, D. Y. Kwok, Wettability interpretation of oxygen plasma modified poly(methyl methacrylate), Langmuir **20** (2004) 10919-10927.

[22] J. Lai, B. Sunderland, J. Xue, S. Yan, W. Zhao, M. Folkard, B. D. Michael, Y. Wang, Study on hydrophilicity of polymer surfaces improved by plasma treatment, Appl. Surf. Sci. **252** (2006) 3375–3379.

[23] A. Bhattacharyya and C. M. Klapperich, Mechanical and chemical analysis of plasma and ultraviolet-ozone surface treatments for thermal bonding of polymeric microfluidic devices, Lab Chip **7** (2007) 876-882.

[24] J. Peeling and D. T. Clark, An ESCA study of the photo-oxidation of the surface of polystyrene film, Polym. Degrad. Stab. **3** (1980-81) 97-105.

[25] J. Peeling and D. T. Clark, ESCA study of the surface photo-oxidation of some non-aromatic polymers, Polym. Degrad. Stab. **3** (1981) 177-185.

[26] H. Kaczmarek, A. Kamińska, A. V. Herk, Photooxidative degradation of poly(alkyl methacrylate)s, Eur. Polym. J. **36** (2000) 767-777.

[27] T. N. Murakami, Y. Fukushima, Y. Hirano, Y. Tokuoka, M. Takahashi, N. Kawashima, Surface modification of polystylene and poly(methyl methacrylate) by active oxygen treatment, Collo. Surf. B **29** (2003) 171-179.

[28] A. Hozumi, H. Inagaki, T. Kameyama, The hydrophilization of polystylene substrates by 172-nm vacuum ultraviolet light, J. Collo. Interf. Sci. **278** (2004) 383-392.

[29] R. Truckenmüller, P. Henzi, D. Herrmann, V. Saile, W. K. Schomburg, Bonding of polymer microstructures by UV irradiation and subsequent welding at low temperatures, Microsyst. Technol. **10** (2004) 372-374.

[30] H. Kaczmarek, H. Chaberska, The influence of UV-irradiation and support type on surface properties of poly(methyl methacrylate) thin films, Appl. Surf. Sci. **252** (2006) 8185-8192.

[31] G. A. Diaz-Quijada, R. Peytavi, A. Nantel, E. Roy, M. G. Bergeron, M. M. Dumoulin, T. Veres, Surface modification of thermoplastics-towards the plastic biochip for high throughput screening devices, Lab Chip **7** (2007) 856-862.

[32] C. W. Tsao, L. Hromada, J. Liu, P. Kumar, D. L. DeVoe, Low temperature bonding of PMMA and COC microfluidic substrates using UV/ozone surface treatment, Lab Chip **7** (2007) 499-505.

[33] Y.-J. Kim, Y. Taniguchi, K. Murase, Y. Taguchi, H. Sugimura, Vacuum ultraviolet-induced surface modification of cyclo-olefin polymer substrates for photochemical activation bonding, Appl. Surf. Sci. **255** (2009) 3648-3654.

[34] J. Liu, H. Qiao, C. Liu, Z. Xu, Y. Li, L. Wang, Plasma assisted thermal bonding for PMMA microfluidic chips with integrated metal microelectrodes, Sens. Actuators B **141** (2009) 646-651.

[35] J. H. Wang and M. B. Ray, Application of ultraviolet photooxidation to remove organic pollutants in the gas phase, Sep. Purif. Technol. **19** (2000) 11-20.

[36] D. M. Mattox, Surface cleaning in thin film technology, Thin Sol. Fil. **53** (1978) 81-96.

[37] S. L. Holl, C. A. Colinge, K. D. Hobart, F. J. Kub, UV activation treatment for hydrophobic wafer bonding, J. Electrochem. Soc. **153** (2006) G613-G616.

[38] Z. Tang, P. Peng, T. Shi, G. Liao, L. Nie, S. Liu, Effect of nanoscale surface topography on low temperature direct wafer bonding process with UV activation, Sens. Actuators A **151** (2009) 81-86.

[39] T. Kaspar, A. Tuan, R. Tonkyn, W. P. Hess, J. W. Rogers Jr., Y. Ono, Role of O(1D) in the oxidation of Si(100), J. Vac. Sci. Technol. B **21** (2003) 895-899.

[40] K. Watanabe, E. C. Y. Inn, M. Zelikoff, Absorption coefficients of oxygen in the vacuum ultraviolet, J. Chem. Phys. **21** (1953) 1026-1030.

[41] V. Dragoi, S. Farrens, P. Lindner, Low temperature wafer bonding for MEMS applications, MST News **2** (2004) 40-42.

[42] V. Dragoi, S. Farrens, P. Lidner, J. Weixlberger, Low-temperature wafer bonding for Microsystems applications, Proc. IEEE Int. Semicon. Conf., (2004) 199-202.

[43] A. Schütze, J. Y. Jeong, S. E. Babayan, J. Park, G. S. Selwyn, R. F. Hicks, The atmospheric-pressure plasma jet: a reviewand comparison to other plasma sources, IEEE Trans. Plasma Sci. **26** (1998) 1685-1694.

[44] H. Shinohara, Y. Takahashi, J. Mizuno, S. Shoji, Surface hydrophilic treatment of polyurea film realized by vacuum ultraviolet light irradiation and its application for poly(methylmethacrylate) blood analysis chip, Sens. Actuators B **132** (2008) 374-379.

[45] Catalog of eximer irradiation unit (from homepage of Ushio Inc.): http://www.ushio.co.jp/documents/products/lamp/ushio_excimer_irradiation_unit.pdf (accessed on December 2009)

[46] W. P. Maszara, G. Goetz, A. Caviglia, J. B. McKitterick, Bonding of silicon wafers for silicon-on-insulator, J. Appl. Phys. **64** (1988) 4943-4950.

[47] Homepage of Mitsubishi Rayon Co., Ltd. (in Japanese): http://www.mrc.co.jp/acrylite/spec/index.html (accessed on December 2009)

[48] Homepage of Kuraray Co., Ltd. (in Japanese): http://www.paraglas.jp/art/index.html (accessed on December 2009)

[49] Homepage of SUMIPEX (in Japanese): http://www.sumitomo-chem.co.jp/acryl/025technoloy.html (accessed on December 2009)

[50] Catalog of ZEONEX (from homepage of Zeon Co.): http://www.zeon.co.jp/business_e/enterprise/speplast/zeonex_e_200809.pdf (accessed on December 2009)

[51] H. Shinohara, J. Mizuno, S. Shoji, Fabrication of a microchannel device by hot embossing and direct bonding of poly(methyl methacrylate), Jpn. J. Appl. Phys. **46** (2007) 3661-3664.

[52] G. P. López, D. G. Castner, B. D. Ratner, XPS O 1s binding energies for polymers containing hydroxyl, ether, ketone and ester groups, Surf. Interf. Anal. **17** (1991) 267-272.

[53] A. Chilkoti and B. D. Ratner, An X-ray photoelectron spectroscopic investigation of the selectivity of hydroxyl derivatization reactions, Surf. Interface Anal. **17** (1991) 567-574.

[54] D. K. Owens and R. C. Wendt, Estimation of the surface free energy of polymers, J. Appl. Polym. Sci. **13** (1969) 1741-1747.

[55] http://www007.upp.so-net.ne.jp/y-kondo/surface.htm (accessed on December 2009) (in Japanese)

[56] Homepage of Anasys Instruments Corp.:
http://anasysinstruments.com/ (accessed on December 2009)

[57] Spectral Database for Organic Compounds (SDBS):
http://riodb01.ibase.aist.go.jp/sdbs/cgi-bin/direct_frame_top.cgi (accessed on December 2009)

[58] T. Okajima, K. Teramoto, R. Mitsumoto, H. Oji, Y. Yamamoto, I. Mori, H. Ishii, Y. Ouchi, K. Seki, Polarized NEXAFS spectroscopic studies of poly(butylenes terephthalate), poly(ethylene terephthalate), and their model compounds, J. Phys. Chem. **102** (1998) 7093-7099.

[59] Mori, T. Araki, H. Ishii, Y. Ouchi, K. Seki, K. Kondo, NEXAFS studies on the rubbing effects of the surface structure of polyimides, J. Electron Spectrosc. Relat. Phenom. **78** (1996) 371-374.

[60] M. C. M. Alves and G. Tourillon, Influence of complexation processes on the catalytic properties of some polymer-based cobalt compounds for oxygen electroreduction, J. Phys. Chem. **100** (1996) 7566-7572.

[61] T. Coffey, S. G. Urquhart, H. Ade, Characterization of the effects of soft X-ray irradiation on polymers, J. Electron Spectrosc. Relat. Phenom. **122** (2002) 65-78.

[62] X. Zhang, C. Jacobsen, S. Lindaas, S. Williams, Exposure strategies for polymethyl methacrylate from in situ x-ray absorption near edge structure spectroscopy, J. Vac. Sci. Technol. B **13** (1995) 1477-1483.

[63] H. Schmid, H. Wolf, R. Allenspach, H. Riel, S. Karg, B. Michel, E. Delamarche, Preparation of metallic films on elastomeric stamps and their application for contact processing and contact printing, Adv. Funct. Mater. **13** (2003) 145–153.

[64] Y. Tsukamoto, H. Kuroda, A. Sato, H. Yamaguchi, Microindentation adhesion tester and its application to thin films, Thin Sol. Fil. **213** (1992) 220-225.

Chapter 4

Surface Modification Using Polyurea[*]

4.1 Introduction

Surface modification methods for hydrophilic surface treatment on microchannel surfaces are classified into two categories as shown in Figure 4.1. One is pretreatment before bonding process. Pretreatments for low-temperature direct bonding as described in Chapter 3 are included in this category. The other is post-treatment obtained by filling the liquid reagents into the microchannel after bonding process [7-10]. Since the pretreated surface had not enough hydrophilic durability to be maintained during bonding, post-treatment methods are generally added. However, it is difficult to find out appropriate reagents enabling efficient treatment without damage on plastic surface. Since wettability of the damage-free reagents such as reagents not containing organic solvents on plastic is low, the post-treatment method often takes long time for filling the reagents into whole plastic microchannels. In addition, the method takes long time for completing the hydrophilic reaction on whole surfaces.

In this work, surface modification and low-temperature bonding processes are combined by using VUV/O$_3$[†]-treated aromatic polyurea film as shown in Figure 4.2. Section 4.2 describes the surface control of plastic using polyurea. The surface control method is applied for low-temperature bonding in Section 4.3. In section 4.4, a polyurea-coated microchip for microchip electrophoresis (MCE) is fabricated.

---

[*]This chapter is based on the published papers listed in the reference section [1-6].
[†]Vacuum UV (VUV) treatment under oxygen atmosphere

Pre-treatment

①**Pre-treatment**
(by plasma, UV, ozone,
coating of other materials, etc.)

②**Bonding**

Microchannel

Channel plate   *Lid*

Post-treatment

①*Fabrication of microchannel*   ②*Post-treatment (by filling liquid reagents)*
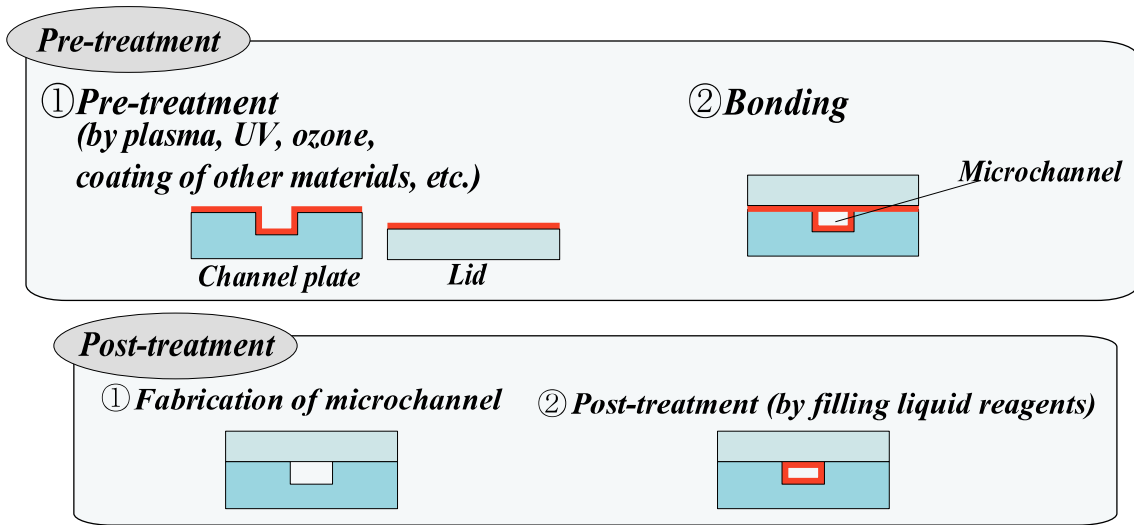
Fig. 4.1: Surface modification methods on microchannel surfaces.

(a)

MDI & MDA

Polyurea

Channel plate   *Lid*

(b)

VUV light (O_2 rich)

(c)

Heat & press
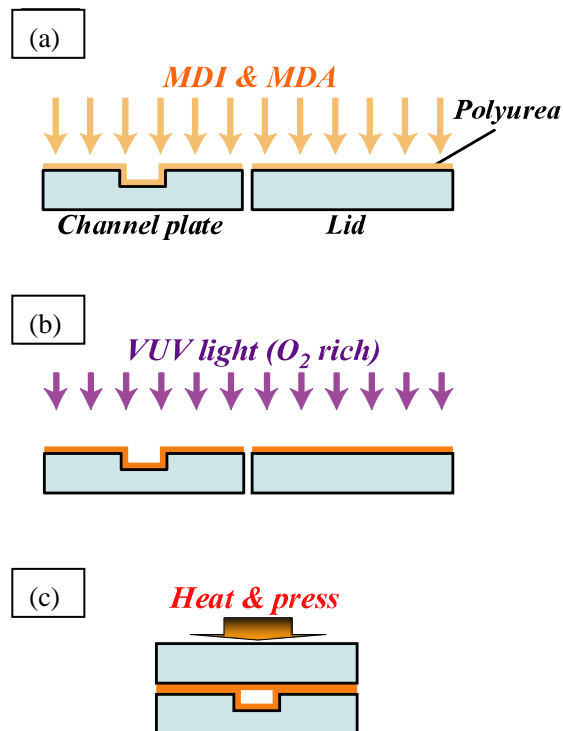
Fig. 4.2: Fabrication process of the polyurea-coated microchip: (a) polyurea coating,
(b) VUV/O_3 treatment, and (c) thermal bonding.

4.2 Surface control of plastic using polyurea

4.2.1 Concept of surface control using polyurea

Aromatic polyurea film is coated on the substrate to hydrophilize the surface [11]. Figure 4.3 shows reaction scheme of aromatic polyurea coated by vapor deposition polymerization [11-15]. Two monomers of 4.4'-diaminodiphenylmethane (MDA) and 4.4'-diphenylmethanediisocyanate (MDI) are heated for evaporation in the process chamber as shown in Figure 4.4. The monomers adsorbed on the surface of a substrate react to copolymerize the aromatic polyurea. The advantages of the polyurea film are its visible transparency, non-toxicity, high purity, and uniform film thickness on microchannel surface. The film can be coated on the substrate so thin that the change in sizes of the microstructures is negligible.
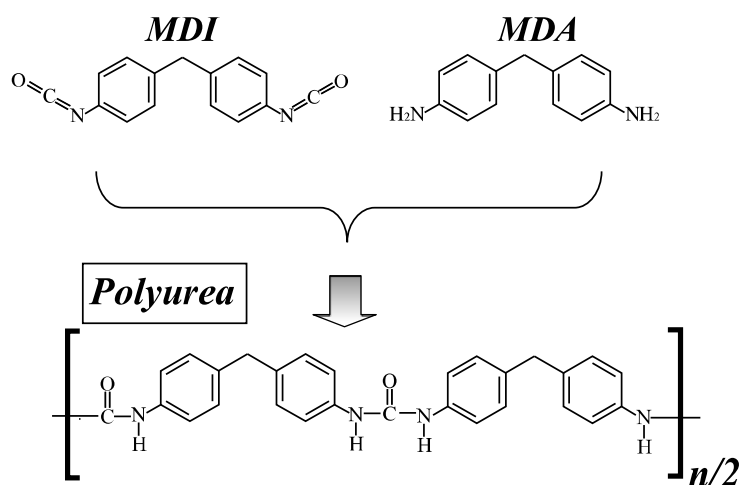
Fig. 4.3: Reaction scheme of aromatic polyurea.

As-deposited polyurea film is low-hydrophilic with water contact angle of about 80 $^\circ$. Highly hydrophilic surface was realized by annealing (50 - 150 $^\circ$C) in O_3 under atmospheric pressure as shown in Figure 4.5 [15]. Figure 4.6 shows changes in water contact angle on O_3-treated polyurea film (thickness: 80 nm) coated on PMMA surface. The O_3-treated film had highly hydrophilic surface, water contact angle was smaller than 30 $^\circ$, and the hydrophilic state on the film kept for long time longer than a month. However, the annealing for hydrophilic surface treatment causes bending of the thermoplastics such as PMMA. On the other hand, the film surface was recovered to hydrophobic after washing by water. For practical microchip applications, surface

stability of the film is required for achieving the reproducibility in observations and measurements.
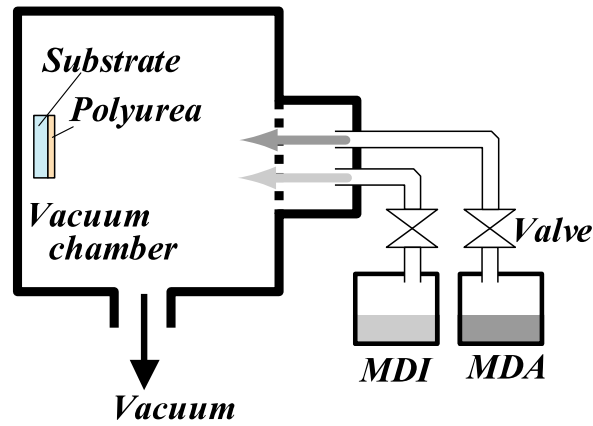
Fig. 4.4: Schematic diagram of equipment for vapor deposition polymerization.
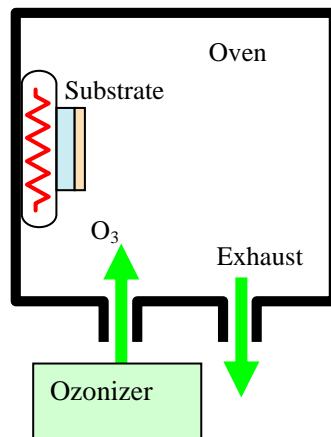
Fig. 4.5: Schematic diagram of conventional hydrophilic surface treatment of polyurea.
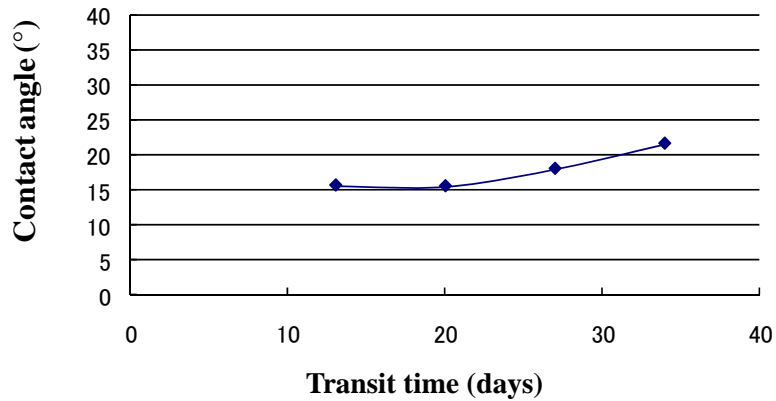
Fig. 4.6: Changes in water contact angle on O_3-treated polyurea film (annealing temperature: 50 $^{\circ}$C) [1].

The author proposes novel surface modification method for hydrophilic surface treatment of polyurea using VUV/O_3 treatment (central UV wavelength of 172 nm). Differences between conventional O_3 treatment and that of VUV/O_3 are listed in Table 4.1. The advantages of the VUV/O_3 treatment are higher density of O_3 and $O(^1D)$, cleaner treatment condition because of under reduced pressure, efficient surface modification by combined effects of O_3, $O(^1D)$, and VUV light, and room temperature process. The deformation of the sample structure and thermal bending are negligible because of its room temperature process. In addition, direct irradiation effect of the VUV light for surface modification is small under oxygen-rich atmosphere. The light intensity on the sample surface decreases, because the UV light is absorbed by oxygen gas in the chamber [16]. Thus, the UV light intensity on the sample surface is controllable by the oxygen pressure p and distance between the light source and the sample surface. O_3 and $O(^1D)$ are only generated near the lamp window and these gases spread over the chamber by diffusion.

Table 4.1: Differences between conventional O_3 treatment and that of VUV/O_3.

Surface treatment	Chamber pressure	Density of O_3 and O(^{1}D)	Annealing temperature (^{o}C)	UV light intensity
O_3	Atmospheric pressure	Low	50 – 150	-
VUV/O_3	Reduced pressure	High	-	Controllable

4.2.2 Experimental procedure

Aromatic polyurea was coated by vapor deposition polymerization on poly-methylmethacrylate (PMMA) surface. Typical preparation conditions were MDA temperature of 100 ^{o}C, MDI temperature of 71 ^{o}C, chamber pressure of approximately 1 × 10^{-3} Pa, the deposition rate of about 10 nm/min, and the substrate temperature of 25 ^{o}C [13]. Thickness of the film was about 140 nm.

VUV/O_3 treatment (equipment: UER20-172 from Ushio Inc.) was carried out with chamber oxygen pressure p of $3.0 \times 10^4 \sim 5.0 \times 10^4$ Pa and treatment time t of 5 ~ 20 min. Oxygen gas was introduced into the chamber after evacuation.

To study the influence of direct VUV irradiation to polyurea, contact angle of de-ionized water droplet on the polyurea at various distances between the lamp window and the sample surface d was measured. To evaluate the long-term stability of hydrophilic state, transit time of water contact angle after VUV/O_3 treatment of the polyurea was measured. In addition, the author also measured water contact angle on the VUV/O_3-treated polyurea before and after washing by ultrasonic cleaning in de-ionized water for 3 min.

4.2.3 Results and discussion

Results of water contact angle measurements at various d are shown in Figure 4.7. The contact angle on the polyurea decreased after VUV/O$_3$ treatment. The contact angle decreased with increasing the distance d, and the smallest contact angle of about 12 $^{\circ}$ was obtained at d = 142 mm. Since the VUV light intensity decreases with distance from the light source, the direct irradiation effect of the VUV light such as cross-linking [13] and over-degradation of polyurea can be avoided.

Figure 4.8 shows water contact angle on the polyurea versus the transit time in various VUV/O$_3$ treatment conditions under the distance d of 142 mm. The treated films kept contact angles smaller than 45 $^{\circ}$ for long time. Especially under the condition of the chamber pressure p of 3.0×10^4 Pa and treatment time t of 20 min, contact angle of smaller than 20 $^{\circ}$ was obtained and kept the state about 2 months. These results in Figure 4.8 indicate that longer t is more important than higher p for hydrophilic treatment. As the treatment time t increased, water contact angle became smaller. Although the chamber pressure is concerned with the volume of O$_3$ and O(^{1}D), the generated volume is saturated at the pressure p higher than 3.0×10^4 Pa.

Figure 4.9 shows measurement results of water contact angle on the O$_3$- and VUV/O$_3$-treated polyurea before and after washing by ultrasonic cleaning in de-ionized water. The O$_3$-treated polyurea was recovered to low-hydrophilic after washing, while the VUV/O$_3$-treated polyurea kept hydrophilic after washing. Especially, contact angle of smaller than 40 $^{\circ}$ after washing was realized with the sample treated within an hour. These results indicate that the VUV/O$_3$-treated polyurea improved surface stability after washing by water.
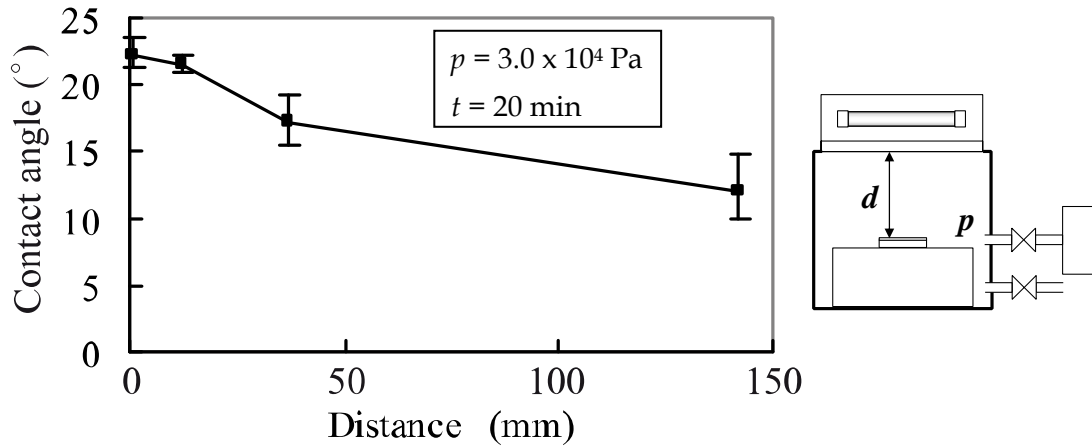
Fig. 4.7: Contact angle of de-ionized water versus distance between the lamp window and the sample d [3].
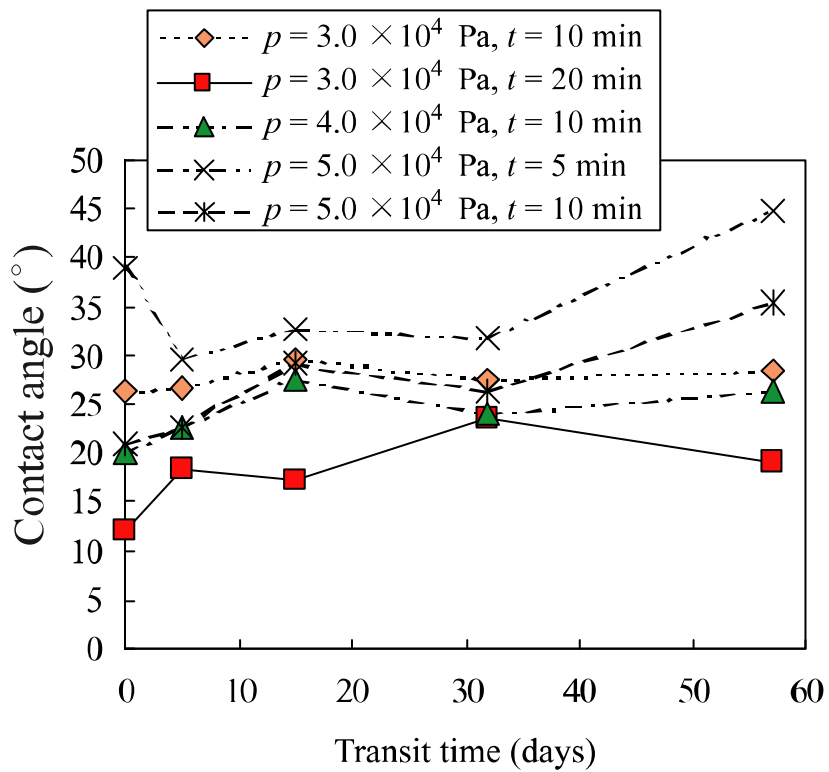
Fig. 4.8: Averaged contact angle of de-ionized water vs. transit time after VUV/O_3 treatment at $d = 142$ mm; p: chamber pressure, t: treatment time [3].
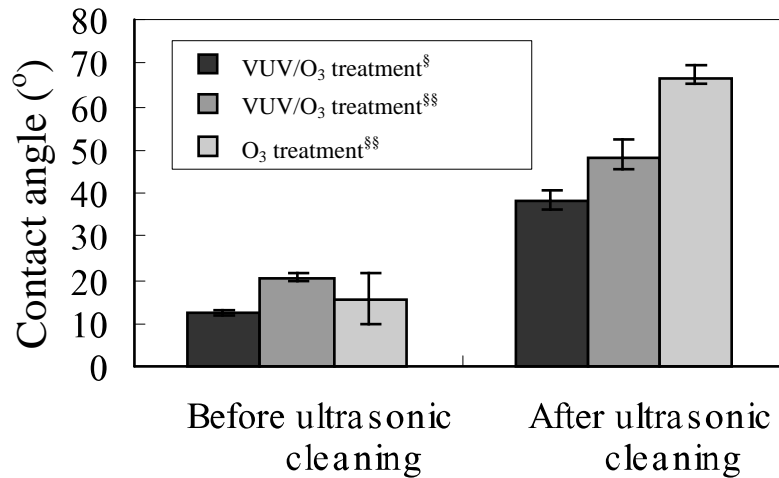
Fig. 4.9: Water contact angle before and after ultrasonic cleaning of de-ionized water at 3 min treated by VUV/O_3 (p = 3.0×10^4 Pa, t = 20 min) at d = 142 mm and conventional O_3 treatment ([§]within 1 h after treatment and [§§]20 days after treatment) [3].

4.3 Application for low-temperature bonding

4.3.1 Concept of low-temperature bonding using polyurea

The author proposes a novel method of low-temperature thermal bonding of plastics using VUV/O_3-treated polyurea film as intermediate layers. In Figure 4.3, the polyurea film of only about five monomers (n = 5) is deposited at room temperature [14]. Further polymerization takes place (n > 5) when the deposited films are annealed by consuming unreacted polymer tails such as NH_2 and N=C=O to form amid bonds [15]. This polymerization occurs at the interface of the two polyurea films during the bonding process. In addition, the generated polar groups by VUV/O_3 treatment cause low-temperature bonding, as in the case of pretreatment in low-temperature direct bonding method described in Chapter 3.

4.3.2 Experimental procedure

Polyurea-coated PMMA was treated by VUV/O_3 under the condition of chamber pressure p of 3.0×10^4 Pa, treatment time t of 20 min. The distance between the VUV lamp window and the polyurea surface d was 142 mm. After the VUV/O_3 treatment, the two plates were brought into contact and then pressed using bonding equipment (EVG520HE). The applied pressure and period were 3 MPa and 20 min.

The bond strength between two polyurea-coated PMMA plates was evaluated by tensile test explained in chapter 3. Bare PMMA plates were used as substrates. Thickness of the polyurea film was about 120 nm.

To investigate the bonding mechanism and annealing effects, surface free energy calculation according to Owens-Wendt theory [17] and X-ray photoelectron spectroscopy (XPS) analyses were carried out for the polyurea surface. For comparison with other low-temperature bonding methods, water contact angles on the plastic plates of cyclo-olefin polymer (COP (Zeonex480)) and PMMA (Comoglass) were also measured. Three kinds of plates were tested, before treatment, after O_2 plasma treatment, and after O_2 plasma treatment and annealing for 20 min. The surface pretreatments were carried out under the same conditions as those of the low-temperature direct bonding explained in Chapter 3.

4.3.3 Results and discussion

Void-free bonding was done at a bonding temperature of 85 $^{\circ}$C. The bond strength measured by the tensile test was 0.60 ± 0.09 MPa. The strength is larger than that of conventional PMMA direct bonding at a temperature of 95 $^{\circ}$C without any surface treatment or coating [19]. The two plates were not bonded at a bonding temperature of 50 $^{\circ}$C. This result indicates that the annealing plays an important role in bonding. Figure 4.10 shows a photomicrograph of the removed surface after the tensile test. Polyurea film peeled from the PMMA surface in some areas. It indicates that the adhesion strength between the polyurea film and the PMMA plate is not enough. To increase the adhesion strength, pretreatment with plasma or UV on the PMMA plate before coating the polyurea will be necessary.
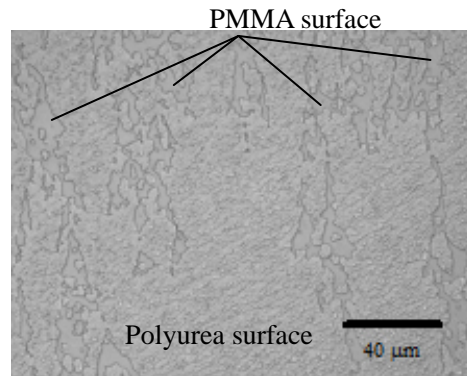
Fig. 4.10: Photomicrograph of the removed surface after the tensile test of the polyurea-bonded sample [5].

The contact angle measurements on the polyurea surface are shown in Figure 4.11. After VUV/O$_3$ treatment, contact angles of water, glycerin, and formamide decreased dramatically, and the contact angles kept even after annealing of 85 ^{o}C for 20 min. The highly hydrophilic surface of the microchannel was also formed after the thermal bonding at 85 ^{o}C.

Figure 4.12 shows calculated surface free energy (γ_s), its polar (γ_s^p) and dispersive (γ_s^d) components of the polyurea. After the VUV/O$_3$ treatment, the γ_s^p was increased significantly, while the γ_s^d was decreased. The additional new polar groups were created after the treatment. After annealing, the γ_s^p was decreased while the γ_s^d was increased.
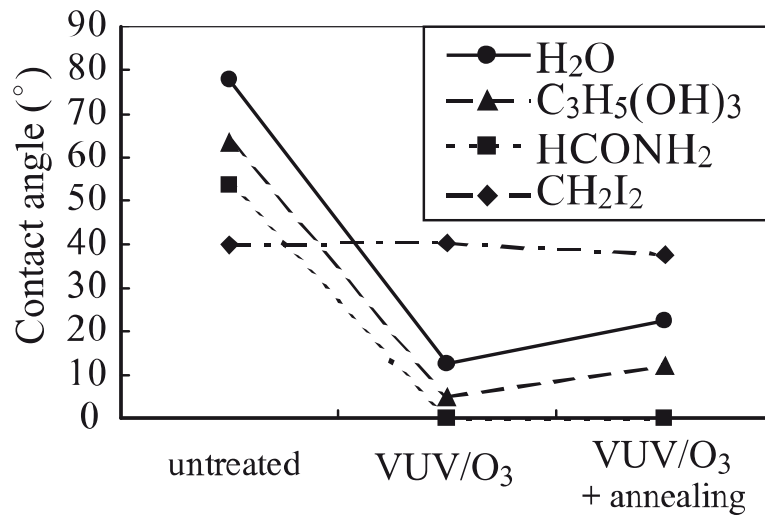
Fig. 4.11: Averaged contact angle of water, glycerin, formamide, and diiodomethane on the polyurea surface before and after VUV/O_3 treatment and annealing of 85 ^{o}C for 20 min [5].
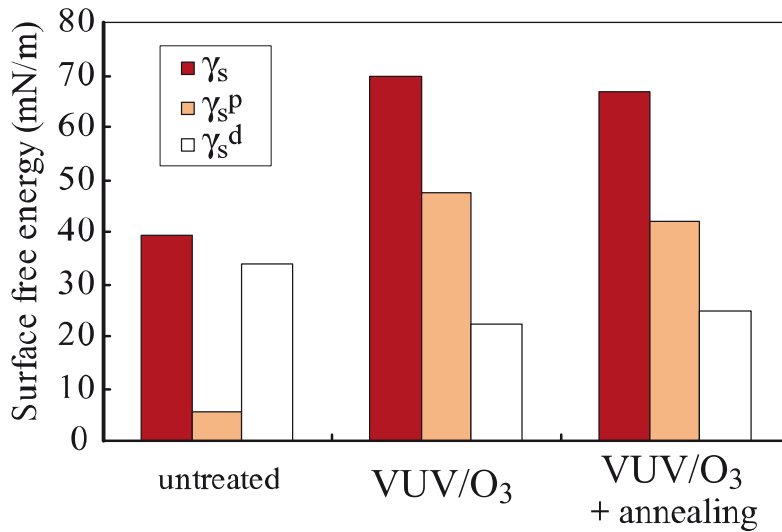
Fig. 4.12: Calculated surface free energy (γ_s), its polar component (γ_s^p), and its dispersive component (γ_s^d) on the polyurea surface before and after VUV/O_3 treatment and annealing of 85 ^{o}C for 20 min [5].
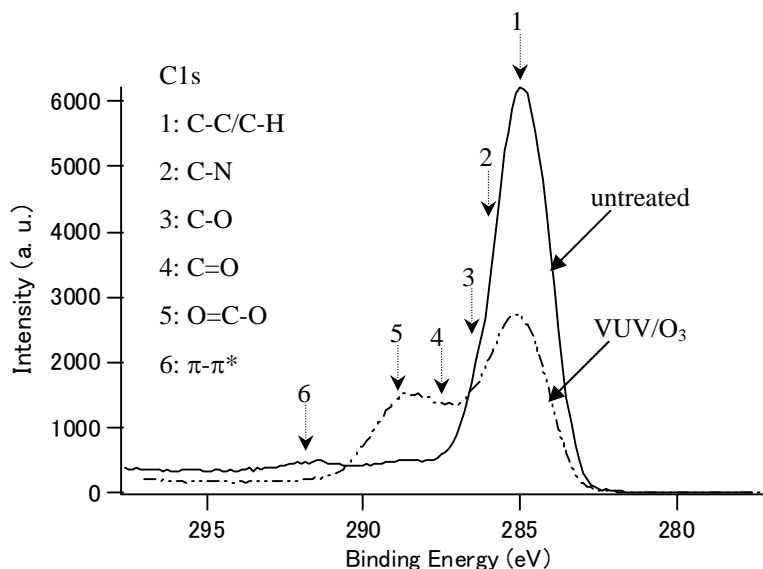
Fig. 4.13: C1s XPS spectra of polyurea before and after VUV/O₃ treatment.

Fig. 4.13 shows C1s XPS spectra of polyurea before and after VUV/O₃ treatment. After treatment, the free C=O peak was increased while the C-C/C-H peak was decreased. C-O (ether or and O-C=O (carboxylic acids or esters) peaks were newly generated. This result follows the surface free energy measurements in Fig. 4.10. These peaks are expected to be originated in -C=O, -CO, -OH, and -COOH. In addition, π-π* peak originated in benzene ring was disappeared after the treatment. This result indicates that the cleavage of the C-C bond in benzene ring was occurred after the treatment [16,19-21]. Oxygen atoms easily attach at the cleaved sites.

The annealing can affect two possible characteristics. One is that hydrogen bond and/or -C-O-C- bond can be generated by dehydration reaction of nearby polar groups such as -OH and -COOH. The other is that unreacted polymer tails of NH_2 and N=C=O were consumed by further polymerization during the annealing. These transformations and polymerization also occurred at the interface of the two polyurea films during the bonding process.

Figure 4.14 shows water contact angle in three conditions on VUV/O$_3$-treated polyurea, oxygen plasma-treated COP, and oxygen plasma-treated PMMA. In the case of the COP, a highly hydrophilic surface (~20 $^\circ$) was realized after O$_2$ plasma treatment. However, the hydrophilic surface was not maintained after the annealing. In the case of the PMMA, the treatment effect was small. From these results, the bonding using the polyurea as the intermediate layer is the best method from the hydrophilicity point of view.
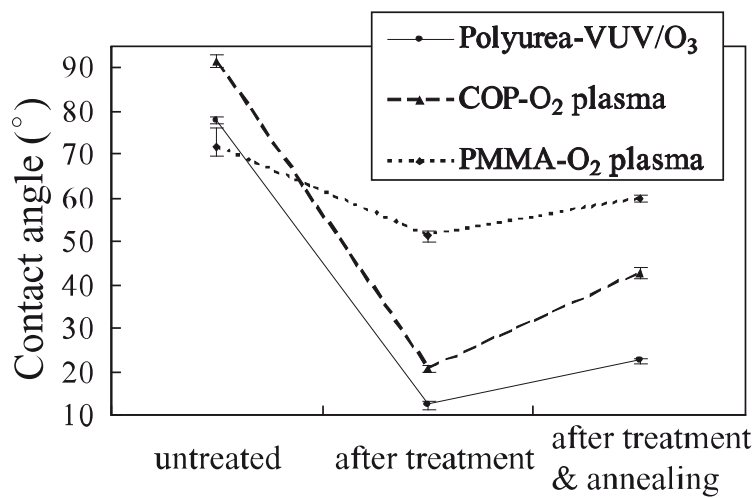
Fig. 4.14: Water contact angle in three conditions (untreated, after treatment, after treatment and annealing of 85 $^\circ$C for 20 min) on VUV/O$_3$-treated polyurea, oxygen plasma-treated COP (P = 100 W, p = 40 Pa, t = 30 sec), and oxygen plasma-treated PMMA (P = 200 W, p = 80 Pa, t = 30 sec) [5]. P: plasma power, p: chamber pressure (oxygen-rich), t: treatment time.

4.4 Application for microchannel fabrication

4.4.1 Experimental procedure

Polyurea-coated PMMA microchip was fabricated by the bonding method explained in Section 4.3. Fabrication process was shown in Figure 4.2. The polyurea was coated on the channel plate and the lid by vapor deposition polymerization (Figure 4.2 (a)). The two plates were made of PMMA. The channel plate was fabricated by hot embossing method described in Chapter 2. Next, the polyurea-coated plates were treated with VUV/O_3 (Figure 4.2 (b)). After VUV/O_3 treatment, the two plates were bonded (Figure 4.2 (c)). The bonding temperature was 85 $^{\circ}$C, and the pressure and period were 3 MPa and 20 min.

A MCE microchip with cross-junction structure was fabricated by this method. The microchannel was 50 μm wide and 19 μm deep. To confirm the compatibility for biogenic compounds, 500 ppm fluorescence-labeled bovine serum albumin (BSA) and borate buffer (pH 9.0) were introduced into the microchannels and keep for 30 min. MCE analysis was carried out using 10 ppm BSA and 10 mM borate buffer (pH 9.0).

4.4.2 Results and discussion

Figure 4.15 shows design and photographs of a prototype polyurea-coated PMMA microchip. The microchannels were 50 μm wide and 19 μm deep. It had a Y-junction, a cross-junction, a T-junction and six ports (diameter: 2 mm). Void-free bonding was realized over the whole sample surface. Since the bonding temperature is lower than the T_g of the PMMA, negligible deformation of the channel structure is obtained. To observe its flow behavior, a 5-μL methylene blue aqueous solution droplet was applied onto a port (as indicated black arrow in Figure 4.15 (a)) on the fabricated microchip. Its flow behavior at the cross-junction is shown in Figure 4.16. All the microchannels were filled by capillary force. There was no leakage or obstacles to smooth fluidic flow at the bonded interface. This result indicates that the fabricated microchip realized enough bond strength for actual use.
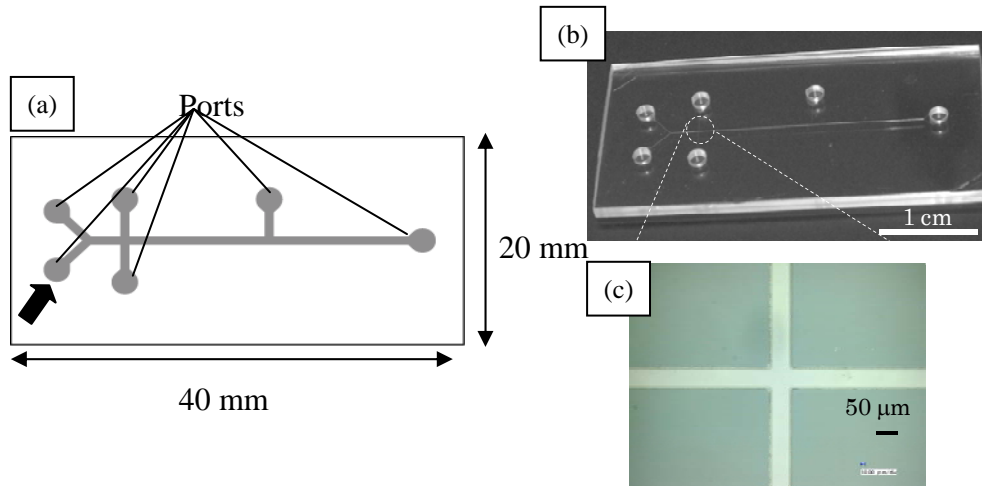
Fig. 4.15: Prototype polyurea-coated microchip: (a) design, (b) whole view, and (c) magnified view at cross-junction [5]. The black arrowed port in (a) was used for introducing methylene blue aqueous solution.

Fig. 4.16: Flow behavior at the Y-junction, the cross-junction and the T-junction in the fabricated microchip using methylene blue aqueous solution [5].

Figure 4.17 shows fluorescent photomicrographs of the microchannels with and without VUV/O$_3$-treated polyurea coating after washing by water. The adhesion of BSA was significant in the conventional unmodified and uncoated PMMA chip (Figure 4.17 (a)), while almost no adhesion was observed in the modified polyurea-coated chip (Figure 4.17 (b)). Fig. 4.18 shows the results of MCE of VUV/O$_3$-treated polyurea coated and uncoated PMMA microchannels. The uncoated microchannel detected the BSA as a broad peak (Figure 4.18 (a)), while the polyurea-coated microchannel detected

as a sharp peak (Figure 4.18 (b)). The theoretical plate number (N)[‡] of polyurea-coated microchannel was about 600. It is six times larger than that of uncoated PMMA microchannel [22]. The sharp peak was realized by negligible adhesion of BSA. Fast migration speed in a positive direction (approximately 1 mm/s) was also observed in polyurea-coated microchip. This result indicates that VUV/O$_3$-treated polyurea surface on the microchannel is negatively charged with high concentrated polar groups of -OH or -COOH. These results indicate that this polyurea-coated microchannel is applicable for high speed MCE analysis.
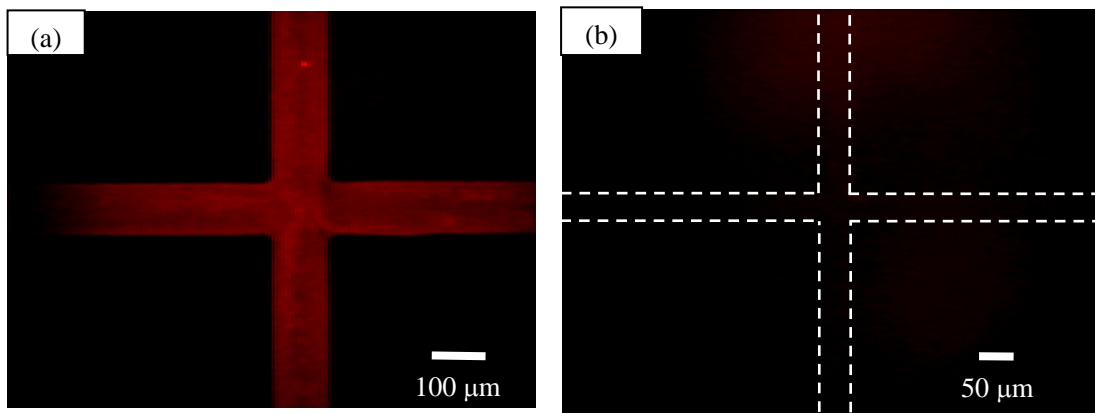
Fig. 4.17: Fluorescent photomicrographs of the (a) unmodified and (b) modified polyurea-coated PMMA microchips after BSA exposure for 30 min [6].
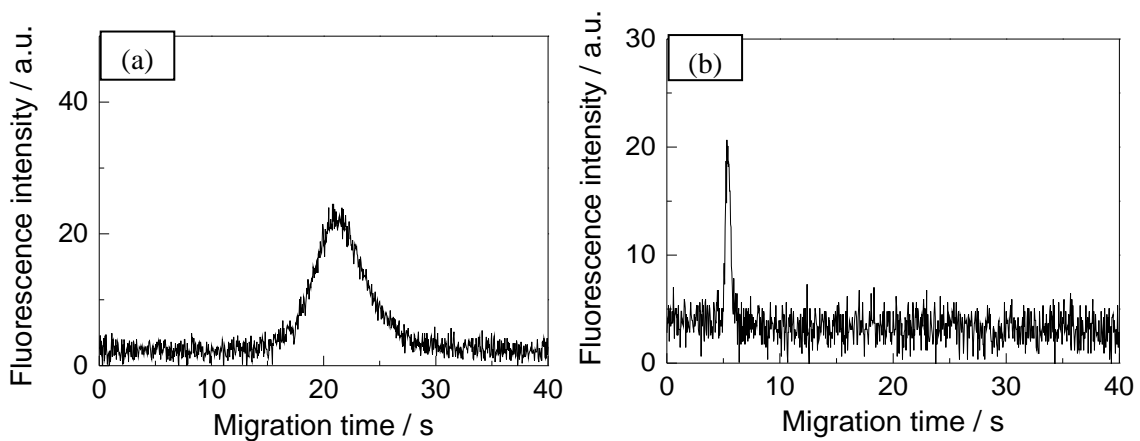
Fig. 4.18: Electropherograms of BSA on the (a) unmodified, (b) modified polyurea-coated PMMA microchips [6].

[‡]a barometer of separation efficiency: $N = 5.54 \, (t_r / W_h)^2$
(t_r: retention time, W_h: half peak height) [23]

4.5 Conclusion

The author developed a novel surface control method using aromatic polyurea film for hydrophilic surface treatment of plastic. The polyurea coated on plastic was changed into highly hydrophilic after VUV/O_3 treatment; water contact angle on the surface was smaller than 20 $^{\circ}$. The treated film kept highly hydrophilic surface for about 2 months. The highly hydrophilic polyurea surface was stable and was kept even after very hard condition of ultrasonic cleaning in de-ionized water.

The method of the hydrophilic surface treatment of polyurea can be applied for low-temperature bonding of plastics. The VUV/O_3-treated polyurea film was used as intermediate bonding layers. A microchannel with a highly hydrophilic surface was realized by the VUV/O_3 treatment. The highly hydrophilic surface of the microchannel was retained even after the thermal bonding process. There was no leakage or obstacles to fluidic flow at the bonded interface. This polyurea-coated microchannel is applicable for high speed electrophoresis analysis.

This is the world's first method to realize highly-stable hydrophilic surface by means of low-temperature bonding. In actual use, post-hydrophilic treatment after bonding can be skipped. This method has remarkable advantages for the fabrication of low-cost PMMA chemical/biochemical microchips.

References

[1]　H. Shinohara, J. Mizuno, G. Tazaki, T. Nishi, M. Nakajima, C. Takahashi, S. Shoji, PU Coated PMMA blood analysis chip, Proc. The 5th Int. Symp. Microchem. Microsys. (ISMM), (2005) 114-115.

[2]　H. Shinohara, Y. Takahashi, T. Nishi, K. Uemura, C. Takahashi, J. Mizuno, S. Shoji, Surface hydrophilic polyurea film for PMMA blood analysis chip realized by vacuum ultraviolet light irradiation, Proc. The 14th Int. Conf. Solid-State Sens. Actuators and Microsys. (Transducers), (2007) 291-294.

[3]　H. Shinohara, Y. Takahashi, J. Mizuno, S. Shoji, Surface hydrophilic treatment of polyurea film realized by vacuum ultraviolet light irradiation and its application for poly(methylmethacrylate) blood analysis chip, Sens. Actuators B **132** (2008) 374-379.

[4]　H. Shinohara, Y. Takahashi, J. Mizuno, S. Shoji, Post-hydrophilic treatment free plastic biochip fabrication method using polyurea film, Proc. The 21st IEEE Int. Conf. Micro Elec. Mech. Sys. (MEMS), (2008) 367-370.

[5]　H. Shinohara, Y. Takahashi, J. Mizuno, S. Shoji, Fabrication of post-hydrophilic treatment-free plastic biochip using polyurea film, Sens. Actuators A **154** (2009) 187-191.

[6]　F. Kitagawa, K. Kubota, H. Shinohara, T. Takahashi, J. Mizuno, S. Shoji, K. Otsuka, The 89th Annual Meeting of CSJ (2009) 2G6-40 (in Japanese).

[7]　J. Liu, T. Pan, A. T. Woolley, M. L. Lee, Surface-modified poly(methyl methacrylate) capillary electrophoresis microchips for protein and peptide analysis, Anal. Chem. **76** (2004) 6948-6955.

[8]　H. Bi, W. Zhong, S. Meng, J. Kong, P. Yang, B. Liu, Construction of a biomimetic surface on microfluidic chips for biofouling resistance, Anal. Chem. **78** (2006) 3399-3405.

[9]　F. Kitagawa, K. Kubota, K. Sueyoshi, K. Otsuka, One-step immobilization of cationic polymer onto a poly(methyl methacrylate) microchip for high-performance electrophoretic analysis of proteins, Sci. Tech. Adv. Mater. **7** (2006) 558-565.

[10] F. Kitagawa, K. Kubota, K. Otsuka, One-step preparation of amino-PEG modified PMMA microchips for electrophoretic separation of biogenic compounds, Proc. The 12th Int. Conf. Miniaturized Sys. Chem. Life Sci. (Micro-TAS), (2008) 1138-1140.

[11] JP2005-213545 (in Japanese).

[12] Y. Takahashi, M. Iijima, E. Fukada, Pyroelectricity in poled thin films of aromatic polyurea prepared by vapor deposition polymerization, Jpn. J. Appl. Phys. **28** (1989) L2245-L2247.

[13] M. Sato, M. Iijima, Y. Takahashi, Photoresist characteristics of polyurea films prepared by vapor deposition polymerization, Jpn. J. Appl. Phys. **33** (1994) L1721-L1724.

[14] X. S. Wang, M. Iijima, Y. Takahashi, E. Fukada, Dependence of piezoelectric and pyroelectric activities of aromatic polyurea thin films on monomer composition ratio, Jpn. J. Appl. Phys. **32** (1993) 2768-2773.

[15] Y. Takahashi, S. Ukishima, M. Iijima, E. Fukada, Piezoelectric properties of thin films of aromatic polyurea prepared by vapor deposition polymerization, J. Appl. Phys. **70** (1991) 6983-6987.

[16] A. Hozumi, H. Inagaki, T. Kameyama, The hydrophilization of polystylene substrates by 172-nm vacuum ultraviolet light, Collo. Interf. Sci. **278** (2004) 383-392.

[17] D. K. Owens and R. C. Wendt, Estimation of the surface free energy of polymers, J. Appl. Polym. Sci. **13** (1969) 1741-1747.

[18] H. Shinohara, J. Mizuno, S. Shoji, Fabrication of a microchannel device by hot embossing and direct bonding of poly(methyl methacrylate), Jpn. J. Appl. Phys. **46** (2007) 3661-3664.

[19] J. K. Stille, R. L. Sung, J. V. Kooi, The reaction of benzene in a radiofrequency glow discharge, J. Org. Chem. **30** (1965) 3116-3119.

[20] J. Friedrich, I. Loeschcke, H. Frommelt, H.-D. Reiner, H. Zimmermann, P. Lutgen, Ageing and degradation of poly(ethylene terephthalate) in an oxygen plasma, Polym. Degrad. Stab. **31** (1991) 97-114.

[21] S. B. Amor, M. Jacquet, P. Fioux, M. Nardin, XPS characterization of plasma treated and zinc oxide coated PET, Appl. Surf. Sci. **255** (2009) 5052-5061.

[22] F. Kitagawa, K. Kubota, K. Otsuka, One-step preparation of amino-PEG modified PMMA microchips for electrophoretic separation of biogenic compounds, Proc. The 12th Int. Conf. Miniaturized Sys. Chem. Life Sci. (Micro-TAS), (2008) 1138-1140.

[23] Homepage of Shimadzu Co. (in Japanese)
http://www.an.shimadzu.co.jp/hplc/support/lib/lctalk/34/34tec.htm (accessed on January 2010)

Chapter 5

<u>Plastic Chemical/Biochemical Microchips</u>[*]

5.1 Plastic micro direct methanol fuel cell (μDMFC)

5.1.1 Introduction

Conventional micro direct methanol fuel cell (μDMFC) was fabricated on the Si or glass substrates [8,9]. Design of Si-μDMFC is shown in Figure 5.1. This design is different from the conventional bipolar structure that the anode and cathode channels are made on two separate substrates and stacked with a polymer electrolyte membrane (PEM). Main features of the device are a plane structure and integration of the anodes and the cathodes side by side onto a polymer substrate. This simple structure enables easy fabrication including the assembly of PEM. This device has two micro channels for introducing new fuel solution and oxidant solution to the reaction area continuously to achieve high performance. The sidewall of the channel is tapered (about 35 °) for easy patterning of electrode on the channel. The tapered channel is formed by KOH anisotropic etching [9].

In view of cost reduction, plastic micro devices were requested in actual use. The author chooses cyclo-olefin polymer (COP) as the plastic material because of its high chemical durability and easy metallization of the electrodes. In order to achieve high power density, 3-D electrodes which increase the catalyst surface area keeping the total size are employed.

---

[*]This chapter is based on the published papers listed in the reference section [1-7].
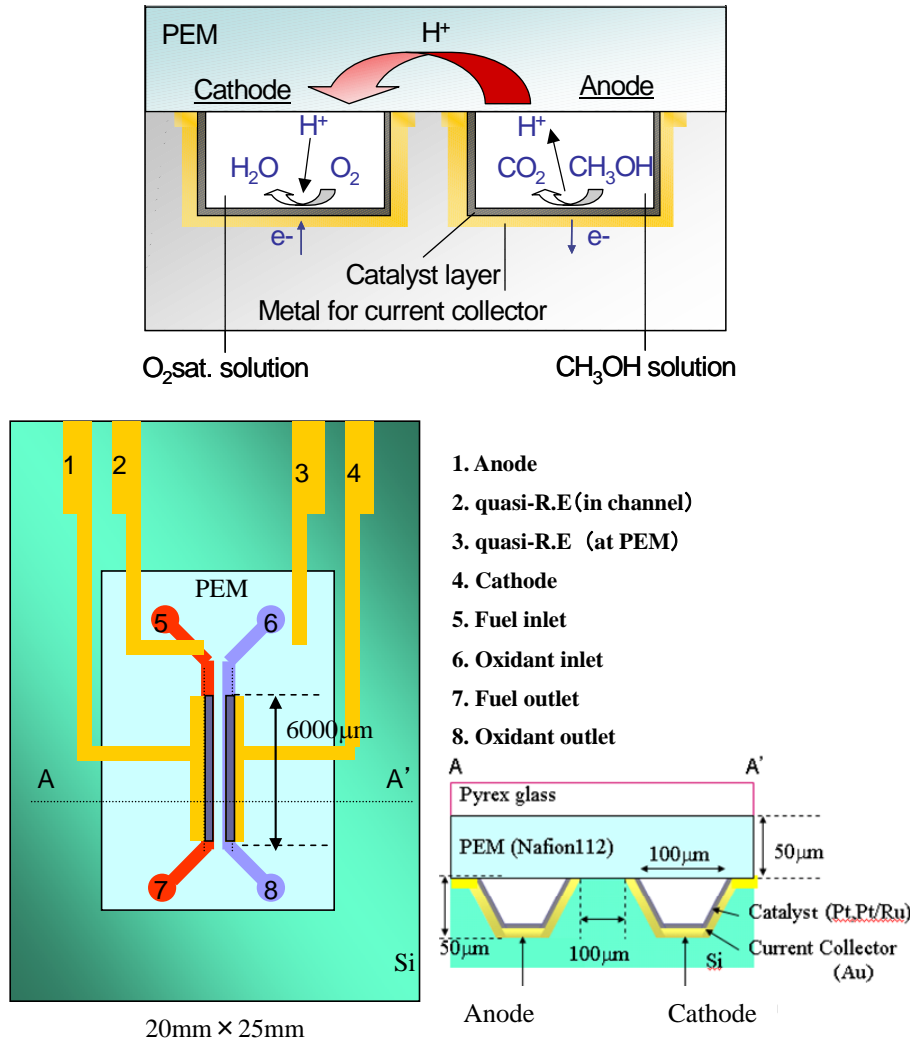
Fig. 5.1: Design of Si-μDMFC [8,9].

5.1.2 Experimental procedure

Fabrication process of COP-μDMFC is shown in Figure 5.2. To use conventional Si-μDMFC design without change, Ni electroplating process was incorporated, and the Ni was used as a mold. First, a (100)-Si wafer was etched anisotropically by KOH solution as in the case of the Si-μDMFC [9]. A seed layer was coated on the substrate (Figure 5.2 (a)). After electroplating of Ni on the substrate (Figure 5.2 (b)), Si was removed by KOH etching (Figure 5.2 (c)). Hot embossing of the COP substrate was performed using hot embossing equipment (EVG520HE from EV Group Co.) (Figure 5.2 (d)). After coating an Au layer on the embossed surface (Figure 5.2 (e)), a photoresist was patterned on the 3-D topographic structures by spray coating and

photolithography methods [9] (Figure 5.2 (f)). Au electrode pattern were formed by wet etching. Catalyst layers of the anode and cathode were formed by electroplating Pt-Ru for the anode and Pt for the cathode, onto the Ti/Au 3-D electrodes (Figure 5.2 (g)). Finally the μDMFC was assembled by placing a PEM membrane between the silicon substrate and the glass cover. These three layers were clamped mechanically (Figure 5.2 (h)).

 The performance of the μDMFC was tested at room temperature using 2M methanol/0.5 M sulfuric acid/H_2O as the fuel and O_2-sat/0.5 M sulfuric acid/H_2O as the oxidant. The O_2 saturated solution was prepared by using oxygen bubbling into 0.5 M sulfuric acid/H_2O solution. The supply of fuel and oxidant was made by a micro syringe pump connected to the fabricated μDMFC unit.
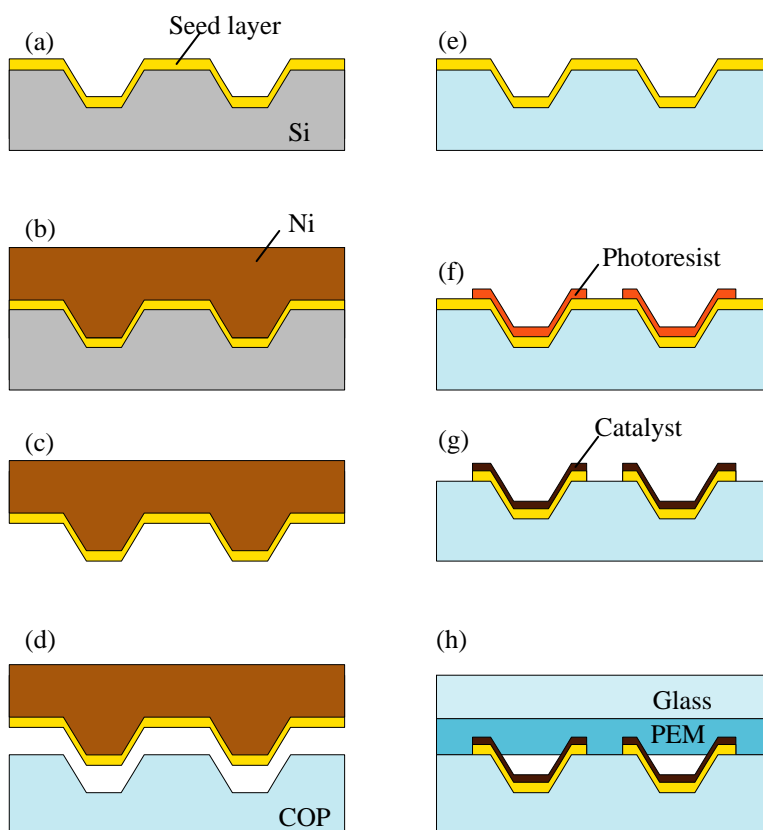
Fig. 5.2: Fabrication process of a COP-μDMFC: (a) wet etching of Si and coating seed layer, (b) Ni electroplating, (c) removal of Si, (d) hot embossing, (e) Au evaporation, (f) photoresist patterning, (g) Au wet etching and electrodeposition of catalysts and (h) assembly.

5.1.2 Results and discussion

The photograph of the plastic μDMFC is shown in Figure 5.3. Figure 5.4 shows the cell voltage and power density vs. current density of the prototype device at the oxidant and fuel flow rate of 10 mL/min. The open circuit voltage of 237 mV and the maximum power density of 0.04 mW/cm² were obtained. In order to realize micro power sources, large numbers of μDMFC are going to be integrated serially on a substrate. This technique can apply to the COP-μDMFC array chip which has many cells in parallel.
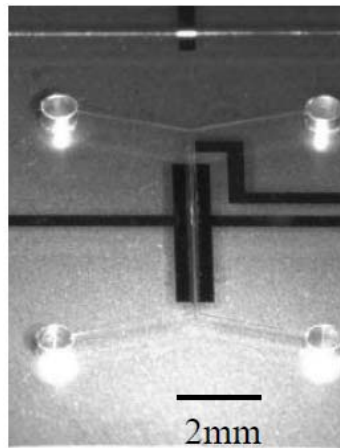
Fig. 5.3: Photograph of the COP-μDMFC (before assembled) [1].
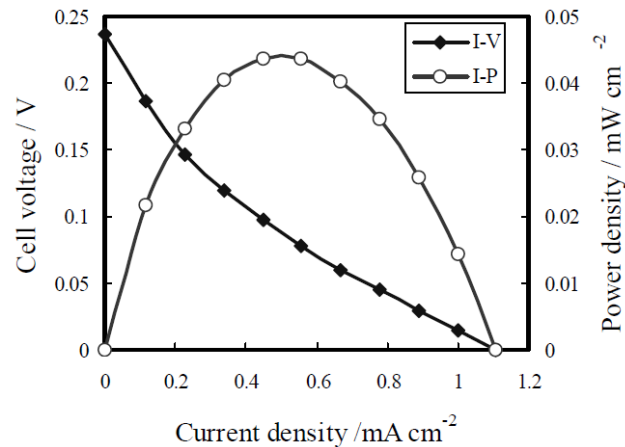
Fig. 5.4: Power generation characteristic of fabricated μDMFC [1].

5.2 MCE-ESI-MS microchip

5.2.1 Introduction

Mass spectrometry (MS) is one of the useful detection methods for microchip electrophoresis (MCE). The advantages of combining MCE and MS (MCE-MS) include high sensitivity, no need for the derivatization of samples and valuable for the analysis of complex mixtures such as biomedical samples. In many cases, the electrospray ionization (ESI) method is used as an interface of MCE-MS (MCE-ESI-MS) [10-15]. Tapered capillary of a spray nozzle was generally connected directly to the channel outlet [12-15]. To generate stable electrospray, ESI voltage is applied through a liquid junction [12-14] or at a spray nozzle having conductive coating [15]. However, there are a few technical problems caused by the dead volume at a connecting joint between the spray nozzle and the microchip. Efficiency of the spray strongly depends on the structure of the nozzle. The conventional microchips for MCE–ESI-MS are generally expensive because the chips were mainly made of glass or quartz. A few polymer ESI-MS chips have been reported. Svedberg et al. [16] fabricated directly from the end of the microchips that were made of polycarbonate (PC) or poly-methylmethacrylate (PMMA) with injection molding. The emitter tip was coated with either polymer-embedded gold particles or graphite particles as the conducting layer for applying ESI voltage. A syringe pump was used for introducing the sample and stable flow rate. Arscott et al. [17] fabricated a microchip which has a free-standing micro-nib made of an epoxy-based negative photoresist SU-8 and a silicon wafer which supported the nib-structure. This chip had no lid and a sample droplet was placed on the reservoir. The ESI voltage was applied via the droplet directly using a Pt wire. Chiou et al. [18] fabricated an ESI nozzle which had no dead volume between the spray nozzle and the microchannel using poly-dimethylsiloxane (PDMS) casting techniques. The ESI voltage was applied through a Pt wire embedded with the PDMS chip. Since these three ESI-MS chips did not have MCE channels, no MCE–ESI-MS analysis results were reported in these references.

In this section, a COP microchip for MCE-ESI-MS is fabricated by hot embossing and low-temperature direct bonding. An ESI emitter tip is fabricated directly on the opening of a separation channel. Stable ESI is achieved at low flow rate without external pump. Since the structure of the nano-electrospray tip enables neglected dead volume in the ESI interface, an efficient spray of a sample solution and higher separation efficiency are expected. MCE-ESI-MS analysis is demonstrated

by using the microchip.

5.2.2 Experimental procedure

Design of the microchip

Figure 5.5 shows design of MCE-ESI-MS microchip. The microchip consists of a conventional cross-type microchannel for MCE separation and a nanospray tip for ESI. An Au electrode was formed around the nanospray tip. The ESI emitter tip was formed directly at the separation channel outlet. Dimensions of the channel are 50 μm in width and 20 μm in depth and 30 mm in length. The width of the outlet channel tapers from 50 μm to 10 μm.

Fabrication process

Fabrication process of the MCE-ESI-MS microchip is shown in Figure 5.6. A silicon mold with the conventional cross-type channel configuration for the MCE separation was fabricated by photolithography and deep-reactive ion etching (Deep-RIE). The microchannel pattern was fabricated by embossing a COP plate (Zeonex480) (Figure 5.6 (a)). The embossing temperature was 165 $^{\circ}$C, and the press strength of 1400 N was applied for 4 min. The dimensions of the COP plate were 12.5 mm × 40 mm × 1 mm. To prevent from bending of the COP plate caused by thermal stress after hot embossing, ten through holes (diameter 2 mm) were drilled on non-embossing area before hot embossing (see Fig. 5.8 (a)). Then, the surface of the microchannel plate and a COP lid are treated by an O_2 plasma activation bonding system (EVG810LT). The dimensions of the lid were 12.5 mm × 40 mm × 1 mm. The treatment was carried out at 100W plasma power and chamber pressure of 0.4 mbar for 30 sec. Direct bonding between the substrates each other was performed under contact force of 1000N at 120 $^{\circ}$C (lower than glass transition temperature (T_g) of the COP) for 5 min using EVG520HE (Figure 5.6 (b)). After bonding, the ESI emitter was machined directly on the COP chip. The tapered tip was structured by a circular saw (Figure 5.6 (c)). Four microchips were fabricated by changing the tip angle α of 180 $^{\circ}$ (non-tapered), 90 $^{\circ}$, 60 $^{\circ}$, and 30 $^{\circ}$. The Au emitter electrode around the spray tip is formed by electron beam evaporation (Figure 5.6 (d)). Thickness of the Au film was 200 nm. To reduce the size of droplets formed at the spray tip, hydrophobic surface around the nozzle is effective. The surface of the Au electrode was modified with alkanethiol by soaking it in 1% mercaptooctadecane in methanol for 30 min. Finally, the surface of Au was washed by ethanol and water.
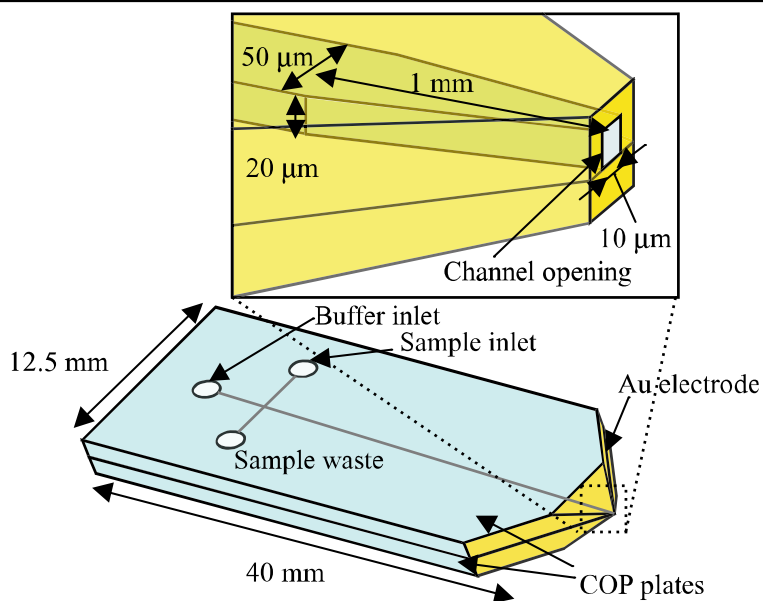
Fig. 5.5: Design of MCE-ESI-MS microchip [3].
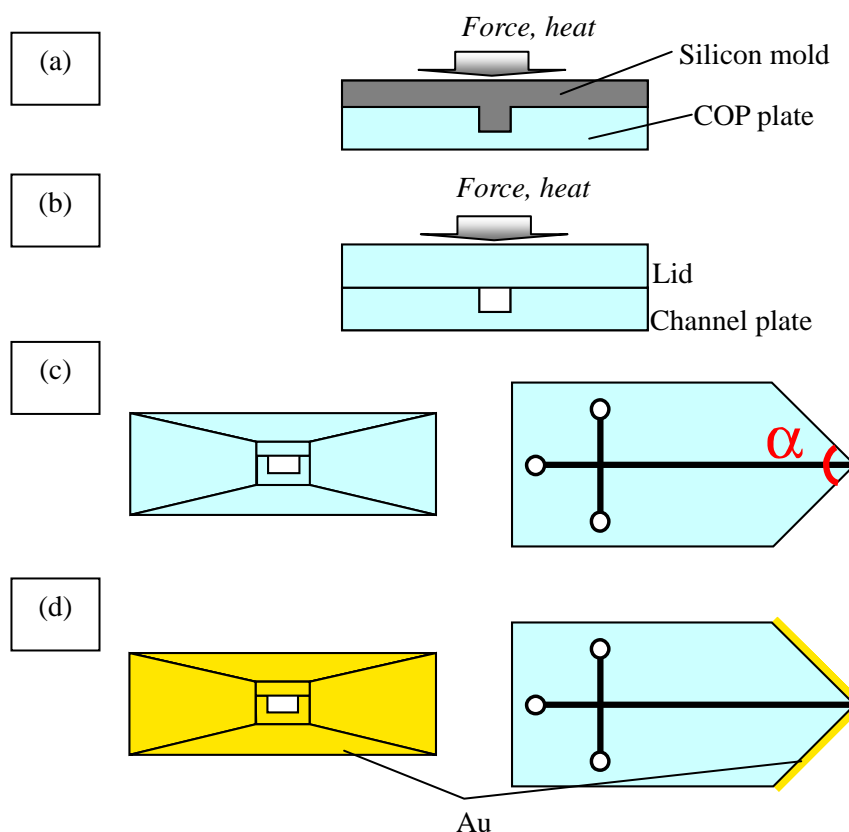
Fig. 5.6: Fabrication process of the MCE-ESI-MS microchip; (a) hot embossing, (b) low-temperature direct bonding, (c) tip structuring: elevational view (left) and top view (right), and (d) Au evaporation [3].

ESI experiments

The COP MCE–ESI-MS microchip was evaluated in ESI experiments including observation of the Taylor cone formation, the infusion analysis, and MCE–ESI-MS analysis using mass spectrometer. Schematic diagram of the experimental setup is shown in Figure 5.7. The target grounded electrode (MS orifice) was spaced a few millimeters from channel opening. V_{SEP} is defined as the potential difference between the buffer inlet and the ESI electrode as shown in Figure 5.7. V_{ESI} is defined as the applied voltage to the ESI electrode.

For observation of the Taylor cone[‡], 20 mM phosphate buffer liquid was used as the sample solution. The V_{SEP} was 1.0 kV, and the V_{ESI} was 2.0 kV. The estimated flow late by measuring the electroosmotic flow (EOF) as reported by Sze et al. [20] was about 0.1 μL/min. The difference in the tip angles α was also observed.

For the infusion analysis with electroosmotic flow, 1000 ppm caffeine (Mw 194) in 10 mM ammonium acetate was continually infused. The V_{SEP} was 1.0 kV, and the V_{ESI} was 1.8 kV. Ionized caffeine was detected by a quadrupole mass spectrometer (LCMS-2010A from Shimadzu Co.).

For the MCE-ESI-MS analysis, 1000 ppm arginine (Mw 174) and caffeine (Mw 194) in 10 mM ammonium acetate were used as sample solutions. The V_{SEP} was 1.3 kV, and the V_{ESI} was 1.8 kV. The sample solutions were injected into the separation channel by the gated injection technique.

For stability and reproducibility test, MCE-ESI-MS analysis was carried out repeatedly, by using caffeine in 10 mM ammonium acetate as a sample solution. A MCE-ESI-MS microchip (α = 30 $^{\circ}$) was reused and the reproducibility of the peak heights detected as MS spectrum was observed.

[‡]Taylor cone is equilibrium shape of a free liquid surface at the end of an ESI electrode in a sufficiently intense electric field [19].
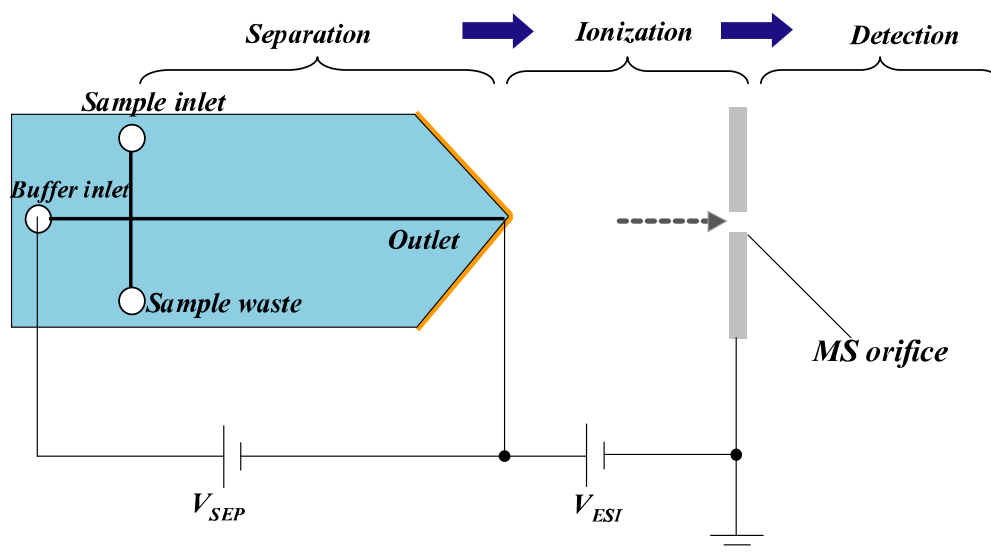
Fig. 5.7: Experimental setup for ESI experiments. The grounded target was spaced a few millimeters from channel opening.

5.2.3 Results and discussion

Fabricated microchip

  Whole view of the COP microchip and scanning electron microscope (SEM) image of the spray tip (α = 90 $^{\circ}$) are shown in Figure 5.8. The channel outlet of 10 μm in width and 20 μm in depth formed at the spray tip was observed. At the direct bonding process, deformation of the channel structure was negligible because bonding is performed at the temperature lower than T_g. Even after ESI tip structuring by a circular saw, there was no crack at the bonded interface because of its sufficient bonding strength.

ESI measurements

  Photomicrographs of the channel outlet at the experiments of Taylor cone formation are shown in Figure 5.9. The Taylor cone was not formed at the non-tapered tip (α = 180 $^{\circ}$) (Figure 5.9 (a)), while it was formed at the tapered emitter tips (α = 90 $^{\circ}$, 60 $^{\circ}$, 30 $^{\circ}$) (Figure 5.9 (b–d)). The success rate of the Taylor cone formation increased with decreasing the tip angle α. This reason was expected that broadening droplet along the tip surface could be avoided by structuring the sharp emitter tip.
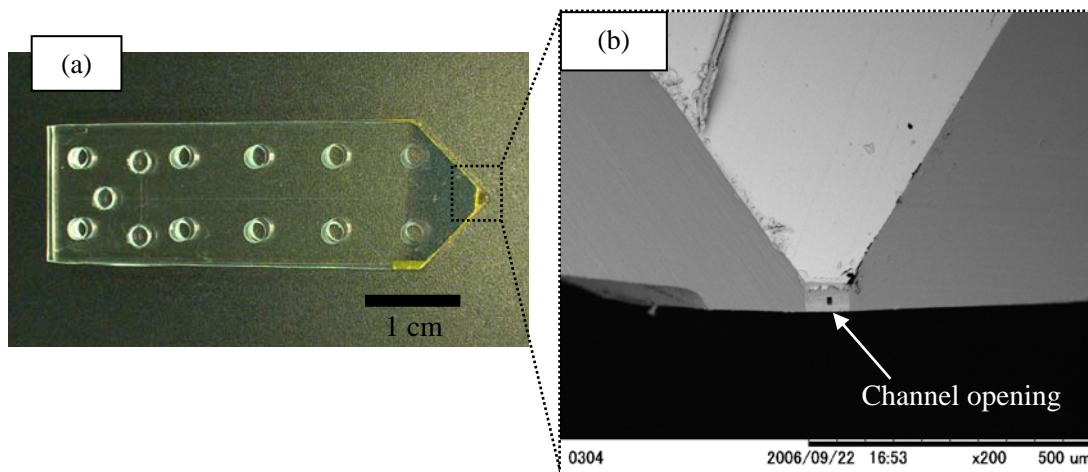
Fig. 5.8: Fabricated MCE-ESI-MS microchip ($\alpha = 90$ °); (a) whole view and (b) SEM image of the ESI tip [3].
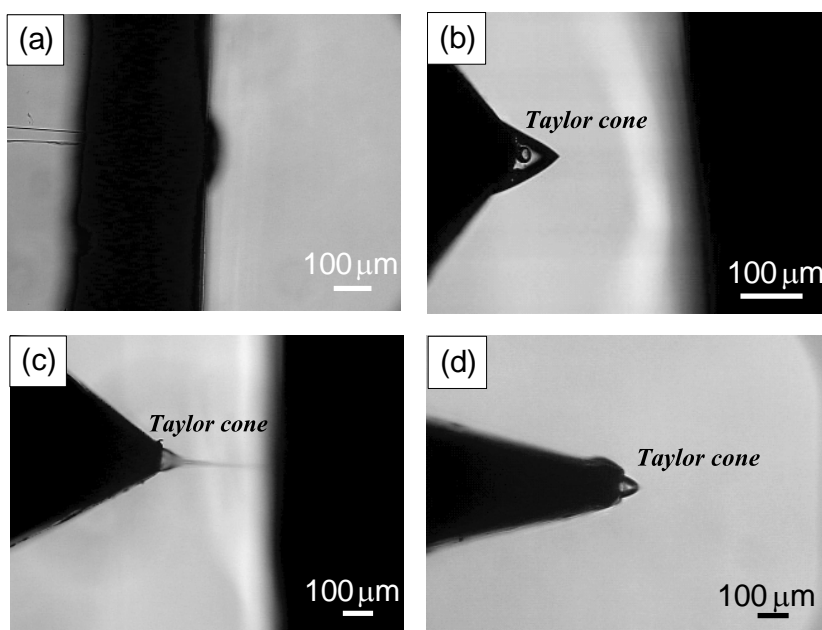
Fig. 5.9: Photomicrographs of the channel outlet at the experiments of Taylor cone formation; the tip angle α of (a) 180 °, (b) 90 °, (c) 60 °, and (d) 30 ° [3].
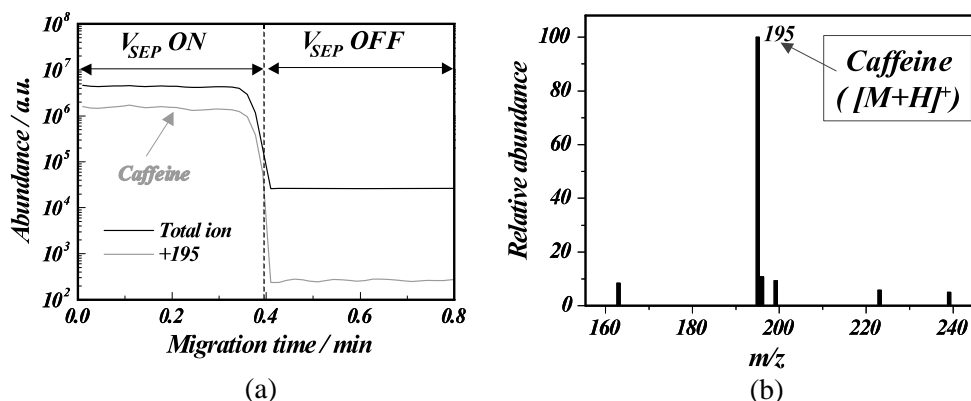
Fig. 5.10: Detection of caffeine by infusion analysis: (a) electropherogram and (b) MS spectrum of caffeine [3].

The electropherogram and the MS spectrum obtained with an infusion analysis of caffeine ($\alpha = 30°$) are shown in Figure 5.10. The protonated ion of caffeine (m/z 195) was observed in the positive ion mode (Figure 5.10 (b)). The electropherogram is stable and the background noise in MS spectrum is very small. These results indicate that stable ESI were achieved.

Figure 5.11 shows the separation of arginine and caffeine by MCE-ESI-MS at $\alpha = 30°$. Injection time was 1 s, and MS detection mode was positive ion mode. Complete separation of the sample in the MCE-ESI-MS analysis was obtained. Arginine and caffeine were successfully detected as protonated molecules [M+H]+. The background noise and contamination noise from the other sample are negligible. Thus, the fabricated COP microchip can be employed as the MCE-ESI-MS analysis device. However, the peak of caffeine is very small in the electropherogram; the values of caffeine are multiplied twenty times in Figure 5.11 (a). Caffeine is neutral and shows lower detection sensitivity compared to cationic species such as arginine. Since the electrophoresis speed of arginine is faster than that of caffeine, concentration of arginine seems to be occurred at sample injection. Another problem is broadening the bands (~ 10 sec) in Figure 5.11 (a). This effect was strongly affected by the negative pressure generated in the MS orifice as reported by Tachibana et al. [13]. This problem can be overcome by using a microchip with the longer separation channel.

103
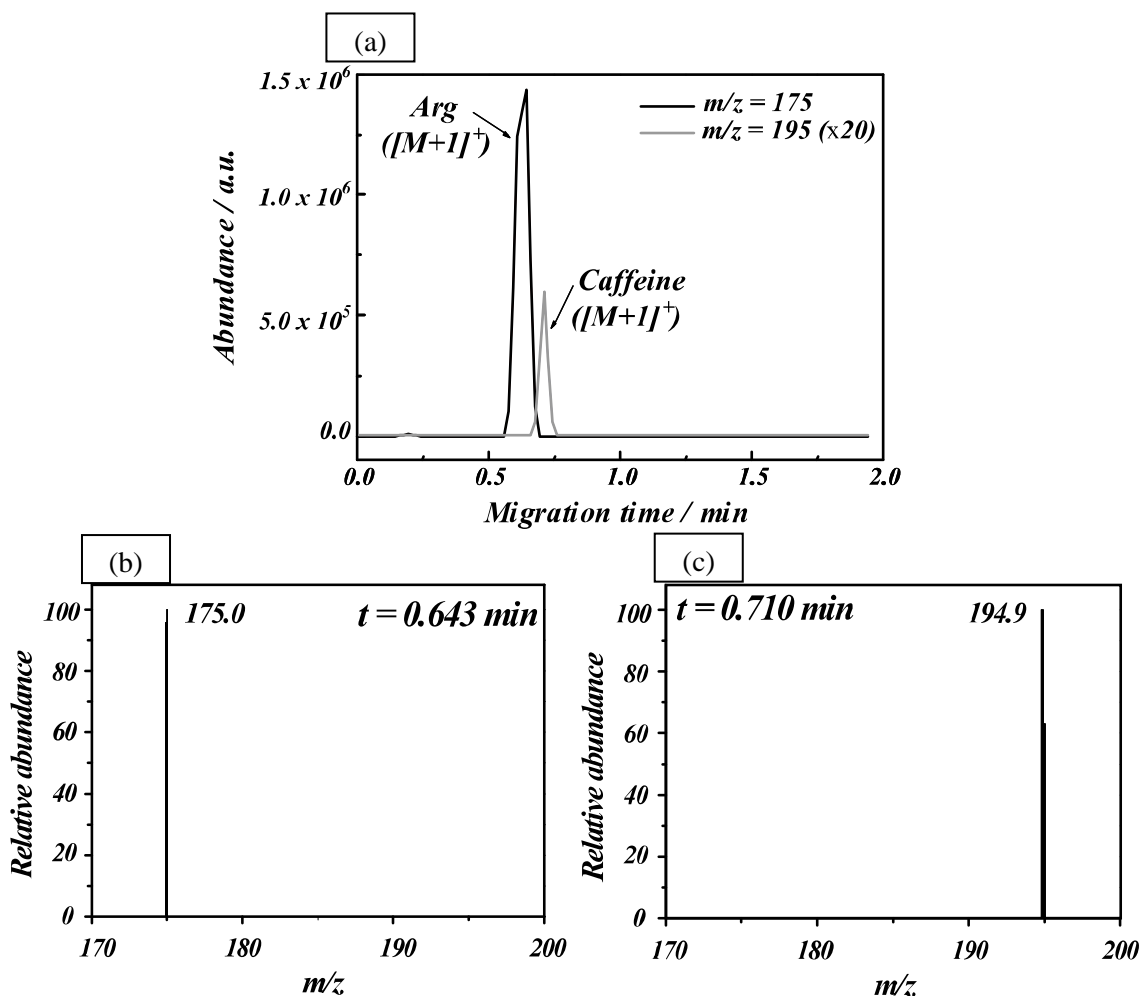
Fig. 5.11: MCE-ESI-MS analysis of caffeine and arginine; (a) electropherogram, (b) MS spectrum of arginine (t = 0.643 min) and (c) caffeine (t = 0.710 min) [3]; t: migration time.

Figure 5.12 (a) shows the peak heights of MS spectrum at 1st, 3rd, 5th, 7th, 10th, 12th, and 14th run in stability and reproducibility test. Stable MS detection was achieved and reproducible peak heights were kept up to 13 times. The residual standard deviation (RSD) of the peak height was 9.4 %. At the 14th run, the peak was not detected. Figure 5.12 (b) shows photomicrographs of the nano-electrospray tip after 1st, 5th, 10th, and 14th run in this test. After 10th run, optical transparency of the tip was increased obviously. It is indicated that thickness of the Au film decreased. After 14th run, the decrease area was expanded, and deformation of the tip structure was

observed. The obvious decrement of the peak at 14th run was caused by the deformation or damage of the Au electrode. The damages of the bonding interface were not observed. The Au thickness looked thinner; however, it was still remained on the COP tip. These results indicate that bonding strength of the COP plates and the adhesion strength of the Au film are strong enough. The stability and reproducibility of the fabricated nanospray tip is sufficient in practical use.
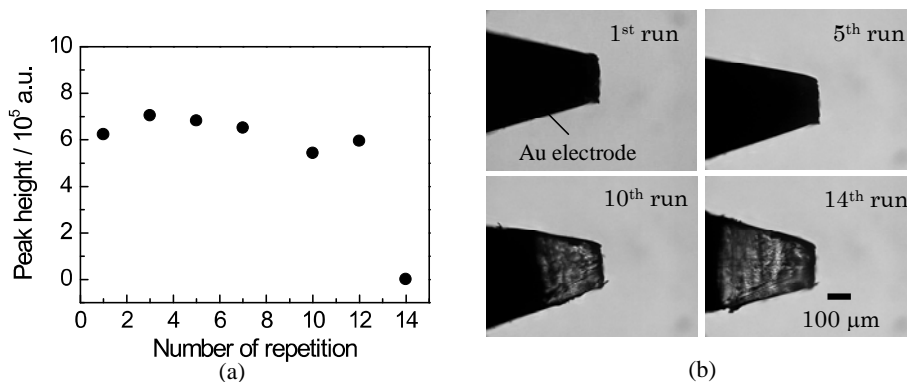
Fig. 5.12: Results of stability and reproducibility test of ESI tip: (a) reproducibility of the peak height detected as MS spectrum; (b) photomicrographs of the nano-electrospray tip after 1st, 5th, 10th, and 14th run [2].

5.3 Plastic blood analysis chip

5.3.1 Introduction

In order to observe blood flow behavior in vivo capillary vessels, Kikuchi et al. developed a blood analysis chip made of silicon [21,22]. This chip has microchannel array, which equivalent diameter is 6 μm. When human blood is flowed into the microchannels, platelet aggregation was observed after channel passage due to activation of platelet. This chip is used for the evaluations of the shear stress sensitivity of platelets, the adhesion of white blood cells and the hardness of red blood cells from blood transit time as well as the blood flow images. Several experiments have been reported by using these chips [23,24]. Since the commercialized blood analysis chips are fabricated by silicon fabrication process, cost of chip is one of the problems in actual use.

In the case of the blood analysis chip made of silicon, thermal oxidation for hydrophilic treatment (changed SiO_2) was performed to introduce blood into the microchannels smoothly. In order to realize reproducible blood analysis, the highly hydrophilic surface modification methods are requested. Long-term stable hydrophilic surface and anti-adhesion of biomaterials (platelets and white blood cells) as well as biocompatibility are also required. However, the surface by thermal oxidization causes adhesion of biomaterials on the chip surface.

The author fabricated the blood analysis chip made of PMMA [25-27] in our previous work. Since the multistep structures are formed at once by hot embossing or injection molding, low-fabrication cost is realized. Hydrophilic organic films (MPC (2-methacryloyloxiethylphosphorylcholine) [25,27] or ozone-treated polyurea [26]) were coated on the PMMA chip for smooth flow and anti-adhesion of biomaterials. On the other hand, since the organic film-coated surfaces were recovered to hydrophobic after washing by water, adhesion of biomaterials were often observed on the microchannel surfaces after washing. For reproducible measurements, improvement of the surface stability is required.

The author applies VUV/O_3-treated polyurea film (see Chapter 4) for the PMMA blood analysis chip. The performance of the surface treatment is evaluated by flowing actual human whole blood.

5.3.2 Experimental procedure

Fabrication process

Fabrication process of the blood analysis chip is shown in Figure 5.13. The blood analysis chip was structured by injection molding of PMMA (PARAPET GH-S from Kuraray Co., Ltd.) (Figure 5.13 (a)). The nickel stamp is fabricated by photolithography and electroforming [25,27]. After evaporation of aluminum on the chip surface to observe with epi-illumination (Figure 5.13 (b)), polyurea film was coated and treated by VUV/O_3 (Figure 5.13 (c)). Thickness of the polyurea film was about 140 nm. The VUV/O_3-treatment conditions were chamber oxygen pressure p of 3.0×10^4 Pa, treatment time t of 20 min, and distance between the lamp window and the sample surface d of 142 mm.
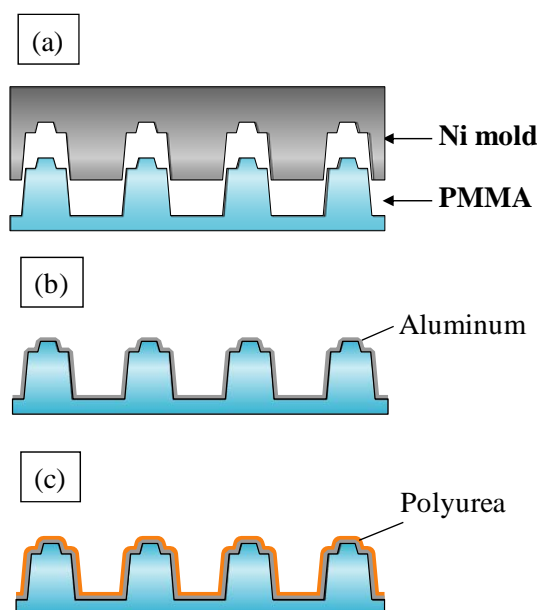
Fig. 5.13: Fabrication process of a blood analysis chip: (a) injection molding of PMMA by using Ni mold, (b) evaporation of Al, and (c) polyurea film coating and VUV/O_3 treatment [6].

Measurement setup

Special chip assembly for blood flow test was used as shown in Figure 5.14. As in the case of a conventional silicon chip [21-24], fabricated PMMA chip was contacted with flat glass plate mechanically.

A micro channel flow analyzer (MCFAN from Hitachi Haramachi Electronics Co., Ltd.) as shown in Figure 5.15 was used to characterize the fabricated PMMA chip. The fresh human whole blood (100 μL, heparin addition (5%)) was flowed into the chip under a pressure difference of 20 cm H_2O. The contentious imaging of the blood flow was performed to evaluate the adhesion of the platelets and white blood cells. For comparison, conventional silicon chip was also measured. The PMMA chip is reused once more after the first blood flow test. The PMMA chip is washed by ultrasonic cleaning in surfactant induced water for removing blood.
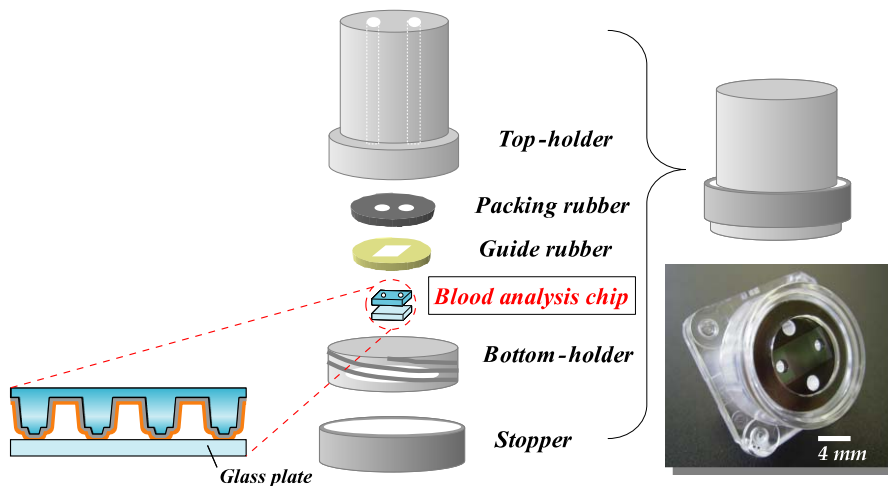
Fig. 5.14: Chip assembly for blood flow test and its photograph [6].
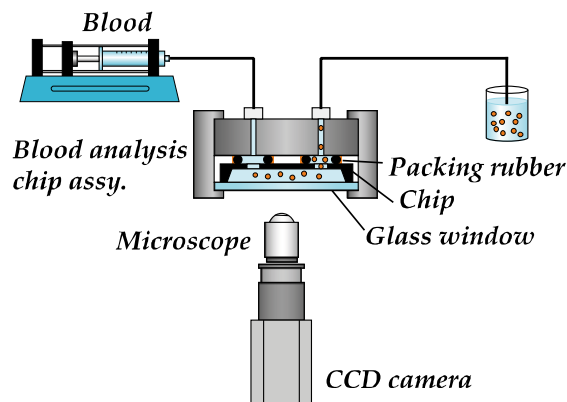
Fig. 5.15: Experimental setup for blood flow analyzer [6].

5.3.3 Results and discussion

Figure 5.16 (a) and (b) is a whole view and SEM micrographs of the fabricated chip. This chip has 300 μm-wide and 85 μm-deep channels for introducing blood sample, and 6 μm-wide and 5 μm-deep microchannels for observation.

The images of human blood flow of the conventional silicon chip and the newly developed PMMA chip are shown in Figure 5.17. The adhesion of platelets and white blood cells was significant in the case of a silicon chip (Figure 5.17 (a)) while almost no adhesion was observed in the case of a PMMA chip coated with the polyurea film (Figure 5.17 (b)). Even the reused polyurea chip shows almost no adhesion (Figure 5.17 (c)). These results indicate that this polyurea film treated by VUV/O_3 has remarkable advantages in the blood analysis chips.
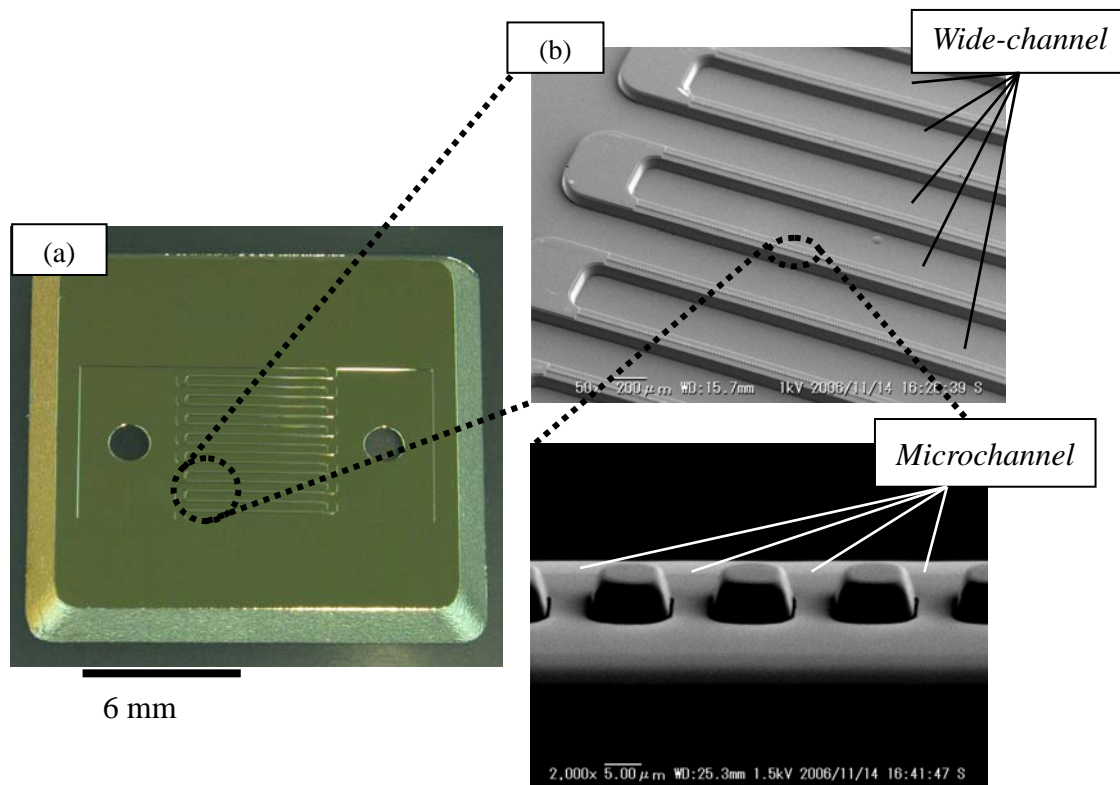
Fig. 5.16: (a) Whole view and (b) SEM micrographs of the fabricated blood analysis chip [6].
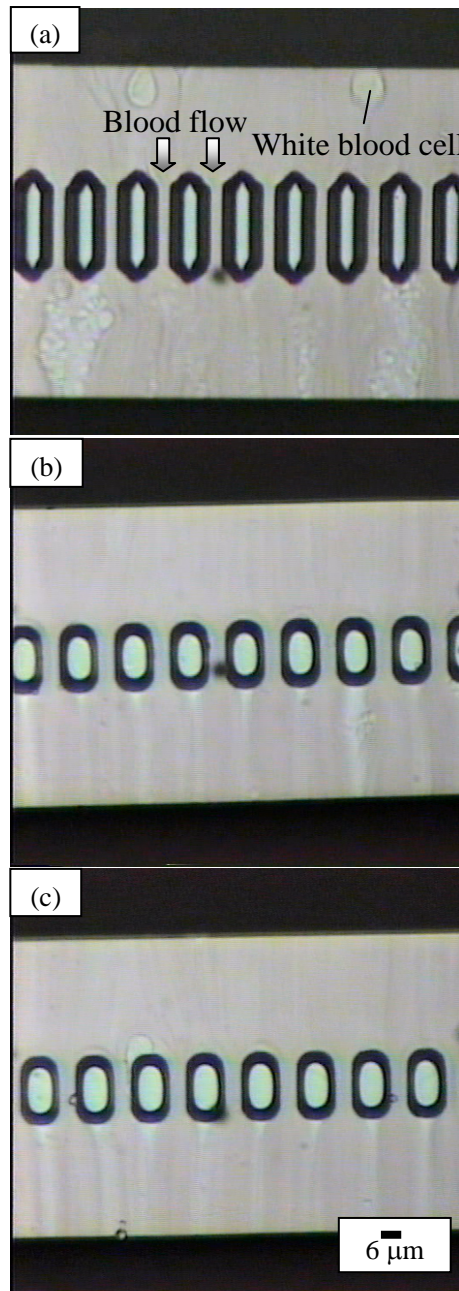
Fig. 5.17: Images of blood flow in (a) Si chip for reference, (b) PMMA chip coated polyurea film, and (c) reused PMMA chip after ultrasonic cleaning with surfactant-induced water [6].

5.4 Conclusion

A μDMFC device was realized on COP substrate. Microchannel pattern was fabricated by hot embossing. The plastic μDMFC with 3-D electrodes succeeded in generating electricity. The open circuit voltage of 237 mV and the maximum power density of 0.04 mW/cm^2 were obtained at room temperature with 2M methanol. This technique can apply for a μDMFC array chip which has numbers of cells in series.

A MCE-ESI-MS microchip was fabricated by hot embossing and low-temperature direct bonding. The ESI emitter tip structure was formed directly at the MCE outlet. Since these microchips enable negligible dead volume at the electrospray port, efficient spray of the sample necessary for acceptable resolution of MS was realized. It also achieved stable spray at the low flow rate of about 0.1 μL/min without an external pump. By applying the fabricated COP chip for actual MCE-ESI-MS chemical analysis, successful separation and detection of caffeine and arginine was achieved. The fabricated COP microchip can be employed as the MCE–ESI-MS analysis device. Long-term stable MS spectrum was obtained and the reproducible results were observed up to 13 times. Low cost and reusable plastic MCE-ESI-MS chip can be realized.

The VUV/O$_3$-treated polyurea film was applied for PMMA blood analysis chip which has blood cell behavior detection microchannels (equivalent diameter: 6 μm). The fresh human whole blood was flowed into the chip. The adhesion of platelets and white blood cells was significant in the case of a silicon chip, while almost no adhesion was observed in the case of VUV/O$_3$-treated polyurea coated chip, even after ultrasonic cleaning in surfactant induced water. This polyurea film treated by VUV/O$_3$ has remarkable advantages in the blood analysis chips.

These applications indicate that the fabrication methods previously described in Chapters 2, 3 and 4 are applicable for fabrication of actual plastic microchips.

References

[1] M. Ishizuka, T. Suzuki, H. Shinohara, H. Houjou, S. Motokawa, J. Mizuno, T. Momma, T. Osaka, S. Shoji, Cost effective plastic micro direct methanol fuel cell (μDMFC), Proc. The 9th Int. Conf. Miniaturized Sys. Chem. Life Sci. (Micro-TAS), (2005) 1212-1214.

[2] H. Shinohara, F. Kitagawa, J. Mizuno, K. Otsuka, S. Shoji, Highly stable and reproducible cyclo-olefin polymer nano-electrospray tip for electrophoresis-mass spectrometry, Proc. The 4th Asia-Pacific Conf. Transducers and Micro/Nano Technol. (APCOT), (2008) 2S45 (in CD-ROM).

[3] H. Shinohara, T. Suzuki, F. Kitagawa, J. Mizuno, K. Otsuka, S. Shoji, Polymer microchip integrated with nano-electrospray tip for electrophoresis-mass spectrometry, Sens. Actuators B **132** (2008) 368-373.

[4] F. Kitagawa, T. Suzuki, H. Shinohara, J. Mizuno, S. Shoji, K. Otsuka, Application of cycloolefin polymer chip directly integrated with an electronanospray tip to electrophoretic separation and mass spectrometric detection, Proc. The 11th Int. Conf. Miniaturized Sys. Chem. Life Sci. (Micro-TAS), (2007) 1405-1407.

[5] T. Suzuki, F. Kitagawa, H. Shinohara, J. Mizuno, K. Otsuka, S. Shoji, Polymer microchip for electrophoresis-mass spectrometry fabricated by hot embossing and low temperature direct bonding, Proc. The 14th Int. Conf. Solid-State Sens. Actuators Microsys. (Transducers), (2007) 1617-1620.

[6] H. Shinohara, Y. Takahashi, J. Mizuno, S. Shoji, Surface hydrophilic treatment of polyurea film realized by vacuum ultraviolet light irradiation and its application for poly(methylmethacrylate) blood analysis chip, Sens. Actuators B **132** (2008) 374-379.

[7] H. Shinohara, Y. Takahashi, T. Nishi, K. Uemura, C. Takahashi, J. Mizuno, S. Shoji, surface hydrophilic polyurea film for PMMA blood analysis chip realized by vacuum ultraviolet light irradiation, Proc. The 14th Int. Conf. Solid-State Sens. Actuators Microsys. (Transducers), (2007) 291-294.

[8] S. Motokawa, M. Mohamedi, T. Momma, S. Shoji, T. Osaka, MEMS-based design and fabrication of a new concept micro direct methanol fuel cell (μ-DMFC), Electrochem. Comm. **6** (2004) 562-565.

[9] M. Ishizuka, H. Houjou, S. Motokawa, J.Mizuno, T. Momma, T. Osaka, S. Shoji, Metallization on three dimensions microstructures using photoresist spray coating for microdirect methanol fuel cell, Jpn. J. Appl. Phys. **45** (2006) 7944-7948.

[10] Q. Xue, F. Foret, Y. M. Dunayevskiy, P. M. Zavracky, N. E. McGruer, B. L. Karger, Multichannel microchip electrospray mass spectrometry, Anal. Chem. **69** (1997) 426-430.

[11] R. S. Ramsey, J. M. Ramsey, Generating electrospray from microchip devices using electroosmotic pumping, Anal. Chem. **69** (1997) 1174-1178.

[12] B. Zhang, F. Foret, B. Karger, High-throughput microfabricated CE/ESI-MS: automated sampling from a microwell plate, Anal. Chem. **73** (2001) 2675-2681.

[13] Y. Tachibana, K. Otsuka, S. Terabe, A. Arai, K. Suzuki, S. Nakamura, Rubust and sinple interface for microchip electrophoresis-mass spectrometry, J. Chromatogr. A **1011** (2003) 181-192.

[14] Y. Tachibana, K. Otsuka, S. Terabe, A. Arai, K. Suzuki, S. Nakamura, Effects of the length and modification of the separation channel on microchip electrophoresis-mass spectrometry for analysis of bioactive compounds, J. Chromatogr. A **1025** (2004) 287-296.

[15] J. Li, C. Wang, J. F. Kelly, D. J. Harrison, P. Thibault, Rapid and sensitive separation of trace level protein digests using microfabricated devices coupled to a quadrupole - time-of-flight mass spectrometer, Electrophoresis **21** (2000) 198-210.

[16] M. Svedberg, A. Pettersson, S. Nilsson, J. Bergquist, L. Nyholm, F. Nikolajeff, K. Markides, Sheathless electrospray from polymer microchips, Anal. Chem. **75** (2003) 3934-3940.

[17] S. Arscott, S. L. Gac, C. Druon, P. Tabourier, C. Rolando, A micro-nib nanoelectrospray source for mass spectrometry, Sens. Actuators B **98** (2004) 140-147.

[18] C. H. Chiou, G. B. Lee, H. T. Hsu, P. W. Chen, P. C. Liao, Microdevices integrated with microchannels and electrospray nozzles using PDMS casting techniques, Sens. Actuators B **86** (2002) 280–286.

[19] A. J. Rulisona and Richard C. Flagan, Scale-up of electrospray atomization using linear arrays of Taylor cones, Rev. Sci. Instrum. **64** (1993) 683-686.

[20] A. Sze, D. Erickson, L. Ren, D. Li, Zeta-potential measurement using the Smoluchowski equation and the slope of the current–time relationship in electroosmotic flow, J. Colloid Interface Sci. **261** (2003) 402–410.

[21] Y. Kikuchi, K. Sato, H. Ohki, T. Kaneko, Optically accessible microchannels formed in a single-crystal silicon substrate for studies of blood rheology, Microvasc. Res. **44** (1992) 226-240.

[22] Y. Kikuchi, K. Sato, Y. Mizuguchi, Modified cell-flow microchannels in a single-crystal silicon substrate and flow behavior of blood cells, Microvasc. Res. **47**

(1994) 126-139.

[23] Y. Kikuchi, Effect of leukocytes and platelets on blood flow through a parallel array of microchannels: micro- and macroflow relation and rheological measures of leukocyte and platelet activities, Microvasc. Res. **50** (1995) 288-300.

[24] Y. Yoshimura, Y. Hiramatsu, Y. Sato, S, Homma, Y. Enomoto, Y. Kikuchi, Y. Sakakibara, Activated neutrophils and platelet microaggregates impede blood filterability through microchannels during simulated extracorporeal circulation, Ann. Thorac. Surg. **75** (2003) 1254-1260.

[25] J. Mizuno, H. Shinohara, M. Ishizuka, T. Suzuki, G. Tazaki, Y. Kirita, T. Nishi, S. Shoji, PMMA micro-channel array for blood analysis fabricated by hot embossing, Proc. The 9th Int. Conf. Miniaturized Sys. Chem. Life Sci. (Micro-TAS), (2005) 1340-1342.

[26] H. Shinohara, J. Mizuno, G. Tazaki, T. Nishi, M. Nakajima, C. Takahashi, S. Shoji, PU Coated PMMA blood analysis chip, Proc. The 5th Int. Symp. Microchem. Microsys. (ISMM), (2005) 114-115.

[27] T. Nishi, K. Hagiwara, M. Fukuda, F. Kinoshita, K. Ito, Y. Kikuchi, S. Shoji, J. Mizuno, H. Shinohara, Examination of blood passage time using an acrylic micro channel array chip, Hemorheol. Relat. Res. **9** (2006) 3-9 (in Japanese).

Chapter 6

<u>Conclusion</u>

　Through creative experiments, the author has being worked to establish the foundations of high precision plastic micro/nanofabrication such as high precision hot embossing, low-temperature direct bonding, and surface modification using aromatic polyurea film. Functional chemical/biochemical microchips were successfully fabricated by combination of these methods.

　The summary of this work discussed in Chapters 1-5 is as follows:

　Chapter 1 introduced the thesis by summarizing the trends in relevant technical fields. The author provided the technical backgrounds of plastic micro/nanofabrication methods which required for low-cost fabrication of chemical/biochemical microchips. The required issues on fabrication methods for plastic microchips were also described.

　Chapter 2 described high precision hot embossing of plastic substrates. Flat embossed surface which is required for successive low-temperature bonding was realized by optimization of mold structure and demolding conditions. Etching condition to realize smaller scallops of deep-reactive ion etching (Deep-RIE) was chosen to decrease the rounded slope at the bottom edge. In hot embossing of poly-methylmethacrylate (PMMA), the failures such as burr height were minimized to be less than 1 μm under the demolding temperature of 80 $^{\circ}$C.

　Chapter 3 described low-temperature direct bonding methods of PMMA and cyclo-olefin polymer (COP). In order to bond plastics at lower than glass transition temperature T_g, pretreatments of oxygen plasma, atmospheric-pressure plasma, UV/O$_3$, vacuum UV (VUV), and VUV/O$_3$ were examined. The mechanisms of low-temperature direct bonding using oxygen plasma, VUV and VUV/O$_3$ treatments were investigated using surface analysis methods. Increment of polar functional groups and/or decrement of the T_g on the surface were observed after the pretreatment. The low-temperature direct bonding is originated in dipolar interactions between the

polar functional groups, and/or cross-diffusion of the low-T_g layers. This bonding method can be applicable for fine microstructures of smaller than micron meter-scale. An Au-electrode-embedded functional COP microchip was also successfully fabricated.

In Chapter 4, surface modification and low-temperature bonding processes were combined by using aromatic polyurea film. The polyurea film was coated on plastic surface and treated by VUV/O$_3$. Highly stable hydrophilic surface was obtained after the treatment. The VUV/O$_3$-treated polyurea film can be used as intermediate layers for low-temperature bonding of PMMA. The highly hydrophilic surface of the microchannel was retained even after the thermal bonding process. This bonding method was applied for fabrication of electrophoresis microchips.

Chapter 5 explained three kinds of plastic chemical/biochemical microchips realized by high precision plastic micro/nano fabrication methods.

A micro direct methanol fuel cell (µDMFC) device was realized by hot embossing of COP. The plastic µDMFC with 3-D electrodes succeeded in generating electricity. The open circuit voltage of 237 mV and the maximum power density of 0.04 mW/cm^2 were obtained at room temperature with 2M methanol.

A MCE-ESI-MS microchip is fabricated by hot embossing and low-temperature direct bonding of COP. The electrospray ionization (ESI) emitter tip structure was formed directly at the microchip electrophoresis (MCE) outlet. Since these microchips enable negligible dead volume at the electrospray port, efficient spray of the sample necessary for acceptable resolution of mass spectrometry (MS) was realized. It also achieved stable spray at the low flow rate ($\sim$ 0.1 µL/min) without an external pump. By applying the fabricated COP chip for actual MCE-ESI-MS chemical analysis, successful separation and detection of caffeine and arginine was achieved.

The VUV/O$_3$-treated polyurea film was applied for PMMA blood analysis chip which has blood cell behavior detection microchannels (equivalent diameter: 6 µm). The fresh human whole blood was flowed into the chip. Almost no adhesion of platelets and white blood cells was observed in VUV/O$_3$-treated polyurea coated chip.

This thesis shows possibility to realize functional plastic microchips of smaller than micron meter-scale. In addition, these fabrication methods are significant stepping stones to technological development of functional plastic micro/nano devices in future.

Thus, the results of these works greatly contribute on various scientific fields such as micro/nanoelectronics, analytical chemistry, biochemistry, and life science.

Future works on high precision plastic micro/nanofabrication will include further investigation of low-temperature bonding mechanisms, optimization of low-temperature bonding conditions. The investigations of this thesis are indispensable for future commercialization of functional chemical and biochemical microchips applicable for life science and human health care.

List of Achievements

\<Referred Journal Papers\>

1. **H. Shinohara**, Y. Takahashi, J. Mizuno, S. Shoji, Fabrication of Post-Hydrophilic Treatment-Free Plastic Biochip Using Polyurea Film, *Sensors and Actuators A: Physical*, Vol. 154, No. 2, 2009, pp.187-191.
2. **H. Shinohara**, M. Fukuhara, T. Hirasawa, J. Mizuno, S. Shoji, Fabrication of Magnetic Nanodots Array Using UV Nanoimprint Lithography and Electrodeposition for High Density Patterned Media, *Journal of Photopolymer Science and Technology*, Vol. 21, No. 4, 2008, pp.591-596.
3. **H. Shinohara**, T. Suzuki, F. Kitagawa, J. Mizuno, K. Otsuka, S. Shoji, Polymer Microchip Integrated with Nano-Electrospray Tip for Electrophoresis-Mass Spectrometry, *Sensors and Actuators B: Chemical*, Vol. 132, No. 2, 2008, pp.368-373.
4. **H. Shinohara**, Y. Takahashi, J. Mizuno, S. Shoji, Surface Hydrophilic Treatment of Polyurea Film Realized by Vacuum Ultraviolet Light Irradiation and Its Application for Poly(methylmethacrylate) Blood Analysis Chip, *Sensors and Actuators B: Chemical*, Vol. 132, No. 2, 2008, pp.374-379.
5. **H. Shinohara**, J. Mizuno, S. Shoji, Fabrication of a Microchannel Device by Hot Embossing and Direct Bonding of Poly(Methyl Methacrylate), *Japanese Journal of Applied Physics*, Vol. 46, No. 6A, 2007, pp.3661-3664.
6. **H. Shinohara**, J. Mizuno, S. Shoji, Low Temperature Direct Bonding of Poly(Methyl Methacrylate) for Polymer Microchips, *IEEJ Transactions on Electrical and Electronic Engineering*, Vol. 2, No. 3, 2007, pp.301-306.
7. T. Shibazaki, **H. Shinohara**, T. Hirasawa, N. Sakai, J. Taniguchi, J. Mizuno, S. Shoji, Desktop Type Equipment of Thermal-assisted UV Roller Imprinting, *Journal of Photopolymer Science and Technology*, Vol. 22, No. 6, 2009, pp.727-730.
8. 北川文彦, **篠原秀敏**, 水野 潤, 大塚浩二, 庄子習一, ナノスプレー一体型ポリマー製マイクロチップにおける電気泳動分離－質量分析検出, *電気学会論文誌E*, Vol. 130, No. 8, 2010 (in press).
9. 西泰治, 萩原清道, 福田始弘, 木下藤寿, 伊藤克之, 菊池佑二, 庄子習一, 水野潤, **篠原秀敏**, アクリル製マイクロチャネルアレイを用いた血液通過時間の再現性の検討, *日本ヘモレオロジー学会誌*, Vol. 9, No. 2, 2006, pp.3-9.

\<Presentations & Papers (referred)\>

1. **H. Shinohara**, J. Mizuno, S. Shoji, Precise Structure Controlled Plastic Hot Embossing Method for Low-temperature Direct Bonding, *International Conference on Electronics Packaging (ICEP2010)*, 2010, Sapporo, Japan (accepted).
2. **H. Shinohara**, J. Mizuno, S. Shoji, NEXAFS Studies on VUV and Oxygen Plasma Pretreated PMMA Surfaces for Investigation of Low-Temperature Bonding Mechanisms, *The 22nd International Microprocesses and Nanotechnology Conference (MNC2009)*, 2009, Sapporo, Japan, pp.726-727.
3. **H. Shinohara**, T. Suzuki, J. Mizuno, S. Shoji, Studies on Low-Temperature Bonding

Mechanism of VUV and Plasma Pretreated Cyclo-Olefin Polymer, *The 15th International Conference on Solid-State Sensors, Actuators and Microsystems (Transducers2009)*, 2009, Denver, Colorado, USA, pp.1039-1042.

4. **H. Shinohara**, J. Mizuno, S. Shoji, Studies on Low-Temperature Direct Bonding Methods of PMMA and COP Using Surface Pretreatment, *International Conference on Electronics Packaging (ICEP2009)*, 2009, Kyoto, Japan, pp.748-753.

5. **H. Shinohara**, J. Mizuno, S. Shoji, High-Throughput Nano-Metal Patterning Process Using UV Nanoimprint Lithography and Electrodeposition, *The 7th International Conference on Nanoimprint and Nanoprint Technology (NNT2008)*, 2008, Kyoto, Japan, pp.148-149.

6. **H. Shinohara**, F. Kitagawa, J. Mizuno, K. Otsuka, S. Shoji, Highly Stable and Reproducible Cyclo-Olefin Polymer Nano-electrospray Tip for Electrophoresis-Mass Spectrometry, *The 4th Asia-Pacific Conference on Transducers and Micro/Nano Technologies (APCOT2008)*, 2008, Tainan, Taiwan, 2S45 (in CD-ROM).

7. **H. Shinohara**, Y. Takahashi, J. Mizuno, S. Shoji, Post-Hydrophilic Treatment Free Plastic Biochip Fabrication Method Using Polyurea Film, *The 21st IEEE International Conference on Micro Electro Mechanical Systems (IEEE-MEMS2008)*, 2008, Tucson, USA, pp.367-370.

8. **H. Shinohara**, Y. Takahashi, T. Nishi, K. Uemura, C. Takahashi, J. Mizuno, S. Shoji, Surface Hydrophilic Polyurea Film for PMMA Blood Analysis Chip Realized by Vacuum Ultraviolet Light Irradiation, *The 14th International Conference on Solid-State Sensors, Actuators and Microsystems (Transducers2007)*, 2007, Lyon, France, pp.291-294.

9. **H. Shinohara**, J. Mizuno, F. Kitagawa, K. Otsuka, S. Shoji, Fabrication of Highly Dimension Controlled PMMA Microchip by Hot Embossing and Low Temperature Direct Bonding, *The 10th International Conference on Miniaturized Systems for Chemistry and Life Sciences (Micro-TAS2006)*, 2006, Tokyo, Japan, pp.158-160.

10. **H. Shinohara**, M. Ishizuka, J. Mizuno, S. Shoji, Low Temperature Direct Bonding of PMMA for Polymer Microchips, *Asia-Pacific Conference on Transducers and Micro-Nano Technology (APCOT2006)*, 2006, Singapore, 95-FT-A0062 (in CD-ROM).

11. S. Matsui, **H. Shinohara**, J. Mizuno, S. Shoji, Studies on Direct Bonding of Poly(Dimethyl Siloxane) with PC, COP and PMMA Using Pretreatment of Atmospheric-Pressure Oxygen Plasma, *International Conference on Electronics Packaging (ICEP2010)*, 2010, Sapporo, Japan (accepted).

12. T. Kasahara, M. Mizushima, **H. Shinohara**, T. Obata, T. Futakuchi, J. Mizuno, S. Shoji, Simple and low cost fabrication of high-sensitive capacitance sensor, *International Conference on Electronics Packaging (ICEP2010)*, 2010, Sapporo, Japan (accepted).

13. T. Kasahara, M. Mizushima, **H. Shinohara**, T. Obata, T. Futakuchi, J. Mizuno, S. Shoji, Simple and Low Cost Fabrication of Capacitance Sensors, *The 22nd International Microprocesses and Nanotechnology Conference (MNC2009)*, 2009, Sapporo, Japan,.pp.736-737.

14. S. Tominaka, H. Nishizeko, **H. Shinohara**, J. Mizuno, T. Osaka, Fabrication of On-Chip Fuel Cells on Polymer Substrates, *ECS Transactions (The 216th ECS Meeting)*, 2009, Vienna, Austria, Vol. 25, No. 1, pp.1961-1969.

15. H. Kurotaki, **H. Shinohara**, K. Sakuma, H. Kobayashi, J. Mizuno, S. Shoji, Low Temperature Wafer Bonding Using Metal Diffusion Technique, *International*

Conference on Electronics Packaging (ICEP2009), 2009, Kyoto, Japan, pp.628-631.

16. S. Ishizuka, M. Nakao, S. Kataza, **H. Shinohara**, S. Mashiko, J. Mizuno, S. Shoji, Batch Transfer Large-Area Gratings for DFB Lasers Fabricated on GaAs Substrates Using Ultraviolet Nano-imprint Lithography, *The 21st International Microprocesses and Nanotechnology Conference (MNC2008)*, 2008, Fukuoka, Japan, pp.554-555.

17. H. Kurotaki, **H. Shinohara**, H. Kobayashi, J. Mizuno, S. Shoji, Study of Low-temperature Wafer Bonding with Au-Au Bonding Technique, *2nd Integration and Commercialization of Micro and Nanosystems International Conference and Exhibition*, 2008, Hong Kong, MicroNano2008-70064.

18. F. Kitagawa, T. Suzuki, **H. Shinohara**, J. Mizuno, S. Shoji, K. Otsuka, Application of Cycloolefin Polymer Chip Directly Integrated with an Electronanospray Tip to Electrophoretic Separation and Mass Spectrometric Detection, *The 11th International Conference on Miniaturized Systems for Chemistry and Life Sciences (Micro-TAS2007)*, 2007, Paris, France, pp.1405-1407.

19. T. Suzuki, F. Kitagawa, **H. Shinohara**, J. Mizuno, K. Otsuka, S. Shoji, Polymer Microchip for Electrophoresis-mass Spectrometry Fabricated by Hot Embossing and Low Temperature Direct Bonding, *The 14th International Conference on Solid-State Sensors, Actuators and Microsystems (Transducers2007)*, 2007, Lyon, France, pp.1617-1620.

20. H. Kurotaki, **H. Shinohara**, H. Ishida, V. Dragoi, T. Glinsner, O. Lindner, J. Mizuno, S. Shoji, Equipments and Technologies for Packaging of Nano/micro-structured Polymer Applications, *The 11th International Conference on the Commercialization of Micro and Nano Systems (COMS2006)*, Tools of the Trade: Equipment and Infrastructure, 2006, Florida, pp.33-34.

21. J. Mizuno, **H. Shinohara**, M. Ishizuka, T. Suzuki, G. Tazaki, Y. Kirita, T. Nishi, S. Shoji, PMMA Micro-channel Array for Blood Analysis Fabricated by Hot Embossing, *The 9th International Conference on Miniaturized Systems for Chemistry and Life Sciences (Micro-TAS2005)*, 2005, Boston, USA, pp.1340-1342.

22. M. Ishizuka, T. Suzuki, **H. Shinohara**, H. Houjou, S. Motokawa, J. Mizuno, T. Momma, T. Osaka, S. Shoji, Cost Effective Plastic Micro Direct Methanol Fuel Cell (μDMFC), *The 9th International Conference on Miniaturized Systems for Chemistry and Life Sciences (Micro-TAS2005)*, 2005, Boston, USA, pp.1212-1214.

23. J. Mizuno, S. Farrens, H. Ishida, V. Dragoi, **H. Shinohara**, T. Suzuki, M. Ishizuka, T. Glinsner, S. Shoji, Cyclo-Olefin Polymer Direct Bonding Using Low Temperature Plasma Activation Bonding, *The 2005 International Conference on MEMS, NANO, and Smart Systems (ICMENS2005)*, 2005, Banff, Alberta-Canada, pp.346-349.

24. J. Mizuno, H. Ishida, S. Farrens, V. Dragoi, **H. Shinohara**, T. Suzuki, M. Ishizuka, T. Glinsner, F. P. Lindner, S. Shoji, Cyclo-Olefin Polymer Direct Bonding Using Low Temperature Plasma Activation Bonding, *The 13th International Conference on Solid-State Sensors, Actuators and Microsystems (Transducers2005)*, 2005, Seoul, Korea, pp.1346-1349.

\<Presentations \>

1. **H. Shinohara**, M. Fukuhara, T. Hirasawa, J. Mizuno, S. Shoji, Fabrication of Magnetic Nanodots Array Using UV Nanoimprint Lithography for High Density Patterned Media, *The 25th International Conference of Photopolymer Science and*

Technology (ICPST-25), 2008, Chiba, Japan, A-41.

2. **H. Shinohara**, J. Mizuno, G. Tazaki, T. Nishi, M. Nakajima, C. Takahashi, S. Shoji, PU Coated PMMA Blood Analysis chip, *The 5th International Symposium on Microchemistry and Microsystems (ISMM2005)*, 2005, Kyoto, Japan, pp.114-115.

3. S. Shoji, K. Kawai, **H. Shinohara**, D. H. Yoon, T. Arakawa, T. Funatsu, MEMS Based Cell Function Analysis Micro Fluidic Systems, *The 11th Korean MEMS Conference (KMEMS2009)*, 2009, Jeju, Korea, pp.1-3.

4. F. Kitagawa, K. Kubota, **H. Shinohara**, Y. Takahashi, J. Mizuno, S. Shoji, K. Otsuka, Electrophoretic Analyses of Biogenic Compounds Using Surface Modified Polymer Microchips, *The 33rd International Symposium on High Performance Liquid Phase Separations and Related Techniques (HPLC2008 Kyoto)*, 2008, Kyoto, Japan, PW045.

5. F. Kitagawa, K. Kubota, **H. Shinohara**, Y. Takahashi, J. Mizuno, S. Shoji, K. Otsuka, Electrophoretic Analyses of Biogenic Compounds Using Surface Modified Polymer Microchips, *The 8th International Symposium on Microchemistry and Microsystems (ISMM2008)*, 2008, Kyoto, Japan, p.26.

6. S. Shoji, T. Arakawa, K. Kawai, **H. Shinohara**, T. Funatsu, MEMS/NT Based Cell Function Analysis Microdevice/Systems, *Micro- and Nano Technologies in Medicine - a Swedish-Japanese Collaborative Workshop*, 2008, p.20.

7. J. Mizuno, **H. Shinohara**, S. Shoji, Compound Nanoimprint Processes and Their Applications for Functional Nanodevices, *The 2008 International Conference on Solid State and Materials (SSDM2008)*, 2008, Tsukuba, Japan, pp.928-929.

8. F. Kitagawa, T. Suzuki, **H. Shinohara**, J. Mizuno, S. Shoji, K. Otsuka, Electrophoretic Separation and Mass Spectrometric Detection on Polymer Microchip Directly Integrated with ESI Spray, *The 22nd International Symposium on Microscale Bioseparations and Methods for Systems Biology (MSB2008)*, 2008, Berlin, Germany, P.055-Mo.

9. F. Kitagawa, T. Suzuki, **H. Shinohara**, J. Mizuno, S. Shoji, K. Otsuka, Microchip Electrophoresis-Mass Spectrometry on Polymer Microfluidic Device Directly Integrated with a Nano ESI Tip, *The 7th Asia-Pacific International Symposium on Microscale Separations and Analysis, (APCE2007)*, 2007, Singapore, p.141.

10. F. Kitagawa, T. Suzuki, **H. Shinohara**, J. Mizuno, S. Shoji, K. Otsuka, Electrophoretic Separation and Mass Spectrometric Detection on Polymer Chip Directly Integrated with a Nano ESI Tip, *The 7th International Symposium on Microchemistry and Microsystems (ISMM 2007)*, 2007, Ibaraki, Japan, p.22.

11. F. Kitagawa, T. Suzuki, **H. Shinohara**, J. Mizuno, S. Shoji, K. Otsuka, Electrophoretic Separation and Mass Spectrometric Detection of Biogenic Compounds on Polymer Microchip Directly Integrated with a Nano Electrospray Tip, *DICP Symposium−Symposium (XIV) on Microscale Bioseparation*, 2007, Dalian, China.

12. F. Kitagawa, T. Suzuki, **H. Shinohara**, J. Mizuno, S. Shoji, K. Otsuka, Electrophoretic Separation and Mass Spectrometric Detection of Biogenic Compounds on Polymer Microchip Directly Integrated with a Nano Electrospray Tip, *DICP Shanghai Satellite Meeting: New Technology on Cell Separation and Detection*, 2007, Shanghai, China.

13. F. Kitagawa, T. Suzuki, **H. Shinohara**, J. Mizuno, S. Shoji, K. Otsuka, Electrophoretic Separation and Mass Spectrometric Detection on Polymer Chip Directly Integrated with an Electronanospray Tip, *The 1st Shenyang International Colloquium on Microfluidics (SICOM I)*, 2007, Shenyang, China.

14. S. Shoji, T. Arakawa, K. Kawai, **H. Shinohara**, T. Funatsu, Cells and Biomolecules Handling Micro/Nanofluidic Systems, *IEEE International Conference on Information Acquisition (IEEE ICIA2007)*, 2007, Jeju, Korea, PT2.

15. F. Kitagawa, T. Suzuki, **H. Shinohara**, J. Mizuno, S. Shoji, K. Otsuka, Fabrication of Integrated Nano ESI Tip for Microchip Electrophoresis−Mass Spectrometry, *The 21st International Symposium on Microscale Bioseparations (MSB2007)*, 2007, Vancouver, Canada, p.286.

\<Presentations in Domestic Conferences\>

1. <u>篠原秀敏</u>, 高橋善和, 西泰治, 植村邦彦, 高橋千栄子, 水野潤, 庄子習一, 真空紫外線を用いたポリ尿素膜親水化処理とその血液チップへの応用, *第 15 回化学とマイクロ・ナノシステム研究会*, 2007, 仙台, p.98.

2. <u>篠原秀敏</u>, 鈴木崇章, 石束真典, 水野潤, 庄子習一, 低温直接接合によるPMMA流体デバイスの製作, *第 11 回化学とマイクロ・ナノシステム研究会*, 2005, 福岡, p.20.

3. 水野 潤, <u>篠原秀敏</u>, 庄子習一, MEMS製造におけるインプリントプロセスとプラズマプロセス, *第 70 回応用物理学会学術講演会*, 2009, 富山, 8p-ZD-10.

4. 松井俊介, <u>篠原秀敏</u>, 白崎善隆, 小原収, 水野潤, 庄子習一, PDMS-熱可塑性樹脂直接接合技術の研究, *第 19 回化学とマイクロ・ナノシステム研究会*, 2009, 広島, p.14.

5. 柴崎智隆, <u>篠原秀敏</u>, 平澤玉乃, 坂井信支, 谷口淳, 水野潤, 庄子習一, デスクトップ型熱アシストUVロールインプリント装置の開発, *第 20 回プラスチック成形加工学会 年次大会*, 2009, 東京, pp.327-328.

6. 北川文彦, 久保田圭, <u>篠原秀敏</u>, 高橋善和, 水野潤, 庄子習一, 大塚浩二, 表面修飾ポリマーマイクロチップを用いる生体試料の電気泳動分析, *日本化学会第 89 春季年会*, 2009, 船橋, 2G6-40.

7. 北川文彦, 久保田圭, <u>篠原秀敏</u>, 高橋善和, 水野 潤, 庄子習一, 大塚浩二, 表面修飾ポリマーマイクロチップを用いる生体試料の電気泳動分析, *第 28 回キャピラリー電気泳動シンポジウム (SCE2008)*, 2008, 八王子.

8. 庄子習一, 荒川貴博, 川合健太郎, <u>篠原秀敏</u>, 船津高志, MEMS/NTを応用した細胞機能解析マイクロシステム, *第 17 回日本コンピュータ外科学会大会*, 2008, 東京, pp.213-214.

9. 北川文彦, <u>篠原秀敏</u>, 水野潤, 庄子習一, 大塚浩二, ESIスプレー集積化ポリマー製マイクロチップによる電気泳動分離−質量分析検出, *日本化学会第 88 春季年会*, 2008, 東京, 4L1-26.

10. 北川文彦, 鈴木崇章, <u>篠原秀敏</u>, 水野潤, 庄子習一, 大塚浩二, ナノESI一体型ポリマー製マイクロチップによる電気泳動分離−質量分析検出, *第 27 回キャピラリー電気泳動シンポジウム (SCE 2007)*, 2007, 浜松, pp.25-26.

11. 北川文彦, 鈴木崇章, <u>篠原秀敏</u>, 水野潤, 庄子習一, 大塚浩二, マイクロチップ電気泳動分離−質量分析検出用ポリマー製デバイスの開発, *日本分析化学会第 56 年会*, 2007, 徳島, I2006.

12. 北川文彦, 鈴木崇章, <u>篠原秀敏</u>, 水野 潤, 庄子習一, 大塚浩二, シクロオレフィンポリマーマイクロチップによる電気泳動分離−質量分析検出, *第 15 回化学とマイクロ・ナノシステム研究会*, 2007, 仙台, p.78.

13. 北川文彦, 鈴木崇章, <u>篠原秀敏</u>, 水野 潤, 庄子習一, 大塚浩二, 電気泳動分離−質量分析検出用ポリマー製マイクロチップの作製, *日本材料学会第 56 期学術講演会*, 2007, 名古屋.

14. 北川文彦, 鈴木崇章, <u>篠原秀敏</u>, 水野 潤, 庄子習一, 大塚浩二, 電気泳動分離−質量

分析検出用シクロオレフィンポリマーマイクロチップの作製（2），*第 55 回質量分析総合討論会*，2007，広島．

15. 北川文彦，鈴木崇章，**篠原秀敏**，水野　潤，庄子習一，大塚浩二，電気泳動分離－質量分析検出用シクロオレフィンポリマーマイクロチップの作製，*第 14 回クロマトグラフィーシンポジウム*，2007，富山．

16. 鈴木崇章，**篠原秀敏**，石束真典，水野潤，庄子習一，Au電極一体型COPマイクロチャネルの作製Ⅱ，*第 12 回化学とマイクロ・ナノシステム研究会*，2005，京都，p.10．

17. 西泰治，鳥原正治，福田始弘，桐田泰三，田崎剛，菊池佑二，庄子習一，水野潤，**篠原秀敏**，樹脂製マイクロチャネルアレイを用いた通過時間の再現性検討，*第 12 回日本ヘモレオロジー学会*，2005，京都，p.51．

18. 西泰治，桐田泰三，福田始弘，菊池佑二，水野潤，庄子習一，**篠原秀敏**，樹脂製マイクロチャネルアレイを用いた血液流動試験，*医科器械学（第 80 回日本医科器械学会大会一般演題講演集）*，Vol.75, No.10, 2005, pp.708-709．

19. 鈴木崇章，**篠原秀敏**，石束真典，水野潤，庄子習一，金電極一体型シクロオレフィンポリマーマイクロチャネルの作製，*第 11 回化学とマイクロ・ナノシステム研究会*，2005，福岡，p.23．

<Books>

1. **H. Shinohara** and J. Mizuno, Subsection 3.3.1 "Ubiquitous NIL Equipment", *Nanotransfer Science and Technology*, KTI-International, 2010 (in press).
2. **H. Shinohara** and J. Mizuno, Section 4.1 "Company Activity", *Nanotransfer Science and Technology*, KTI-International, 2010 (in press).
3. **H. Shinohara**, J. Mizuno, S. Shoji, Chapter 22 "Low-Temperature Polymer Bonding Using Surface Hydrophilic Treatment for Chemical/Bio Microchips", *Solid State Circuits Technologies*, IN-TECH, 2010, pp.445-462.
4. **篠原秀敏**，庄子習一，水野潤，「分析デバイスへの応用」，*2009 ナノインプリント技術大全*，(株)電子ジャーナル社，第 3 編，第 5 章，第 2 節，2009, pp.177-180.
5. **篠原秀敏**，庄子習一，水野潤，「ナノインプリント技術のLEDへの応用」，*2009 ナノインプリント技術大全*，(株)電子ジャーナル社，第 3 編，第 6 章，2009, pp.181-184.
6. **篠原秀敏**，庄子習一，水野潤，「分析デバイスへの応用」，*2007 ナノインプリント技術大全*，(株)電子ジャーナル社，第 3 編，第 5 章，第 2 節，2007, pp.193-197.

<Patents>

1. S. Kajiwara, S. Shoji, J. Mizuno, **H. Shinohara**, Method for Manufacturing Patterned Magnetic Recording Medium, US20090218313, 2009.
2. 庄子習一，水野潤，後藤峰生，加藤友也，**篠原秀敏**，船津高志，荒川貴博，小原收，白崎善隆，三次元シースフロー形成構造及び微粒子集束方法，特願 2009-135665, 2009.
3. 梶原　里美，庄子習一，水野潤，**篠原秀敏**，パターン化磁気記録媒体の製造方法，特開 2009-20577, 2009.

<Media>

1. 「室温で親水性プラに」日経産業新聞，2008 年 4 月 8 日，p.11.